JUSTUS-LIEBIG-
UNIVERSITÄT
GIESSEN

Institut für Tierphysiologie
AG Molekulare Zellphysiologie
Prof. Dr. W. Clauss

Universitäten Gießen und
Marburg Lungen Zentrum
Prof. Dr. W. Seeger
AG Vadasz

Impact of hypercapnia on alveolar Na^+-transport

Establishing a system for ENaC-protein detection

Inaugural Dissertation

zur Erlangung des Doktorgrades Dr. rer. nat.
der naturwissenschaftlichen Fachbereiche
der Justus-Liebig-Universität Gießen

Vorgelegt von Benno Andreas Buchbinder

Gießen, Oktober 2013

Dekan:	Prof. Dr. Volker Wissemann
Interner Betreuer:	Prof. Dr. Wolfgang Clauss
Externer Betreuer:	Prof. Dr. Werner Seeger

Table of Contents

Table 1 Abbreviations

[m/v]	mass per volume
[v/v]	volume per volume
7-AAD	7-Aminoactinomycin
A549	human adenocarcinoma cell line
A6 cells	*Xenopus laevis* kidney cell line
AD/DA	analog-digital / digital-analog
AECC	American-European Consensus Conference on ARDS
AMPK	adenosine-monophosphate-activated kinase
AQP5	aquaporin 5
ARDS	acute respiratory distress syndrome
ATI / ATII	alveolar epithelial cell type I and II
CaMKK-ß	Ca^{2+}-calmodulin dependent kinase kinase ß
CD90	cluster of differentiation 90
cDNA	complimentary deoxyribonucleic acid
CFTR	cystic fibrosis transmembrane conductance regulator
CHO	chinese hamster ovary cell line
COS-7	fibroblast-like cell line derived from monkey kidney tissue
Deg	Degenerin
DNA	deoxyribonucleic acid
E-cadherin	epithelial cadherin

ECL	enhanced chemiluminescence
EDTA	ethylenediaminetetraacetic acid
ENaC	epithelial Na^+- channels
ER	endoplasmic reticulum
ERK	extracellular signal-regulated kinase
et al.	et alii
FACS	fluorescence-activated cell sorting
FBS	fetal bovine serum
FIO_2	fracture of inspired oxygen
GFP	green fluorescent protein
GRE	glucocorticoid responsive element
h	hour
H441 cells	human lung adenocarcinoma epithelial cell line
HA	heme aggluttinin
HEK-293	human embryonic kidney cell line 293
HPRT	hypoxanthin-phosphoribosyl-transferase
HSC	highly selective channels
I_{Ami}	amiloride-sensitive current
IFN-ɔ	interferon-gamma
IgG	immunoglobulin G
IKKɓ	inhibitor of nuclear factor kappa-B kinase subunit ɓ

IL-1ϐ	interleukin-1ϐ
I_{Na}	electrical current produced by transepithelial Na+-transport
I_{sc}	electrical short circuit current
IU	international unit
JNK	c-Jun N-terminal kinase
kDa	kilo Dalton
LB	Luria broth
LDH	lactate dehydrogenase
LPS	lipopolysaccharide
LSC	low selective channel
MAPK	mitogen-activated protein kinase
MDCK	Madin-Darby canine kidney type 1
MEC	mechanosensory abnormality protein
MG-132	proteasome inhibitor
miRNA	micro ribonucleic acid
mmHg	mm of mercury
mRIPA	modified radio-immunoprecipitation assay buffer
mRNA	messenger ribonucleic acid
MSC	mesenchymal stem cell
N	number of é
n.s.	not significant

NCBI	National Center for Biotechnology Information
Nedd4-2	neural precursor cell expressed developmentally down-regulated protein 4-2
NET	neutrophil extracellular traps
NIH	National Institutes of Health
NKCC	$Na^+,K^+,2Cl^-$ cotransporter
P	probability
P_0	open probability
P38	p38-mitogenactivated proteinkinase
Pa	partial pressure
PBS	phosphate buffered saline
PEEP	positive end-expiratory pressure
PKC-ε	protein kinase-C-ε
PY-motifs	conserved proline rich sequence in all ENaC subunits
RNA	ribonucleic acid
rpm	rounds per minute
rtPCR	reverse transcription polymerase chain reaction
SDS	sodium dodecyl sulphate
SEM	standard error of the mean
SGK1	serum- and glucocorticoid regulated kinase
SNP	single nucleotide polymorphisms
SOC-medium	salt-optimized with carbon (glucose)-medium

SP	surfactant protein
TAE	Tris-acetate-EDTA-buffer
TBS-T	Tris buffered saline incl. tween 20
TE-buffer	Tris-EDTA-buffer
TNF-Ŭ	tumor necrosis factor- Ŭ
U	unit
Ub	ubiquitin
UNC	uncoordinated (protein)
V5	epitope tag derived from paramyxovirus of simian virus 5
VE-cadherin	vascular endothelial cadherin
VEGF	vascular endothelial growth factor
VILI	ventilator-induced lung injury
V_T	tidal volume
WW-domain	tryptophane rich sequence of a protein, here Nedd4-2
YFP	yellow fluorescent protein
ZO-1	zona-occludens protein-1

1. Introduction

1.1. Acute Respiratory Distress Syndrome (ARDS)

ARDS has first been described in 1967, as a life-threatening respiratory condition characterized by acute onset of tachypnea, hypoxemia and loss of compliance, induced by different stimuli, including severe trauma, viral infection and pancreatitis (Ashbaugh et al., 1967). Approximately 190,000 cases and 74,000 deaths each year (mortality ~ 40 %) are estimated for the United States alone, underlining the clinical importance of ARDS (Rubenfeld and Herridge, 2007).

Until now, intensive research has been done on the mechanism and treatment of ARDS. The initial definition was revised in 1994 by the *American-European consensus conference on ARDS* (AECC) (Bernard et al., 1994) and further modified in the ñBerlin Definitionò in 2013 to match clinical criteria and to improve diagnosis of ARDS. The current definition of ARDS includes the acute onset within one week of a known clinical insult or new / worsening symptoms, non-cardiogenic bilateral infiltrates and hypoxemia, with the severity based on the degree of hypoxemia calculated as the ratio of oxygenation (PaO_2) to the fraction of inspired O_2 (FIO_2) (mild ARDS: 200 mmHg < PaO_2 / FIO_2 Ò 300 mmHg; moderate ARDS: 100 mmHg < PaO_2 / FIO_2 Ò 200 mmHg; severe ARDS PaO_2 / FIO_2 Ò 100 mmHg). Since the oxygenation is dependent on the ventilation of patients, these criteria have to be applied when the patient is ventilated with a *positive end-expiratory pressure* (PEEP) higher than 5 cmH_2O.

The main causes of ARDS are categorized into direct and indirect. Direct risk factors include all conditions that directly target the lung, such as pneumonia, inhalational injury or near-drowning, whereas indirect risk factors can be quite diverse. Major trauma, non-pulmonary sepsis, severe burns or drug overdose can all trigger ARDS (Ranieri et al., 2012).

1.1.1. Ventilation during ARDS

Currently, there are only supportive treatment options for the different kinds of ARDS. These include the mode of ventilation, conservative fluid management and prone positioning (Guérin et al., 2013; Wiedemann et al., 2006; Young et al., 2013). PEEP was recognized to be effective in reducing mortality in ARDS patients already in 1967, while only a small subset of patients improved with steroids, antibiotics or digitalis (Ashbaugh et al., 1967). Especially in combination with low tidal volume ventilation it is highly beneficial, as it prevents the alveoli from collapsing thus keeping the lung open (Hickling et al., 1994). Subsequently, oxygenation is improved, even more when combined with fluid management (Wiedemann et al., 2006). But mechanical ventilation is not only beneficial for the lung. When inadequate pressures are applied, the lung can be damaged, a condition called ventilator-induced lung injury (VILI) (Biehl et al., 2013), leading to increased morbidity and mortality (Parsons et al., 2005; Ranieri, 1999; Ranieri et al., 2000). Optimal ventilation strategies are still under debate. Studies aiming to elucidate the effect of lower versus higher PEEP are controversial and a meta-analysis in 2010 came to the conclusion that only patients suffering from severe ARDS benefit from higher PEEP levels (Briel et al., 2010). The authors who published the most recent meta-analysis conclude that high PEEP levels neither reduced mortality before hospital discharge, nor significantly increase the risk of barotrauma but improve oxygenation within the first seven days of treatment (Santa Cruz et al., 2013). But not only the level of PEEP should be considered when determining the optimal ventilation settings. Another important variable in ventilating patients is the tidal volume (V_T). Low V_T ventilation has been shown to be safe compared to conventional ventilation (6 vs. 12 ml/kg predicted body weight) (Cheng et al., 2005), minimize damage to the lung, reduce mortality and increase the number of days without ventilator (The Acute Respiratory Distress Syndrome Network, 2000) and according to a recent clinical trial it also acts protective on the cardiovascular system (Natalini et al., 2013).

1.1.2. Permissive hypercapnia

Lung-protective ventilation with low tidal volume and reduced minute-ventilation (volume of air inspired per minute) leads to a decreased elimination of CO_2 from the alveolar space, ultimately resulting in systemic hypercapnia with or without acidosis. Under normal conditions humans exhibit a partial pressure of arterial CO_2 (Pa_{CO2}) of 35-45 mmHg, but during several pulmonary diseases it can even exceed 200 mm Hg (Connors et al., 1996; Feihl and Perret, 1994; Mutlu et al., 2002; Sheikh et al., 2011). Clinical studies suggest that slightly elevated CO_2 levels are not detrimental for the patients and can be accepted (Hickling et al., 1994; The Acute Respiratory Distress Syndrome Network, 2000). Now, permissive hypercapnia as a consequence of lung protective ventilation is widely accepted, although not without reservation (Curley et al., 2011). Several clinical studies not only show hypercapnia is not harmful, but they even support a beneficial effect on the lung and on survival of patients (Ryu et al., 2012). In a rat model of systemic sepsis induced lung injury for example, hypercapnia only reduced the severity of lung injury when accompanied by acidosis, while buffered hypercapnia failed to provide any benefit (Higgins et al., 2009). This is interesting, because in another infection-based lung injury model sustained hypercapnia worsened lung injury (OõCroinin et al., 2008). Generally, hypercapnia impairs lung host defense in different ways. It has been shown to alter the innate immune response (Sporn et al., 2011), but also phagocytosis (Wang et al., 2010) and generation of reactive oxygen species (Gates et al., 2011).

pH independent effects of hypercapnia

Positive and negative effects of hypercapnia *in vivo* cannot be well investigated without any contribution of pH. But in several *in vitro* models pH-independent hypercapnia induced mechanisms have been identified that are highly detrimental in the context of ARDS. Hypercapnia was shown to inhibit epithelial cell wound repair and the inhibition was still present, when acidosis was buffered to normal pH (OõToole et al., 2009). Highly relevant is the finding, that alveolar epithelial function is significantly impaired during hypercapnia. This process has also been proven to be pH independent and is discussed in detail later (Briva et al., 2007; Chen et al., 2008; Vadász et al., 2008; Welch et al., 2010). Another event that has been demonstrated to be pH independent is blunting of the immunological response (Helenius et al., 2009).

1.1.3. Pathophysiology of ARDS

ARDS is characterized by dysregulated inflammation, inappropriate accumulation and activity of leukocytes and platelets, uncontrolled activation of coagulation and disrupted epi- as well as endothelial barrier function (Matthay et al., 2012).

Inflammation by activation of the innate immune response is triggered by microbial products or cell injury-associated endogenous molecules that are recognized by pattern-recognition receptors located on the surface of the lung epithelium and alveolar macrophages (Opitz et al., 2010). Dependent on the cause of the disease, several other mechanisms can contribute to the inflammatory process, such as formation of *neutrophil extracellular traps* (NET) (Caudrillier et al., 2012) or interaction of inflammatory and hemostatic cells (Looney et al., 2009). Since ARDS can be induced by many different stimuli, inflammatory processes are not good or bad *per se*, but need fine adjustment to clear pathogens from the lung without worsening the damage.

Another important characteristic of ARDS is the disruption of the microvascular and epithelial barrier causing the accumulation of protein-rich edema fluid, as well as leukocytes and erythrocytes in the alveolar space thereby impairing gas exchange.

Disruption of the endothelial barrier is caused by destabilization of its major component *vascular-endothelial cadherin* (VE-cadherin) by several factors like cytokines (TNF-Ŭ and IFN-ɔ), lipopolysaccharide (LPS) (Herwig et al., 2013) or VEGF (Chen et al., 2012) that are associated with different models of ARDS. Not only increased permeability of the endothelium is a problem in ARDS. Clinical data link obstruction and destruction of the microvascular bed in the lung, assessed by the pulmonary dead-space fraction, to increased mortality of ARDS patients (Nuckton et al., 2002). When only the endothelial barrier is disrupted, with the epithelium still intact, no increased permeability was observed and the alveolar epithelial liquid clearance was normal, indicating that a loss of endothelial barrier function does not necessarily induce ARDS (Wiener-Kronish et al., 1991).

Less is known about the mechanism of epithelial barrier damage. In patients that died from ARDS a variety of events are reported to happen at the alveolar epithelium, including cytoplasmic swelling, vacuolization and necrosis leading ultimately to a loss of epithelial cells (Bachofen and Weibel, 1977). Taken into account that the epithelial barrier is much tighter than the endothelial barrier (Taylor and Gaar, 1970) its disruption is an important event in the development of pulmonary edema. Besides

prevention of flooding of the airspace another critical function of the alveolar epithelium is the precise regulation of fluid transport.

Maximal fluid clearance has only been observed in 13 % of ARDS patients which is highly relevant when considering, that the hospital mortality was 62 % when fluid clearance was impaired or submaximal, compared to a mortality of ñonlyò 20 % in patients having maximal fluid clearance rates (Ware and Matthay, 2001).

The resolution of ARDS is quite complex and different events have to be synchronized. The epithelial and the endothelial barriers have to be reestablished and edema fluid, as well as inflammatory cells and exudate, need to be cleared from the airspace.

1.1.4. Alveolar epithelial barrier – function and repair

The alveolar epithelium is comprised of two different cell types: Alveolar epithelial cells type I (ATI) and type II (ATII). ATI cells cover approximately 93 % of the alveolar surface due to their large, flat morphology, thus keeping the diffusion barrier thin to enable proper gas exchange (Wang and Hubmayr, 2011). ATII cells are cuboidal, twice as abundant as type I cells and cover approximately 7 % of the alveolar surface. They account for 16 % of the all alveolar cells and have half of the volume of ATI cells (Crapo et al., 1982). Main functions are absorbance of excess alveolar fluid, a process later described in detail and secretion of surfactant (Kawada et al., 1990; Press et al., 1982). Surfactant, short for *surface active agent* consists of different components (10 % proteins, 90 % lipids) some of which reduce surface tension (surfactant proteins B and C (SP-B, SP-C) and phospholipids). Others play a role in host defence (SP-A and SP-D), underlining the immunological importance of ATII cells (Günther et al., 2001). Unidirectional amino acid and protein uptake from the apical side has also been described (Buchäckert et al., 2012; Uchiyama et al., 2008).

In the normal lung, proliferation of this cell-type is minimal, with a reported proliferative subpopulation of 0.5-1 % of all ATII cells (Kalina et al., 1993). In different models of lung injury in rats ATII cells have been reported to function as progenitors for type I cells, indicating their importance in reestablishing the alveolocapillary barrier following lung injury by proliferation and differentiation (Adamson and Bowden, 1974; Clegg et al., 2005; Evans et al., 1973). In the mouse model of hyperoxia-induced lung injury ATII cells have been identified to promote alveolar epithelial regeneration (Adamson and Bowden, 1974). This process seems to be activated generally upon injury of the epithelium, independent of the specific stimulus.

Lately, evidence for pluripotent stem cells that differentiate into alveolar epithelial cells is rising. Those cells have been found in the adult human lung and express markers of *mesenchymal stem cells* (MSCs) like CD90 as well as pro-surfactant protein-C that is associated with ATII cells but can also express *aquaporin 5* (AQP5), a marker of ATI cells. Still, it is not known whether this cell type directly differentiates into ATI or ATII cells or both (Chapman et al., 2011; Fujino et al., 2011).

Repopulation of the injured epithelium and restoration of the epithelial barrier function alone is not sufficient to resolve ARDS. Once the epithelium is tight again, the excess fluid needs to be cleared from the airspace.

Under normal conditions the alveolar surface liquid volume is precisely regulated. By low temperature scanning electron microscopy of the rat lung an area-weighted average thickness of 0.2 µm was estimated (Bastacky et al 1995). The primary regulators of the alveolar liquid layer are ATII cells. For many years, ATI cells have been believed to represent only a physical barrier, but recently studies showed that ATI cells express molecules crucial for fluid reabsorption and that they can as well actively contribute to fluid clearance (Johnson et al., 2002).

The regulation of alveolar surface liquid volume is controlled by an orchestrated active absorption and secretion of Na^+- and Cl^-- ions, which create an osmotic driving force for water to follow. Key elements are epithelial Na^+- channels (ENaCs) and Cl^- - channels for example *cystic fibrosis transmembrane conductance regulator* (CFTR), located in the apical surface of alveolar epithelial cells and the Na^+,K^+-ATPase, a cation transporter located in the basolateral membrane.

Especially in the fetal lung Cl^--transport is extremely important, since it drives distention of the lung, enabling growth and development (Olver and Strang, 1974). The mechanism is independent of pulmonary vascular filtration (Carlton et al., 1992a) indicating that it is taking place at the alveolar epithelium. This process is described to be secondary active, with Cl^- being cotransported into the cell by the $Na^+,K^+,2Cl^-$ cotransporter (NKCC) located in the basolateral membrane and induced by the electrochemical Na^+-gradient created by the Na^+,K^+-ATPase (Carlton et al., 1992b; Cassin et al., 1986). This results in an excess of Cl^- in the cell that is then secreted apically into the airspace. Around the time of birth, the predominance of Cl^--secretion fades and Na^+-absorption takes over to clear the lung from excess fluid.

The alveolar Na^+-transport is mediated by ENaCs and the Na^+,K^+-ATPase. As mentioned above, the Na^+,K^+-ATPase pumps Na^+-ions out of the cell in exchange for

K^+, more precisely three Na^+-ions and two K^+-ions. The result is a Na^+-gradient between the airspace and the interstitium. Early studies in the rabbit urinary bladder, another tight epithelium exhibiting Na^+-transport similar to the lung, investigating the properties of the apical and the basolateral membrane conclude that the Na^+-conductivity of the apical membrane is limiting the transcellular Na^+-flux (Lewis et al., 1977). This also applies to the lung (Canessa et al., 1994).

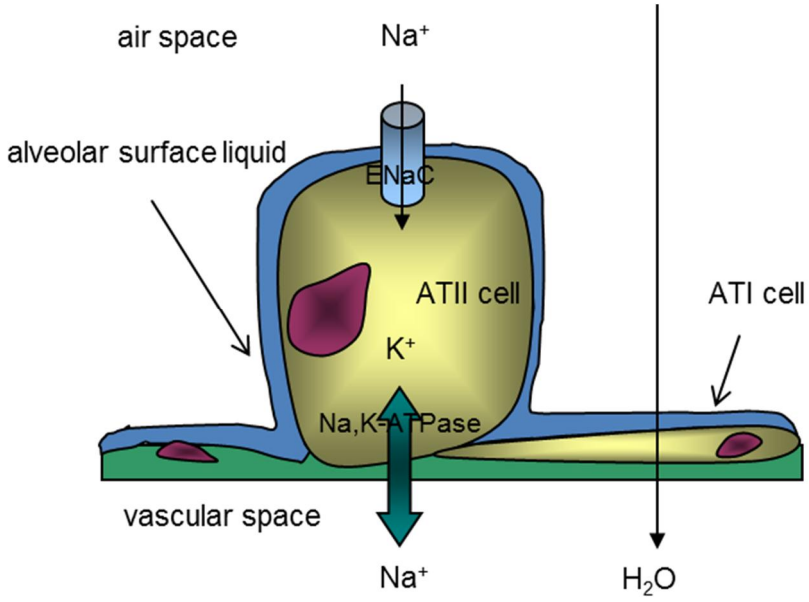

Figure 1 Scheme of alveolar Na^+-transport

The Na^+,K^+-ATPase removes Na^+ from the cytosol, creating a gradient for Na^+ to enter the apical side of the alveolar cells. This is happening both in ATI and ATII cells. Water is following the osmotic gradient that is created. The result is a reduction of alveolar surface liquid.

1.2. Deg/ENaC superfamily

ENaCs have first been reported from studies using frog skin and toad urinary bladder that were mounted in an Ussing chamber to measure transepithelial ion transport. ENaC or ENaC-like Na^+-channels are widely distributed among different animal species. Molecules belonging to the Degenerin/ENaC-superfamily have been identified from different epithelia in nematodes (Lai et al., 1996), flies, several species of rodents (Canessa et al., 1994; Letz et al., 1995), frog, chicken (Goldstein et al., 1997), cow (Fuller et al., 1995), lungfish (Li et al., 1995) and man (Fronius et al., 2010) underlining the evolutionary importance of this protein family.

1.2.1. Common structure

All members of the Deg/ENaC superfamily share invariable topology: Two transmembrane domains are connected with a large extracellular loop, that contains cysteine-rich domains (Renard et al., 1994). The N- as well as the C-termini are located in the cytoplasm of the cells and represent only a small fraction of the full-length protein (Mano and Driscoll, 1999). Many proteins including ENaCs assemble in homo- or hetero-multimeric complexes with varying composition (Firsov et al., 1998; Kosari et al., 1998; Snyder et al., 1998).

1.2.2. Various functions

The functions mediated by members of the Deg/ENaC superfamily are as diverse as their regulation. Touch sensation in *C. elegans* has been shown to be dependent on the *mechanosensory abnormality protein*s (MEC-4 and MEC-10) that assemble in a heteromeric complex containing at least two copies of each subunit (Hong and Driscoll, 1994; Huang and Chalfie, 1994). Proprioception is another sense that involves members of that family (*uncoordinated* (UNC-8) (Tavernarakis et al., 1997) and UNC-105 (Garcia-Anoveros Garcia Liu)).

Other functions of the Deg/ENaC superfamily involve neurodegeneration (Chalfie and Wolinsky, 1990) and sensing of protons (Chen et al., 1998). pH-dependency of ASIC channels in vitro required very low pH and the result was a rapidly inactivating cation current (Lingueglia et al., 1997; Waldmann et al., 1997).

Most important for the elaborated study is the regulation of salt absorption controlled by ENaCs located in epithelial cells of the kidney, colon and lung. As published by Bentley in 1968 amiloride is a very potent inhibitor of ENaC (Bentley, 1968). Several types of

channels have been described, all of which are sensitive to amiloride namely highly selective channels (HSC) for Na^+ and Li^+ with a low conductance of 5 pS, and low selective channels (LSC) with a conductance of 9 pS and 28 pS (Palmer, 1992).

1.2.3. Epithelial Na^+-channels

Four subunits have been identified in mammals, Ŭɓɔŭ-ENaC. The first subunit that was identified in the rat colon was Ŭ-ENaC (Canessa et al., 1993). When heterologously expressed in *Xenopus* oocytes, it showed characteristics that were found previously of channels expressed in native epithelia, namely high amiloride-sensitivity, high permeability for Li^+ and no K^+-conductivity. The only difference was that the currents were much smaller, compared to injection of whole colon RNA. Subsequently the authors searched for further subunits and found two more subunits, ɓ- and ɔ-ENaC which, when expressed individually, did not form Na^+-conducting, amiloride-inhibitable channels (Canessa et al., 1994). When ɓ- and ɔ-ENaC were coexpressed together with Ŭ-ENaC, the current was more than 100 fold higher, compared to Ŭ-ENaC alone (Canessa et al., 1994), suggesting that Ŭ-ENaC is the pore-forming subunit whose properties are modulated by ɓ- and ɔ-ENaC.

ŭ-ENaC has been identified in 1995. This subunit shares some features with, but also exhibits some important differences to Ŭ-ENaC: Similar to Ŭ-ENaC, ŭ-ENaC expressed individually forms amiloride-sensitive channels and the current is increased by two orders of magnitude, when ɓ- and ɔ-ENaC are coexpressed. Different to Ŭ-ENaC it is more permeable for Na^+, than for Li^+ and the sensitivity for amiloride was approximately 30 times higher (Waldmann et al., 1995). Closely related to ŭ-ENaC, functionally as well as structurally, is Ů-ENaC a subunit that is exclusively expressed in the clawed frog *X. laevis* (Babini et al., 2003).

Although the structure of all ENaC-subunits is quite similar, the tissue expression pattern differs markedly. Ŭ- and ɓ-ENaC are predominantly expressed in lung and kidney, whereas ɔ- and ŭ-ENaC are found in a variety of epithelial and non-epithelial tissues of different organs (Ji et al., 2012). ŭ-ENaC is expressed in heart, liver, brain and lung, but also found in pancreas, skeletal muscle and blood leukocytes (Su et al., 2004; Waldmann et al., 1995).

The functions of ɓ- and ɔ-ENaC are not as clear as for the other subunits. ɓ-ENaC has been postulated to regulate trafficking of ENaC complexes to the plasma membrane. Its Clara cell specific overexpression in the mouse resulted in increased Na^+-transport of

tracheal tissue that caused a cystic-fibrosis-like phenotype with mucus accumulation and postobstructive enlargement of distal airspaces, while overexpression of Ŭ- and ɔ-ENaC did not affect Na^+-transport (Mall et al., 2004). An explanation for this phenomenon might be that ɓ-ENaC is normally the least abundant and thus limiting subunit in the lung (Farman et al., 1997; Talbot et al., 1999; Yue et al., 1995). Genetic knockdown studies on the other hand showed, that the fluid clearance in the lung is impaired, when ɓ-ENaC expression is reduced (Randrianarison et al., 2008).

Stochiometry of ENaC is still under debate. Generally it is believed that ENaC is a heterotetrameric complex composed of two Ŭ-, one ɓ- and one ɔ-subunit (Firsov et al., 1998). Using the very sophisticated approach of atomic force microscopy a trimer composed of one copy each of Ŭ-, ɓ- and ɔ-ENaC or even a trimer-of-trimers was described (Stewart et al., 2011). Considering the discovery of ŭ- and Ů-ENaC which might replace Ŭ-ENaC or could even be added to the conventional heteromeric complex, various subunit assemblies in native tissues and different *in vitro* models might explain the great variations that can be observed studying ENaC function.

1.2.4. Regulation

Since the control of Na^+-transport is crucial to maintain proper water and salt homeostasis, ENaC function is tightly regulated on different levels by a variety of factors.

Regulation of gene expression is limited to long term regulation and less important than acute effects. Significant changes of the single channel conductance due to regulatory or genetic changes could not be demonstrated. The predominant elements of acute ENaC regulation are the number of channels in the membrane (N) and their open probability (P_0) which indicates the ratio of time the channel is in the ñopenò as opposed to the ñclosedò conformation (Butterworth, 2010).

Only a very small portion of all ENaC proteins is located in the plasma membrane. The vast majority is located in trafficking vesicle pools (Hanwell et al., 2002). When introduced into the plasma-membrane ENaCs form near-silent channels, which require activation by proteolytic processing of the Ŭ- and ɔ-subunit to be fully functional (Carattino et al., 2008; Sheng et al., 2006).

Stimuli involved in ENaC regulation include hormones, especially aldosterone (Lee et al., 2008; Masilamani et al., 1999) and insulin (Blazer-Yost et al., 2003; Deng et al., 2012) as well as estrogen and progesterone (Gambling et al., 2004).

Also, anorganic chemicals regulate ENaC activity. Na^+ itself, for example, has a dual role on ENaC function. Intracellular Na^+ has been shown to reduce proteolytic activation of the channel by rendering its cleavage sites inaccessible to proteases by changing the conformation of the complex. This process happens relatively slow (within minutes) and is called ñfeedback inhibitionò. The physiologic function is to prevent the cells from Na^+ overload and thus cell swelling (Knight et al., 2008; Komwatana et al., 1996; Uchida and Clerici, 2002).

Extracellular Na^+ on the other hand triggers ñNa^+ self-inhibitionò. When the extracellular Na^+-concentration is increased rapidly, ENaC activity is impaired. In contrast to the feedback inhibition this response is happening within seconds, induced by a decrease of the open probability P_0. This process can not be explained by saturation of Na^+-transport, because increasing the Na^+-concentration stepwise does not result in a comparable inhibition (Fuchs et al., 1977). The molecular principle of ñNa^+ self-inhibitionò has been shown to involve a conformational change in the proximal part of the extracellular loop of Ŭ- and Ů-ENaC (Babini et al., 2003). Also other stimuli independent of Na^+, like acidity, seem to act on ENaC via the ñNa^+ self-inhibitionò as has been described for human ENaC (Collier and Snyder, 2009).

Oxygen tension is an important factor in the conversion of non-seletive to high-selective channels. Culture of ATII cells with only 5 % O_2 resulted in predominantly non-selective channels. However after 2 h with 95 % O_2 the majority of channels was highly selective (Jain et al., 2008).

Chlorine has also been reported to reduce ENaC expression in the membrane and its activity, in the mouse as well as in isolated ATII cells (Lazrak et al., 2012).

Further stimuli modulating ENaC activity are redox state (Downs et al., 2013; Helms et al., 2008) and physical factors such as shear stress (Fronius et al., 2010).

1.2.5. Signaling pathways

There are multiple signaling pathways that are known to regulate ENaC. Several steroids have been implicated in the translational regulation of ENaC, mediated probably via interaction with the *glucocorticoid responsive element* (GRE) located upstream of the promotor of Ŭ-ENaC (Dagenais et al., 2008). Recent studies show that translation of ENaC is modulated also by miRNA (Tamarapu Parthasarathy et al., 2012).

Interleukin-1ɓ (IL-1ɓ), an important cytokine in ARDS, was shown to reduce ENaC mRNA levels via the P38 *mitogen-activated protein kinase* (MAPK) (Roux et al., 2005). Another member of the MAP-kinase family, the *extracellular signal-regulated kinase* (ERK), is also a regulator of ENaC and has been associated with phosphorylation of ɓ- and ɔ- ENaC. This phosphorylation is likely to enhance interaction with the E3-ubiquitin-ligase *neural precursor cell expressed developmentally down-regulated protein 4-2* (Nedd4-2) (Yang et al., 2006), a protein that directly attaches the small molecule ubiquitin to specific target proteins, leading to endocytosis and subsequent degradation (Kabra et al., 2008). Ubiquitination of ENaC is a highly complex mechanism to differentially regulate protein stability in the cytoplasm and in the plasma membrane. Nedd4-2 is the most prominent E3-ligase known to regulate ENaC, but there is evidence for other E3-ligases that interact with ENaC (Downs et al., 2013). Upon activation Nedd4-2, preferably its domains WW2 and/or WW3 (Itani et al., 2009), binds to the highly conserved PY-motifs, located at the Cï terminus of all ENaC subunits, leading to ubiquitination of lysines located at the N-terminus of ENaC subunits, rendering proteins located in the cytosol susceptible for proteasomal degradation, whereas complexes containing Ŭɓɔ-ENaC located in the plasma membrane appear to be targeted for lysosomal degradation (Staub et al., 1997).

Another way of Nedd4-2 mediated ENaC regulation is a conformational change of the extracellular domain upon ubiquitination that impairs proteolytical processing, thus preventing activation of immature channels (Ruffieux-Daidie and Staub, 2010).

Several pathways seem to converge in ubiquitination. The important effector of aldosterone the *serum- and glucocorticoid regulated kinase* (SGK1) (Debonneville et al., 2001; Lee et al., 2008) but also *inhibitor of nuclear factor kappa-B kinase subunit ɓ* (IKKɓ) (Edinger et al., 2009) and the metabolic sensor *adenosine-monophosphate-activated kinase* (AMPK) (Almaça et al., 2009) phosphorylate Nedd4-2, disrupting its interaction with ENaC.

1.3. State of the art

Elevated CO_2 levels have been shown to reduce alveolar epithelial function independently of pH by downregulation of the Na^+,K^+-ATPase (Briva et al., 2007). Further studies elucidating the underlying pathway identified AMPK to be activated during hypercapnia and to be involved in endocytosis of the Na^+,K^+-ATPase (Vadász et al., 2008). The exact mechanism upstream of AMPK is incompletely understood, especially the sensor for CO_2 is still unknown.

AMPK phosphorylates Nedd4-2 thus promoting its translocation to the membrane where it ubiquitinates individual or all ENaC subunits (Almaça et al., 2009; Bhalla et al., 2006; Myerburg et al., 2010). Ubiquitinated channels are then retrieved from the membrane and degraded by either the lysosome or the proteasome (Lazrak et al., 2012; Malik et al., 2006).

A pharmacological study elucidating the role of several AMPK-activators on alveolar epithelial Na^+-transport provides evidence for a differential effect of AMPK on ENaC and the Na^+,K^+-ATPase (Woollhead et al., 2007). Specific modulation of ENaC and the Na^+,K^+-ATPase by AMPK could be relevant in the resolution of pulmonary edema.

Detection of ENaC proteins in the lung is difficult. Antibodies against endogenous proteins are poor and often recognize either the full length form or the cleaved form of Ŭ- and ɔ-ENaC (Boncoeur et al., 2009; Downs et al., 2013; Jain et al., 1999). Even if both forms are recognized, antibodies against each cleaved fragment produce inconclusive protein sizes (Albert et al., 2008). Many investigators, especially in the field of nephrology are working with overexpression of modified ENaC-subunits that can be recognized better than the endogenous proteins, but reliable systems for detection of ENaC protein in lung cells are not well established.

The aim of the present study was initially to decipher the effect of CO_2 on ENaC function according to the working hypothesis illustrated in **Figure 2**. Due to insufficiencies of the available systems a second aim was added later:

Establishment of a system to detect and immunoprecipitate immature and mature ENaC proteins in lung epithelial cells.

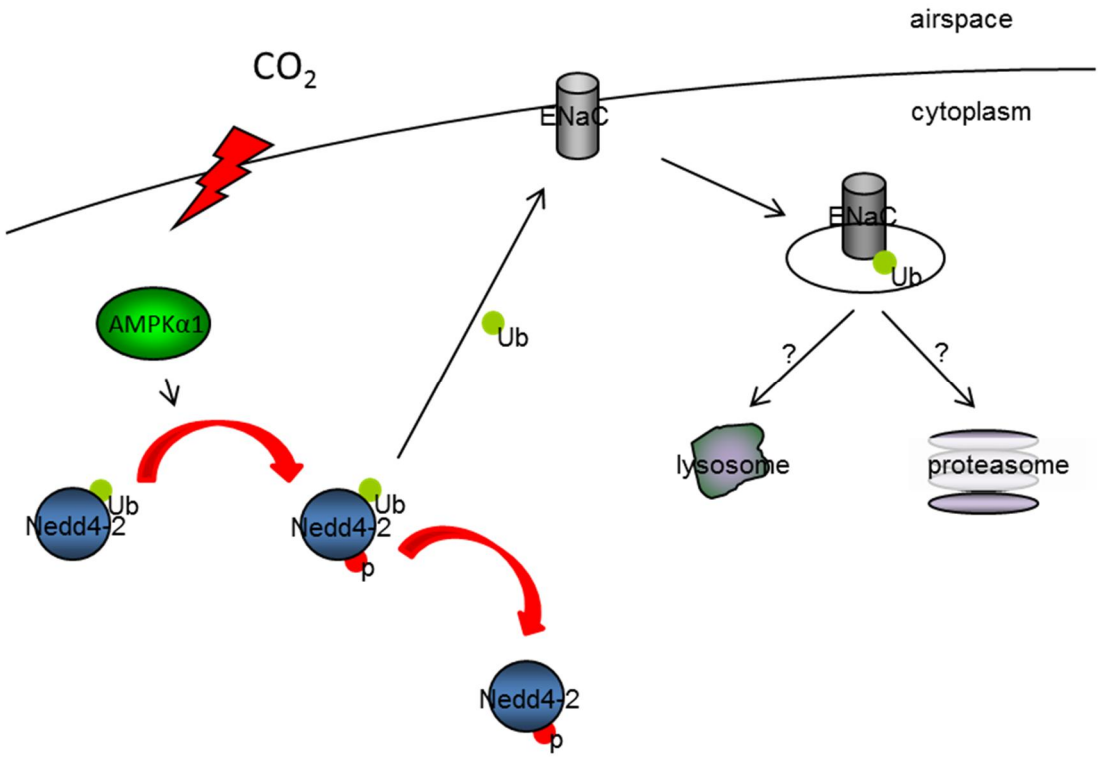

Figure 2 Proposed mechanism of CO_2 regulated endocytosis of ENaC

CO_2 is indirectly activating AMPKŭ1 which is phosphorylating Nedd4-2. Nedd4-2 attaches ubiquitin (Ub) to membrane bound ENaC to target it for endocytosis and subsequent degradation or trafficking back to the membrane.

2. Methods

2.1. Cell culture

2.1.1. Culture of A549 cells

A549 cells show characteristics of alveolar epithelial cells and can be transfected easily. Cells were grown in 100 mm cell culture dishes. The full medium contained DMEM (4.5 g/l glucose incl. stable L-glutamine) and 10 % [v/v] fetal bovine serum (FBS). No antibiotics were used and the cells were maintained in a humidified incubator at 37 °C, 5 % CO_2, 100 % relative humidity.

For treatment with high CO_2-levels the medium had to be modified to compensate for the influence of CO_2 on the pH. For that 3 ml of basal DMEM (4.5 g/l glucose incl. stable L-glutamine), 1 ml F12-supplement and 0.5 ml of Tris-solution (0.5 M, pH 7.3 or pH 10 for normocapnia and hypercapnia respectively) and the solutions incubated in 5 % respectively 18 % CO_2 cell culture incubators to achieve an identical pH of 7.4 and P_{O2} but a P_{CO2} in the medium of either 40 or 110 mmHg, as published previously (Briva et al., 2007; Vadász et al., 2008).

2.1.2. Transfection of A549 cells

For transfection of plasmid DNA 6 x 10^5 A549 cells were plated on 60 mm cell culture plates in 3 ml of full medium. The following day 12 µl Lipofectamine 2000 were diluted in 500 µl DMEM, incubated for 5 min, then 4 µg plasmid-DNA was added and the mixture incubated for 30 min. The transfection mixture was then directly added to the cells without aspiration of the medium. After transfection no media change was performed, since cytotoxicity was minimal and higher expression rates were obtained. Experiments were conducted 18-24 h after transfection.

Transfection with siRNA was performed using Lipofectamine RNAiMAX. 6 x 10^5 A549-cells were plated on a 60 mm cell culture dish in 2 ml DMEM. The next day cells were starved with preequilibrated DMEM (1.5 g/l glucose) without serum for 30 min. Per reaction, 17 µl siRNA and 17 µl Lipofectamine RNAiMAX were diluted in 250 µl OptiMEM medium each, mixed by pipetting and combined. After a 30 min incubation time, medium was aspirated from the cells and the 500 µl transfection solution applied to the cells. During a period of 4 h the cells were agitated every 15 minutes, before 1 ml of

OptiMEM was added. Cells were replated and transfected the next day with ENaC-plasmids as stated above in this paragraph.

2.1.3. Culture of H441 cells

To elucidate the effect of hypercapnia on epithelial Na^+-transport Ussing chamber experiments were conducted on H441 cells. H441 cells, in contrast to A549 cells, form polarized monolayers and are established as a model for investigation of Na^+-transport in alveolar epithelial cells (Albert et al., 2008; Brown et al., 2008; Ramminger et al., 2004).
The basal medium for subculturing H441 cells was RPMI 1640 incl. L-glutamine, 10 % [v/v] FBS, 100 IU/ml Penicillin, 100 µg/ml Streptomycin, 1 mM Na^+-Pyruvat, 5 µg/ml Insulin, 5 µg/ml Transferrin, 5 µg/ml Na^+-Selenit.
For functional measurements cells were seeded on snapwell-inserts with a growth area of 1 cm^2. The following day the medium on the apical side was aspirated so that the apical compartment was exposed to air. Furthermore the medium on the basolateral side was supplemented with 200 nM dexamethasone. Experiments were performed 5-7 days later with the medium replaced every two days.

2.1.4. Optimization of H441 cell transfection

Transfection of H441 cells by Lipofectamine 2000 is not efficient, so another system had to be used. A new method designed for primary cells and hard-to-transfect cell lines is Nucleofection, a modified electroporation technique. Basic principle is the formation of pores in the plasma membrane as well as in the nuclear envelope by specifically combining solutions with different ionic compositions with electrical impulses of different frequencies, durations and intensities. The best combination has to be established empirically for every cell-type.
Nucleofection was performed using a Lonza 4D-Nucleofector and preselected cell type-specific solutions. For optimizing Nucleofection of cells in suspension H441 cells were cultured for 24 h. Cells were then trypsinized, counted and the appropriate amount of cells (1.5×10^5 cells per reaction) centrifuged at 90 g for 10 min. The supernatant was discarded, the cells resuspended in Nucleofection mixture (20 µl reaction: 16.4 µl Solution SF, 3.6 µl of supplement + 0.4 µg pMaxGFP Vector) and transferred to the Nucleofection cuvette. Nucleofection was conducted in the X-Unit of the device. After Nucleofection 80 µl of prewarmed medium was added into the cuvette to resuspend the cells and 50, 25 and 12.5 µl of cell-suspension were plated in 150, 175 and 187.5 µl respectively of prewarmed

medium in a 96-well plate. 24 h after Nucleofection efficiency and viability were estimated and the best program selected.

2.1.5. Transfection of H441 cells

For transfection of H441 cells in suspension the 4D-Nucleofector System and the SF Cell Line 4D-Nucleofector X Kit was used.

Cells were plated such, that they reached not more than 50 % confluence 24 h later. The next day cells were washed with PBS, detached from the culture plate with trypsin, counted and the desired amount of cells (1 x 10^6 cells per reaction) was centrifuged at 90 g for 10 min. The supernatant was discarded and the cells were resuspended in nucleofection solution (82 µl solution SF, 18 µl supplement), combined with the desired amount of nucleic acid, e.g. 2 - 4 µg pMaxGFP Vector and transferred to the Nucleofection cuvette. The program used for Nucleofection was CM 138. Cells were then incubated at room temperature for 10 min, diluted in app. 300 µl of prewarmed medium and plated. For transwell supports and 60 mm cell culture dishes 1 x 10^6 cells were plated, 0.5 x 10^6 cells for 35 mm dishes. Analysis was conducted 24 - 48 h later.

2.1.6. Isolation of primary rat alveolar epithelial cells

Primary rat alveolar epithelial type II cells (ATII) were isolated as described previously (Buchäckert et al., 2012; Dobbs, 1990) and cultured in DMEM with 4.5 g/l glucose, 10 % [v/v] FBS and 100 IU/ml Penicillin, 100 µg/ml Streptomycin.

2.1.7. Establishment of ATII cell transfection

Transfection of ATII cells was performed by Nucleofection using a Lonza 4D-Nucleofector and preselected cell type-specific solutions as recently published (Grzesik et al., 2013). For optimizing Nucleofection of primary ATII cells in suspension, cells were cultured for 24 h. Cells were then trypsinized, counted and the appropriate amount of cells (1.5 x 10^5 cells per reaction) centrifuged at 90 g for 10 min. The supernatant was discarded, the cells resuspended in Nucleofection mixture (20 µl reaction: 16.4 µl Solution P1 or P3, 3.6 µl of supplement + 0.4 µg pMaxGFP Vector) and transferred to the Nucleofection cuvette. Nucleofection was conducted in the X-Unit of the device. After Nucleofection 80 µl of prewarmed medium was added into the cuvette to resuspend the cells and 50, 25 and 12.5 µl of cell-suspension were plated in 150, 175 and 187.5 µl respectively of prewarmed

medium in a 96-well plate. 24 h after Nucleofection efficiency and viability were estimated and the best program selected.
Further optimization revealed no loss of transfection efficiency, when using up to 3.5 x 10^6 cells per 100 µl reaction. Attempts to transfect freshly isolated cells resulted in significant cell death.

Some cell types that are cultured in high-calcium-medium (e.g. DMEM) require a recovery step after transfection to prevent an influx of calcium through the not yet closed pores in the plasma-membrane. For that step low-calcium-medium (e.g. RPMI 1640) is added directly to the Nucleofection cuvette and the cells are incubated at 37 °C for 10 minutes. This step proved not to be necessary for ATII cells. Also, removal of Nucleofection solution after transfection by diluting the cells in preequilibrated medium and subsequent centrifugation did not result in higher viability, nor transfection efficiency.

2.1.8. Final protocol for the Nucleofection of ATII cells

For the optimized protocol freshly isolated rat AT II cells were plated in 60 mm cell culture dishes to recover from the isolation. The next day cells were washed with PBS, detached from the culture plate with trypsin, counted and the desired amount of cells (3.5 x 10^6 cells per reaction) was centrifuged at 90 g for 10 min. The supernatant was discarded and the cells were resuspended in nucleofection solution (82 µl solution P3, 18 µl supplement), combined with the desired amount of nucleic acid, e.g. 3-5 µg pMaxGFP Vector and transferred to the Nucleofection cuvette. The program used for Nucleofection was EA-104. Cells were then incubated at room temperature for 10 min, diluted in app. 300 µl of prewarmed medium and plated. For transwell supports and 60 mm cell culture dishes 3.5 x 10^6 cells were plated, 2 x 10^6 cells for 35 mm dishes. Analysis was conducted 48 h later (day 3 after isolation).

2.1.9. Flow cytometry

For determination of transfection efficiency, cells were washed with PBS, trypsinized, centrifuged at 90 g and resuspended in FACS buffer (PBS without Ca^{2+} and Mg^{2+}, 7.4 % EDTA, 0.5 % FBS, pH 7.2). To evaluate viability, cells were stained with 7-AAD (1:10) and incubated for 5 min prior to FACS analysis which was conducted with a LSR Fortessa and analyzed by FACS Diva Software.

2.1.10. Fluorescence microscopy

GFP expression of transfected cells was visualized by fluorescence microscopy. Living cells were imaged in medium using a fluorescence microscope (Leica DMIL), a camera (Leica DFC 420C) and the software Leica application suite 330.

2.1.11. Cytotoxicity assay

Early cell death was evaluated by release of *lactate-dehydrogenase* (LDH) into the medium. Cells were transfected and plated on permeable supports as described above. The medium was collected at 4 h, replaced by fresh medium and collected again 24 h after transfection. The assay was performed as instructed by the manufacturer. Minimal cell death was measured in non treated cells, maximal cell death was determined by lysing cells with 1 % Triton X 100.

2.2. Ussing chamber measurements

Ussing chamber experiments were conducted on H441 cells. For those experiments cells were plated confluent on snapwell permeable supports. One day after plating, medium was removed from the apical side to culture the cells at liquid-air-interface and dexamethasone 200 nM was added to the medium. Measurements were conducted on day 7 - 9 after plating.

Experiments were performed using a custom built Ussing chamber setup. The electrical signal was recorded and amplified by a *voltage-clamp*-amplifier (custom built; Institut for animal physiology Gießen), converted from analog to digital by an AD/DA-converter (MacLab Interfaces) and recorded by a two-channel chart-strip recorder (Kipp & Zonen, *Netherlands*) plus recorded digitally using an Apple-PC, (Macintosh, Apple) and the software *Chart* (Version 3.6.3, *MacLab*). Electrical interference was neutralized with a 50 Hz filter that was included in the software. The relevant data where also noted manually.

The regular perfusion solution contained in mM: NaCl 130, KCl 2.7 KH_2PO_4 1.5, $MgCl_2$: 0.5, $CaCl_2$, D-glucose 10. Unless otherwise stated, 55 mM Tris base was added. For normocapnia (pCO_2 ~ 40 mm Hg) and hypercapnia (pCO_2 > 100 mm Hg) the solutions were continuously bubbled with 5 % CO_2, 21 % O_2, 74 % N_2 and 20 % CO_2, 21 % O_2, 59 % N_2 respectively and the pH adjusted accordingly to obtain a final pH of about 7.4.

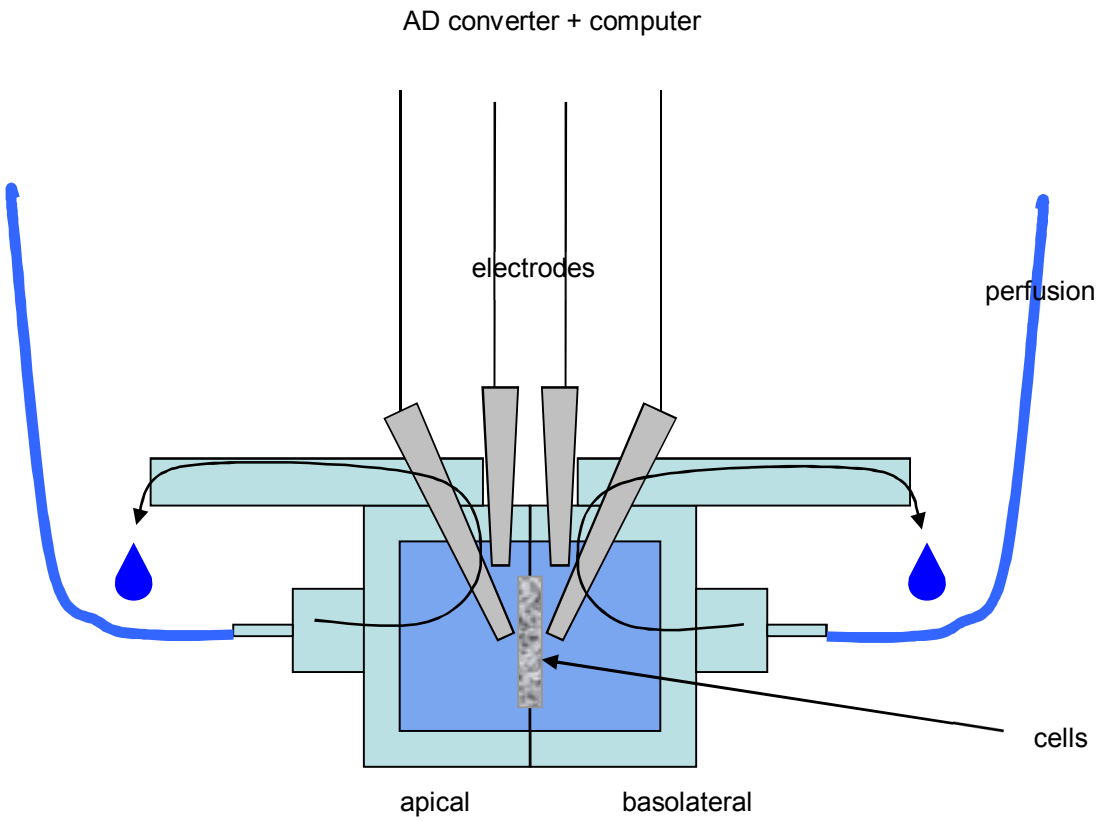

Figure 3 Scheme of the custom build Ussing chamber.

Both chambers of the setting were perfused seperately so it was possible to specifically target the apical or the basolateral compartment.

2.3. Real-time rtPCR

To study the expression of endogenous ENaC subunits on the mRNA level, real-time rtPCR experiments were performed. After incubating the cells in normo- versus hypercapnic conditions for 6 resp. 24 h, cells were lysed and mRNA isolated using the RNeasy-Kit according to the instructions supplied by the manufacturer. The mRNA was reverse transcribed (iScript cDNA Synthesis Kit (**Table 2**) and PCR performed with iTaqTM Sybr Green Supermix with ROX. The reaction composition is depicted in **Table 3**. The expression of the housekeeeping gene *hypoxanthin-phosphoribosyl-transferase* (HPRT) was used to normalize the data.

Calculation of data: $\Delta Ct = Ct_{housekeeping\ gene} - Ct_{target\ gene}$

$\Delta\Delta Ct = Ct_{CO2} - Ct_{control}$

Table 2 Composition cDNA synthesis (20 µl reaction)

component	volume
Reaction buffer (5x)	4 µl
reverse transcriptase	1 µl
RNA (1µg)	x µl
H_2O	to 20 µl

Table 3 Composition real-time PCR (25 µl reaction)

component	volume
iTaq Sybr Green Supermix with ROX	12.5 µl
cDNA (1:5 diluted)	2.0 µl
Primer forward	0.5 µl
Primer reverse	0.5 µl
H_2O	9.5 µl

Table 4 Real time PCR conditions

initial denaturation	95°C	2:00	min	
denaturation	95°C	1:15	sec	35 cycles
primer annealing + elongation	55°C	0:30	sec	
cool down	4°C	-		

Following primers were used for real-time PCR:

Table 5 Real-time PCR Primer

gene	primer	primer-sequence	reference-sequence
ŭENaC	hscnn1a_F	5`-acttcagctaccccgtcagc-3´	NM_001038
	hscnn1a_R	5`-gagcgtctgctctgtgatgc-3´	
ɓ ENaC	hscnn1b_F	5`-gcaccgtgaatggttctgag-3´	NM_000336.2
	hscnn1b_R	5`-cggatcatgtggtcttggaa-3´	
ŭ ENaC	hscnn1d_F	5`-cagcatccgagaggacgag-3´	NM_001130413.3
	hscnn1d_R	5`-aggagcaggtctccaccatc-3´	
ɔ ENaC	hscnn1g_F	5`-gctgcctactcgctccagat-3´	NM_001039
	hscnn1g_R	5`-ttcctggacaaaggctcgat-3´	
HPRT	HPRT_human_F	5`-cctggcgtcgtgattagtga-3´	NM_000194.2
	HPRT_human_R	5`-atggcctcccatctccttc-3´	

2.4. Generation of genetically modified ENaC-constructs

The expression levels of ENaC-subunits are generally low. Furthermore the majority of ENaC proteins is located in submembranous vesicles and in the endoplasmatic reticulum, making the detection of functional ENaC proteins in the plasmamembrane even more challenging (Hanwell et al., 2002). To enhance the expression ŭ, ɓ and ɔ-ENaC were cloned into expression vectors. The generated constructs were genetically modified: Epitope-tags were added to increase the recognition for commercially available antibodies. eYFP-ŭ-ENaC-Flag, ɓ-ENaC-V5, and Myc-ɔ-ENaC-HA were generated (see **Table 6**). ɓ-ENaC was the first vector generated and cloned from the human cellline A549 (see **2.1.1**). Later, ŭ- und ɔ-ENaC were cloned from previously generated plasmids (pTNT-Oocyte expression vector; (Fronius et al., 2010)) tagged with the respective epitope-tags and ligated into expression vectors.

Table 6 Cloning primers and genetic modifications

protein	primer	primer sequence	destination-vector	tag
ŭENaC	SCNN1A_for2	5`-catggaggggaacaagct-3ó		
	SCNN1A_rev2	5´-ccttggtgtgagaaacctctcc -3`		
ŭENaC	SCNN1A_for3	5`-gaattcaatggaggggaacaagctggagg-3ć	pE-eYFP	eYFP
	SCNN1A_rev	5´-ggatcc<u>cttgtcatcgtcatccttgtaat</u>cggg` cccccccagaggac-3`[1]		Flag
ɓ ENaC	SCNN1Bfor	5`-ctcggatccacatgcacgtgaagaagtacct-3`	pcDNA3.1V5/ Hyg	V5
	SCNN1Brev	5`-gcactcgaggatggcatcaccctcactgt-3`		
ɔ ENaC	SCNN1G_forHA	5`-aggcccgaattcatggcacccggagagaagat-3`	pCMV-HA-C	HA
	SCNN1G_revHA	5`-gtagccggtaccgagctcatccagcatctggg-3`		
	SCNN1G_formyc	5`-gagatcggatccaatggcacccggagagaagat-3`	pCMV-tag 3	Myc
	SCNN1G_revmyc	5`-ccccccctcgagttaagcgtaatctggaacat-3`		

[1] Highlighted is the sequence for the FLAG-epitope-tag that was added by PCR

2.4.1. Subunit-specific cloning procedure

2.4.1.1. β-ENaC

For the cloning of β-ENaC, mRNA was isolated from A549 cells and reverse transcribed into cDNA. Amplification of the coding sequence with the appropriate restriction sites attached was performed with Pfu-Ultra DNA polymerase. The sequence of the primers used is provided in **Table 6.** The composition of the PCR-mix is listed in **Table 7**, the cycler-conditions are given in
Table 8.

Table 7 PCR reaction β-ENaC (25 µl)

component	volume
H_2O	to 25.0 µl
buffer	2.5 µl
dNTP	0.4 µl
primer forward	0.5 µl
primer reverse	0.5 µl
cDNA	1.0 µl
Pfu DNA polymerase	1.0 µl

Table 8 PCR conditions for cloning of β-ENaC

initial denaturation	97°C	10:00	min	
denaturation	95°C	1:30	min	35 cycles
primer annealing	65°C	0:30	min	
elongation	72°C	4:00	min	
final elongation	72°C	10:00	min	
cool down	4°C	-		

The PCR-product was analyzed in a 1 % agarose-TAE-buffer gel and the fragment size compared to the expected size of the amplicon.
The PCR product was purified using the Wizard® SV Gel and PCR Clean-Up System. The product and the vector pcDNA3.1 V5/Hyg were then digested with XhoI und BamHI at

37°C over night (**Table 9**) and again purified with the PCR Clean-up System. Complete digestion was verified by electrophoretical determination of the fragment size.

Table 9 Restriction digestion for β-ENaC

component	volume
H_2O + DNA	40.0 µl
enzymebuffer B 10x	5.4 µl
BSA acetylated	5.4 µl
XhoI	1.4 µl
BamHI	1.4 µl

The digested vector and a two-fold excess of insert were ligated over night at 4°C with T4 ligase. As a negativ control the ligation was performed without insert.

Table 10 Ligation reaction

component	volume
H_2O	to 20 µl
buffer 10x	2 µl
vector	100 ng
insert	140 ng
T4 ligase (3 U/µl)	1 µl

2.4.1.2. α-ENaC

Since the Ŭ-subunit of ENaC undergoes proteolytical processing during maturation, the two major fragments were modified to contain individual epitope tags. The primers needed for the modification were relatively long with a brief overlap at the coding region of the protein, resulting in special conditions for the PCR. Increased difficulties arose from the sequence of the human Ŭ-ENaC being rich in the nucleotides guanine and cytosine, aggrevating the cloning process.

Therefore the plasmid was cloned in two steps. First the coding region plus some overhang was amplified from a preexisting plasmid (pTNT-Oocyte expression vector (Fronius et al., 2010)) with the newly distributed Q5 polymerase which has a higher fidelity and acuracy compared to the Pfu-polymerase used to clone the ɓ-subunit. The primers were designed to only amplify the coding region and some overhang. The PCR product of this reaction was

then used as a template for the next reaction, that was performed with primers that included restriction sites and the tag to reduce non-specific annealing. The destination vector pEYFP-C1 contained the epitope-tag eYFP at the N-terminus. To add another tag at the C-terminus of the fusion protein the sequence for the FLAG-tag (5´-gat tac aag gat gac gat gac aag-3`) was incorporated in the reverse-primer between the coding sequence and the stop codon (see **Table 6** highlighted).

Table 11 PCR reaction for α-ENaC (25 µl)

component	volume
H_2O	15.75 µl
buffer	5.00 µl
dNTP	0.50 µl
primer forward	1.25 µl
primer reverse	1.25 µl
cDNA	1.00 µl
Q5 DNA polymerase	0.25 µl

Table 12 First PCR condition for cloning of α-ENaC

initial denaturation	95°C	0:30	min	
denaturation	95°C	0:10	min	35 cycles
primer annealing	65°C	0:30	min	
elongation	72°C	2:10	min	
cool down	4°C	-		

Table 13 Second PCR condition for cloning of α-ENaC

initial denaturation	95°C	0:30	min	
denaturation	95°C	0:10	min	35 cycles
primer annealing + elongation	72°C	2:10	min	
cool down	4°C	-		

The PCR product and the vector were purified and digested with fast-digest restriction enzymes at 37°C for 15 minutes (see **Table 14**) and purified again for ligation.

Table 14 Restriction digestion α-ENaC (40 µl volume)

component	volume
H_2O + DNA	32 µl
buffer FDgreen 10x	4 µl
EcoRI	2 µl
BamHI	2 µl

For the ligation the insert and vector were mixed at a molar ratio of 3:1 and ligated with the T4 ligase kit. As a negative control ligations without vector were performed.

Table 15 Ligation for α-ENaC T4 ligase kit (20 µl)

component	volume
H_2O	to 20 µl
buffer 10x	2 µl
vector	100 ng
insert	140 ng
T4 ligase (3 U/µl)	1 µl

2.4.1.3. γ-ENaC

Cloning of the double-tagged ɔ-ENaC was also performed in two steps: The coding sequence was first amplified, ligated in the vector pCMV-HA-C, containing the c-terminal HA-tag and transformed into bacteria (see **2.4.2**). Successful transformation was controlled by colony-PCR with the primer-pair SCNN1G_for/revmyc. This step provided two benefits: Since one primer was designed to align to a region on the first destination-vector the stringency for the screening was increased. Additionally, the sequence of the plasmid containing the HA-tag was included in the PCR-fragment, so that the PCR product could not only be visualized electrophoretically, but also purified and ligated directly into the second vector pCMV-tag 3 that added a N-terminal Myc-tag. Both PCR-reactions were performed with the conditions given in **Table 11** and **Table 13**. Restriction digestion was performed according to **Table 14**, ligation as described in **Table 15**.

2.4.1.4. Site directed mutagenesis α-ENaC

Two *single nucleotide polymorphisms* (SNP) were included in the original Ŭ-ENaC plasmid that caused a change in the aminoacid sequence (A334T and T663A) compared to the reference sequence NM_001038. Although they were reported earlier (rs11542844 and rs2228576), site directed mutagenesis was performed to eliminate possible effects on the biology of the protein.

Table 16 Primers for site directed mutagenesis

primer	primer sequence
A2365G_for	5`-gtccctgatgctgcgcgcagagcagaatgacttc-3`
A2365G_rev	5`-gaagtcattctgctctgcgcgcagcatcagggac-3`
G3352A_for	5`-ggggccagttcctccacctgtcctctggg-3`
G3352A_rev	5-cccagaggacaggtggaggaactggcccc-3`

The mutagenesis was performed with the QuikChange Site-Directed Mutagenesis Kit. The reaction conditions are described in **Table 17** and **Table 18**.

Table 17 QuikChange site directed mutagenesis reaction

component	volume
H_2O	to 25.0 µl
buffer	2.5 µl
dNTP	0.5 µl
primer forward	62.5 ng
primer reverse	62.5 ng
Pfu Turbo DNA polymerase (2.5 U/µl)	1.0 µl
template (~ 20 µg plasmid)	1.0 µl

Table 18 QuikChange site directed mutagenesis thermal profile

initial denaturation	95°C	0:30	min	
denaturation	95°C	0:30	min	16 cycles
primer annealing	55°C	1:00	min	
elongation	68°C	7:00	min	
cool down	4°C	-		

The parental, non modified vector was digested with 1 µl DpnI at 37°C for 1 h and the reaction with now only the modified plasmids directly transformed into XL1-Blue supercompetent cells, supplied with the QuikChange Kit. For that the cells were thawed on ice and a 25 µl aliquot transferred to a prechilled 14 ml polypropylene tube. One µl of the digested DNA was added and the bacteria incubated on ice for 30 minutes, before they were heat-shocked at 42°C for 45 seconds and placed back on ice for 2 minutes. To promote bacterial proliferation 250 µl prewarmed NZY^+-broth medium were added and the bacteria incubated at 37°C for 1 hour with shaking at 225-250 rpm. Half of the bacterial suspension was then plated on LB-Agar plates as described in the next chapter (**2.4.2**).

2.4.2. Transformation

To amplify the generated plasmids for endotoxin free transfection in alveolar epithelial cell lines the plasmids were transformed into *E. coli JM-109* by heat-shock.

Bacteria were thawed on ice and 50 µl of the suspension were transferred to a precooled reaction tube. Two to 5 µl of the ligation were added and the mixture incubated for 10 min on ice. Bacteria were then heat-shocked for 45-50 seconds at 42°C and immediately incubated on ice for another 2 minutes. Now, 450 µl SOC-medium were added and the bacteria incubated for 1 hour at 37°C, until 100 µl were plated on LB-agar plates containing the appropriate antibiotic (pCMV3A und pE-eYFP: kanamycin; pcDNA3.1: ampicillin) to select for successfully transformed bacteria.

2.4.3. Plasmid preparation

The bacterial colonies that were obtained had to be screened for containing the right, non-modified plasmid. Small liquid cultures were prepared in 15 ml polypropylene tubes by inoculating 5 ml of LB-medium with bacteria picked directly from the agar-plate with a pipette tip, incubated over night at 37°C. Colony PCR (see **Table 19**) was performed to test for integration of the right insert with the primers used for cloning. The liquid culture was stored at 4°C to be able to inoculate a large scale bacterial culture and to prepare glycerol stocks (1:1 [v/v], stored at -80°C) for further amplification. The PCR-products were electrophoretically analyzed for the right size. Plasmids of promising clones were isolated with the Qiaprep Spin Miniprep Kit from the small liquid cultures exactly as instructed by the manufacturer and sent to sequencing for validation (Seqlab, Göttingen, Germany).

Table 19 PCR reaction colony-PCR (20 µl)

Component	volume
H_2O	14.4 µl
buffer	2.0 µl
dNTP	0.4 µl
primer forward	0.5 µl
primer revers	0.5 µl
bacterial culture	2.0 µl
Taq DNA Polymerase	0.2 µl

To generate large amounts of plasmids that are needed for transfections 100 ml LB-medium containing the appropriate antibiotic were inoculated with bacterial culture either from the stored mini-culture or from the glycerol stock and incubated over night at 37°C with shaking. Plasmids were isolated with the Qiagen Plasmid Maxi-Kit exactly as instructed by the manufacturer. Plasmid DNA was disolved in 200-300 µl TE-buffer, the concentration measured with a NanoDrop photometer and stored at -20°C.

2.5. Western-Immuno-Blotting

Quantification of protein levels was done using the western-immunoblot technique. Cells were treated as indicated and washed three times with ice-cold PBS incl. Ca^{2+} and Mg^{2+}. After complete removal of PBS cells were lysed with 300 µl of lysis buffer (mRIPA: 50 mM Tris pH 8.0; 150 mM NaCl; 1 % Igepal; 1 % Na^{+}-deoxycholate) with protease inhibitor cocktail (complete; 40 µl/ml) on ice for 10 min. The cell lysate was collected and cleared by centrifugation (10,000 rpm/10 min). Protein concentration was determined with the Quick-Start Bradford-Assay. Equal protein amounts were diluted in 2 x sample-buffer, denatured under agitation (97 °C, 350 rpm; 7-10 min) and separated electrophoretically in a 10 % acrylamide-gel using standard techniques. Proteins were then transferred to a nitrocellulose membrane with a semi-dry transfer chamber (45-60 minutes, Biorad) and unspecific binding sites blocked with 5 % [m/v] skim milk powder in TBS-T for 1 hour. After removal of blocking buffer the membranes were incubated in the primary antibodies at 4°C over night (see **Table 20**).

Table 20 Antibodies for Western-Blotting

antibody	buffer	dilution	species	company
V5	TBST + 5 % BSA	1:2000	mouse	Invitrogen
E-cadherin	TBST	1:400	rabbit	Santa Cruz
Actin	TBST	1:2000	rabbit	Sigma
GFP	TBST	1:1000	mouse	Roche
HA	TBST	1:1000	mouse	Covance
Myc	TBST	1:2000	mouse	Invitrogen
Nedd4-2	TBST	1:1000	rabbit	Santa Cruz
Flag M2	TBST	1:1000	mouse	Sigma
tGFP	TBST	1:5000	rabbit	Evrogen

The unbound primary antibodies were removed by washing the membrane in TBS-T three times for 10 minutes. Membranes were then incubated with the appropriate horse-raddish peroxidase linked secondary antibodies (rabbit anti-mouse IgG 1:5000; goat anti-rabbit IgG 1:2000). Excess antibody was removed again by washing the membrane as stated above, drained and incubated with chemiluminescent substrate (SuperSignal West Pico). The signal was quantified by exposing an autoradiography film (BioMax MR or Amersham Hyperfilm ECL) that was developed in a Curix 60 developer. Films were

scanned with a CanoScan LIDE 90 and densitometry was performed with ImageJ software (NIH).

In some cases the signal intensity was too low to be detected by the standard protocol. In these cases the concentration of the secondary antibody was reduced to 1:50,000-100,000 and the membrane incubated with the SuperSignal West Femto substrate to obtain maximal detection sensitivity.

2.6. Biotin-Streptavidin-Pulldown

Discrimination between the total cellular amount of ENaC and the functional fraction located in the plasma-membrane was carried out with biotin-streptavidin-pulldown. The underlying principle is the conjugation of a modified, membrane impermeable biotin to lysines located in the extracellular domains of membrane proteins and the subsequent pulldown with immobilized streptavidin that binds to biotin with high affinity (Gottardi et al., 1995).

Briefly, cells were rinsed with PBS incl. Ca^{2+} and Mg^{2+} and incubated on ice with EZ-Link Sulpho-NHS-LC-biotin-solution (1 mg/ml in PBS) for 20 min. To quench unbound biotin cells were washed three times for 10 minutes with PBS containing 100 mM glycine. After a final washing with PBS cells were lysed as described in chapter 2.5. For each experiment equal amounts of protein (150-1000 µg) were incubated with 60-100 µl streptavidin-agarosebeads at 4 °C over night in a rotator with the volume adjusted with mRIPA-buffer to obtain equal protein concentrations.

The following day the beads were washed with the solutions indicated below to eliminate unbound proteins and proteins that were bound unspecifically. Washing solutions were applied, the tube inverted a couple of times, beads collected at the bottom of the tube by centrifugation in a mini centrifuge and the supernatant aspirated almost completely after each step.

1 x solution A: 150 mM NaCl, 50 mM Tris pH 7.4, 5 mM EDTA

2 x solution B: 500 mM NaCl, 50 mM Tris pH 7.4, 5 mM EDTA

3 x solution C: 500 mM NaCl, 20 mM Tris pH 7.4, 0.2 % BSA [m/v]

1 x solution Tris: 10 mM Tris, pH 7.4

Finally the last washing solution was aspirated completely, sample buffer added and the samples were denatured at 99°C for 8-10 minutes. Analysis was performed as described above (chapter **2.5**). To prove that changes were not caused by varying transfection

efficiencies, total cell lysate of every sample was subjected to western blotting without pulldown.

2.7. Pulse-chase-experiments

To determine the stability of ENaC subunits located membrane, cells were biotinylated as stated above. After quenching the unreacted biotin with glycine cells were not yet lysed. Instead, preequilibrated medium was applied and cells put back in the cell culture incubator for up to 6 hours. After different time points the cells were washed with PBS, lysed with m-RIPA buffer supplemented with MG-132 (10 µM) and processed as described in chapter **2.6**.

2.8. Immunoprecipitation of detergent insoluble fraction of ENaC

The cell surface expression and composition of the ENaC-complexes are strongly dependent on the celltype and the underlying culture conditions. Especially for kidney cell lines it has been reported, that the subunits aggregate to complexes that are insoluble in several non-ionic detergents (Prince and Welsh, 1998). To test whether this also applies to alveolar epithelial cell lines the detergent soluble and insoluble fractions were analysed.

A549 and H441 cells were transfected and cultured for 24-48 h in the presence of amiloride (10 µM) to prevent cell swelling when coexpressing all three ENaC-subunits. Next, cells were rinsed three times with PBS containing Ca^{2+} and Mg^{2+} before cells were lysed in Tris-buffered saline (TBS) containing 1% Triton X-100 [v/v] and protease inhibitors (complete, 40 µl/ml). The insoluble fraction was pelleted by centrifugation 16,000 g for 10 minutes at 4 °C. Supernatant was collected in another tube and the pellet lysed in 100 µl of solubilization-buffer (50 mM Tris (pH 7.4); 2 % SDS [w/v]; 1 % β-mercaptoethanol [v/v]; 1 mM EDTA) at 90°C for 5 min. After heating the samples were diluted in 1 ml TBS containing 1 % Triton X-100. ENaC subunits were immunoprecipitated from both fractions with subunit specific antibodies (FLAG M2, 0.5 µg/reaction; GFP, 2 µl/reaction) and 100 µl protein A/G beads at 4°C over night.
Samples were finally washed three times with TBS incl. 1 % Triton X-100, denatured in sample buffer and further processed as described in chapter **2.5**.

2.9. Statistical analysis and graphical illustration

Data are presented as mean ± SEM, if not described otherwise. Statistical comparison between two groups was done using an unpaired *Student`s t-test.* Multiple data sets were compared by ANOVA and subsequent post hoc analysis. GraphPad prism 6 (GraphPad software, San Diego, CA) was used for the analysis and data presentation. Data obtained from Ussing chamber experiments were visualized with FreeHand 10.

2.10. Materials

Table 21 Electronic devices

4D-Nucleofector System	Lonza, Köln, Germany
BioPhotometer	Biorad, München, Germany
Developer Curix 60	Agfa, Mortsel, Belgium
Electrophoresis system	Biorad, München, Germany
Galaxy MiniStar	VWR, Bruchsal, Germany
Hera Cell 150 incubator	Thermo Scientific, Dreieich
Heraeus Fresco 17 thermo centrifuge	Thermo Scientific, Dreieich
KNF Laboport Pumpe	KNF Freiburg, Germany
Magnetstirrer MR 3002	Heidolph, Schwabach, Germany
Mettler H20T precicion scale	Mettler Toledo, Gießen, Germany
Milli-Q water purification	Millipore, Schwalbach, Germany
Mini-PROTEAN Tetra Cell	Biorad, München, Germany
Msc-Advantage	Thermo Scientific, Dreieich, Germany
NanoDrop (ND-1000)	Kisker-Biotech, Steinfurt
Neubauer counting chamber	Labor Optik, Friedrichsdorf, Germany
PB303 DeltaRange scale	Mettler Toledo, Gießen, Germany
pH-Meter 766 Calimatic	Knick, Berlin, Germany
pipettes	Gilson, Limburg-Offheim/Biohit, Rosbach, Germany
Pipetus	Hirschmann, Eberstadt, Germany
Polymax 1040 Orbitalshaker	Heidolph, Schwabach, Germany
PowerPac Basic	Biorad, München, Germany
Stratagene MX 3000P	Stratagene, Waldbronn, Germany
Thermocycler Biometra T Personal	Biometra GmbH, Göttingen, Germany
Thermomix ME waterbath	B.Braun Biotech, Melsungen, Germany
Thermomoxer comfort	Eppendorf, Hamburg, Germany
Transblot SD Semi-Dry Transfer Cell	Biorad, München, Germany
VV3 vortex	VWR, Darmstadt, Germany

Table 22 Reagents

β-mercaptoethanol	Sigma-Aldrich, Steinheim, Germany
2-propanol	Merck, Darmstadt, Germany
7-AAD	Invitrogen, Darmstadt, Germany
A549 cells	LGC, Wesel, Germany
Agarose	Fermentas, St. Leon-Rot, Germany
Amersham Hyperfilm ECL	GE life sciences, Freiburg, Germany
Ammoniumpersulfat (APS)	Promega, Mannheim, Germany
Ampicillin	Sigma-Aldrich, Steinheim Germany
BamHI	Fermentas, St. Leon-Rot, Germany
BioMax MR autoradiography film	Kodak (distributed Sigma-Aldrich)
Bovine serum albumin (BSA)	Sigma-Aldrich, Steinheim, Germany
Bromphenolblue	Merck, Darmstadt, Germany
Complete Protease Inhibitor	Roche, Basel, Switzerland
Cytotoxicity Detection Kit (LDH)	Roche, Basel, Switzerland (#11644793001)
Dexamethasone	Sigma-Aldrich, Steinheim, Germany
DMEM 1.5 g/l glucose, stable L-glutamine	PAA, Cölbe, Germany
DMEM 4.5 g/l glucose, stable L-glutamine	PAA, Cölbe, Germany
DNAse/RNAse free water	Gibco, Darmstadt, Germany
DPBS with Ca^{2+} and Mg^{2+}	PAA, Cölbe, Germany
DPBS without Ca^{2+} and Mg^{2+}	PAA, Cölbe, Germany
E. coli JM 109	Promega, Mannheim, Germany
EcoRI	Fermentas, St. Leon-Rot, Germany
Ethanol 70 %, 96 % and 100 %	Otto Fischer GmbH, Saarbrücken, Germany
Ethylene-diamin-tetraacetic-acid (EDTA)	Sigma-Aldrich, Steinheim, Germany
EZ-linked-sulpho-NHS-LC-biotin	Thermo Scientific, Dreieich, Germany
F12 supplement solution	Gibco, Darmstadt, Germany
Filter paper	Biorad, München, Germany
Glycerol	Sigma-Aldrich, Steinheim, Germany
Glycine	Sigma-Aldrich, Steinheim, Germany
Goat anti-rabbit IgG	Cell signaling, Frankfurt am Main, Germany
H441 cells	LGC, Wesel, Germany
HCl	Carl Roth, Karlsruhe, Germany
Igepal	Sigma-Aldrich, Steinheim, Germany
iScript cDNA Synthesis Kit	Biorad, München, Germany
iTaq Sybr Green Supermix with ROX	Biorad, München, Germany
ITS	Sigma-Aldrich, Steinheim, Germany
Kanamycin	Sigma-Aldrich, Steinheim, Germany
KCl	Merck, Darmstadt, Germany

KH_2PO_4	Merck, Darmstadt, Germany
LB agar	Invitrogen, Darmstadt, Germany
LB-medium	Invitrogen, Darmstadt, Germany
Lipofectamine 2000	Invitrogen, Darmstadt, Germany
Lipofectamine RNAiMAX	Invitrogen, Darmstadt, Germany
Methanol	Sigma-Aldrich, Steinheim, Germany
Na^+-deoxycholate	Sigma-Aldrich, Steinheim, Germany
Na^+-Pyruvat	Sigma-Aldrich, Steinheim, Germany
Na^+-Selenit	Sigma-Aldrich, Steinheim, Germany
Na_2HPO_4	Merck, Darmstadt, Germany
Na_3VO_4	Sigma-Aldrich, Steinheim, Germany
NaCl	Carl Roth, Karlsruhe, Germany
$NaHCO_3$	Merck, Darmstadt, Germany
NaN_3	Carl Roth, Karlsruhe, Germany
NaOH	Carl Roth, Karlsruhe,Germany
Natriumdodecylsulfat (SDS)	Promega, Mannheim, Germany
Opti-MEM	Gibco, Darmstadt, Germany
P3 Primary Cell 4D-Nucleofector X Kit	Lonza, Köln, Germany
pcDNA3.1V5/Hyg	Invitrogen, Darmstadt, Germany
pCMV-HA-C	Clontech, Saint-Germain-en-Laye, France
pCMV-tag 3	Clontech, Saint-Germain-en-Laye, France
Penicillin/Streptomycin-mixture	PAA, Cölbe, Germany
Pfu Ultra DNA polymerase	Agilent, Böblingen, Germany
Polypropylene reaction tube 14 ml	BD Falcon, Heidelberg, Germany
Primer	Metabion, Martinsried, Germany
Protein A/G agarose beads	Santa Cruz, Heidelberg, Germany
Q5 DNA polymerase	New England Biolabs, Frankfurt am Main, Germany
Qiagen Plasmid Maxi-Kit	Qiagen, Hilden, Germany
Quick-Start Bradford solution	Biorad, München, Germany
QuikChange Site-Directed Mutagenesis Kit	Agilent, Böblingen Germany
Rabbit anti-mouse IgG	Thermo Scientific, Dreieich, Germany
RNeasy-Kit	Qiagen, Hilden, Germany
RPMI 1640	Gibco, Darmstadt, Germany
SafeSeal PCR reaction tubes 0.5 und 1.5 ml	Sarstedt, Nümbrecht, Germany
SF Cell Line 4D-Nucleofector X Kit	Lonza, Köln, Germany
Snapwell permeable supports #3801	Corning, (Sigma-Aldrich, Steinheim, Germany)
SOC Medium	Invitrogen, Darmstadt, Germany
Streptavidin-agarose beads	Thermo Scientific, Dreieich, Germany
SuperSignal West Femto substrate	Pierce, Bonn, Germany

SuperSignal West Pico substrate	Pierce, Bonn, Germany
SYBR Safe	Invitrogen, Darmstadt, Germany
T4 DNA Ligase	Promega, Mannheim, Germany
Tetramethylethylendiamin (TEMED)	Carl Roth, Karlsruhe, Germany
Transwell supports #353090	BD Falcon, Heidelberg, Germany
Tris Base	Sigma-Aldrich, Steinheim, Germany
Triton-X 100	Sigma-Aldrich, Steinheim, Germany
Trypsin/EDTA	PAN, Aidenbach, Germany
Tween 20	Sigma-Aldrich, Steinheim Germany
Wizard SV Gel and PCR Clean-Up System	Promega, Mannheim, Germany

Table 23 Buffers

Running buffer westernblot 1 l		
30	g	Tris
144	g	Glycin
100	ml	SDS (10 %)
Adjusted with millipore water to 1 l		
Transfer buffer 1 l		
2.45	g	Tris
12.20	g	Glycin
20.00	%	Methanol [vol/vol]
Adjusted with millipore water to 1 l		
Washing buffer Tris buffered saline TBS-T pH 7.6; 1 l		
1.00	ml	Tween 20
2.42	g	Tris
8.00	g	NaCl
Adjusted with millipore water to 1 l, pH corrected to 7.6		

Sample buffer 2 x; 50 ml			**10 x**	
5	ml	Tris 1 M; pH 6.8	6.25 ml	Tris 1 M; pH 6.8
20	ml	SDS (10 %)	2.50 ml	SDS (20 %)
10	ml	Glycerol	5.00 ml	Glycerol (99 %)
		Bromphenol blue		Bromphenol blue
Adjusted with millipore water to 50 ml				
Stripping buffer 25 ml				
2.5	ml	Glycin 1 M		
22.5	ml	H_2O		
250	µl	HCl (37 %)		
Incubation for 1 h at room temperature with agitation				
Blocking buffer				
5	g	Skim milk powder		
100	ml	Washing buffer		

m-RIPA lysis buffer 100 ml

10	ml	Tris 0.5 M; pH 8
3	ml	NaCl 5 M
1	ml	Igepal (NP-40 substitute)
1	g	Na^+-Dexycholat

Adjusted with millipore water to 100 ml

Tris acetic acid EDTA buffer (TAE), DNA electrophoresis 1 l

4.8	g	Tris
57.0	ml	Acetic acid
100.0	ml	0.5 M EDTA pH 8

Adjusted with millipore water to 1 l, pH 8

3. Results

3.1. Functional Ussing chamber measurements

3.1.1. pH changes of the buffer have no influence on alveolar Na^+-transport

To elucidate the impact of hypercapnia on alveolar Na^+-transport, Ussing chamber experiments were performed. This technique measures the electrogenic transport of ions through flat tissue like bladder, frog lung, and skin or through artificial cell-monolayer. The electrical current detected (*short circuit current* (I_{sc})) is the sum of all ion transport processes. Applying pharmacological inhibitors specific for individual ion transporters or channels makes it possible to fractionate the I_{sc} into different elements. Common inhibitors used to study Na^+-transport are amiloride, that blocks epithelial Na^+-channels and ouabain, which inhibits the Na^+,K^+-ATPase.

Due to the effect of CO_2 on the pH of the buffer, all solutions were buffered with Tris to compensate for changes of pH, when bubbled with CO_2-containing gas-mixtures. Protons respectively acidification have been shown to regulate ENaC (Awayda et al., 2000; Collier and Snyder, 2009), so the first set of experiments was performed to show that the slight changes of pH caused by reperfusion of the solutions that were expected in this open system did not alter the amiloride-sensitive current I_{Ami}. A drop of the pH from 7.4 to 7.2 and an increase from 7.2 to 7.6 did not result in a significant change of I_{Ami} (**Figure 4**). Controls received a constant pH buffer and time-matched amiloride applications.

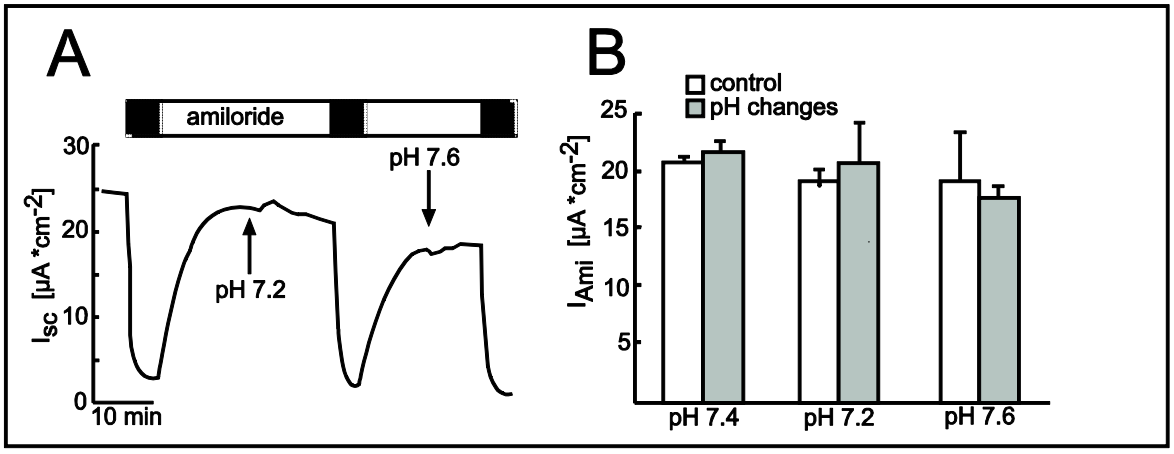

Figure 4 Amiloride-sensitive current during pH variations

The amiloride-sensitive current (I_{Ami}) of polarized H441 cell monolayers was measured during different acidities of the Ringerós solution (pH: 7.2; 7.4; 7.6) in voltage clamp mode. Controls were perfused with Ringerós solution with a constant pH of 7.4 and received time-matched amiloride applications (bars show mean ± SEM; n = 4; *: $P < 0.05$).

3.1.2. Hypercapnia reduces total I_{Na}

Due to the complexity of this Ussing chamber-setting with every solution bubbled separately, hypercapnia could only be applied at one compartment at a time. When hypercapnic solution was administered at the apical compartment for 20 minutes, a significant decrease of I_{Ami} was detected (**Figure 5**) that was absent when administered at the basolateral compartment (**Figure 6**).

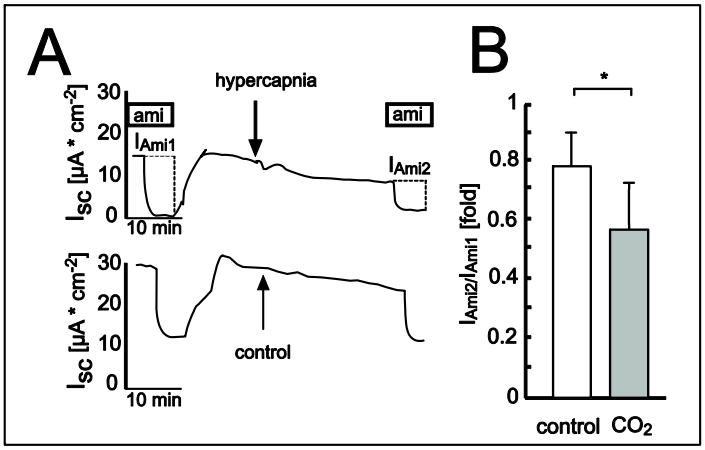

Figure 5 Apical application of hypercapnic solution

H441 cells were exposed to normocapnic and hypercapnic Ringerós solution and the I_{Ami} measured before and after 20 min (ami: amiloride 10 µM). Hypercapnic solution was administrated only from the apical side (graphs show mean ± SEM; n = 4; *: $P < 0.05$).

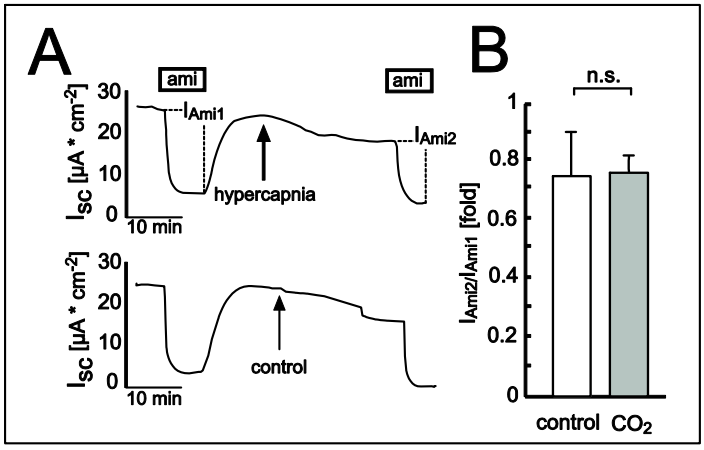

Figure 6 Basolateral application of hypercapnic solution

H441 cells were exposed to normocapnic and hypercapnic Ringerós solution and the I_{Ami} measured before and after 20 min (ami: amiloride 10 µM). Hypercapnic solution was administrated only from the basolateral side (graphs show mean ± SEM; n = 4; *: $P < 0.05$).

3.1.3. Membrane-permeabilization experiments

The epithelial Na^+-transport is mainly the product of the activity of the Na^+,K^+-ATPase located in the basolateral membrane of polarized epithelial cells and the conductance of the Na^+-channels, situated in the apical membrane. To locate the element(s) affected by hypercapnia, permeabilization studies were performed. To target only the basolateral membrane, all amiloride-sensitive channels were blocked, the apical membrane permeabilized by the antimycotic nystatin and the ouabain-sensitive current I_{Oua} measured after 20 min hypercapnia.

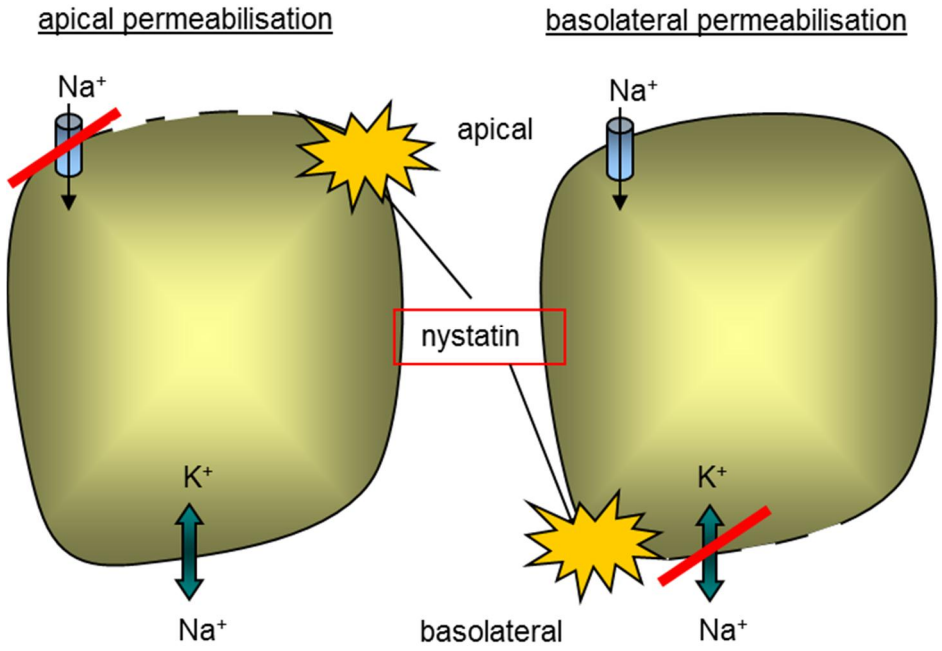

Figure 7 Principle of apical and basolateral membrane permeabilization

During apical permeabilization, Na^+-channels are inhibited by amiloride and the apical membrane is permeabilized by nystatin, enabeling to directly measure the activity of the Na^+,K^+-ATPase, located in the basolateral membrane. During basolateral membrane permeabilization, the Na^+,K^+-ATPase is inhibited by ouabain and the basolateral membrane permeabilized by nystatin. Since the Na^+,K^+-ATPase usually creates the Na^+-gradient, but is now deactivated, an artificial Na^+-gradient has to be generated by the investigator.

During apical permeabilization a large decrease in I_{Oua} was detected indicating a strong inhibition of the Na^+,K^+-ATPase during hypercapnia (**Figure 8**). This is in line with previous findings (Briva et al., 2007; Vadász et al., 2008, 2012).

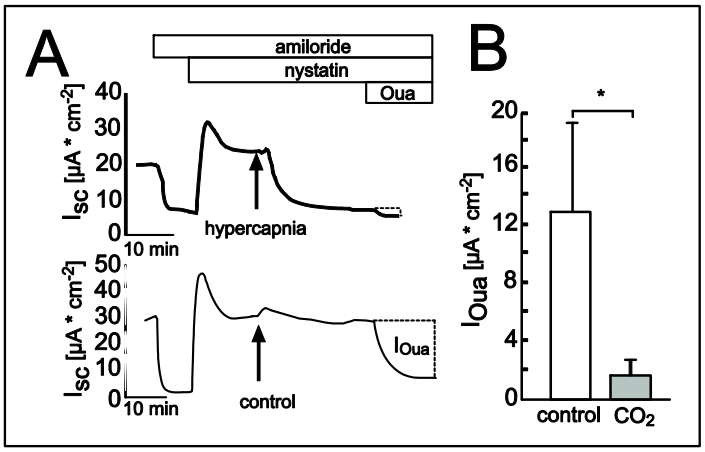

Figure 8 Ouabain-sensitive Na^+-transport during short-term hypercapnia.

Amiloride-sensitive Na^+-channels were blocked using amiloride and the apical membrane was permeabilized with nystatin. Next, control or hypercapnic solution was applied for 20 min and the ouabain-sensitive current I_{Oua} measured (graphs show mean ± SEM; n = 4; *: $P < 0.05$).

Permeabilization of the basolateral membrane is more complex compared to permeabilization of the apical membrane. The Na^+,K^+-ATPase is inhibited by ouabain and the basolateral membrane permeabilized by nystatin. Since the Na^+,K^+-ATPase creates the driving force for Na^+ to enter the cells, a Na^+-gradient had to be generated artificially. To prevent a falsification of the current by Cl^--ions and to stabilize the electrogenic gradients, Cl^- -ions were substituted with the also negatively charged gluconate. The resulting I_{Ami}, in the control as well as in the hypercapnia treated cells, was extremely small (**Figure 9**). No significant changes between control and hypercapnia-treated cells were detected, but due to the small current, an effect of CO_2 can not be excluded.

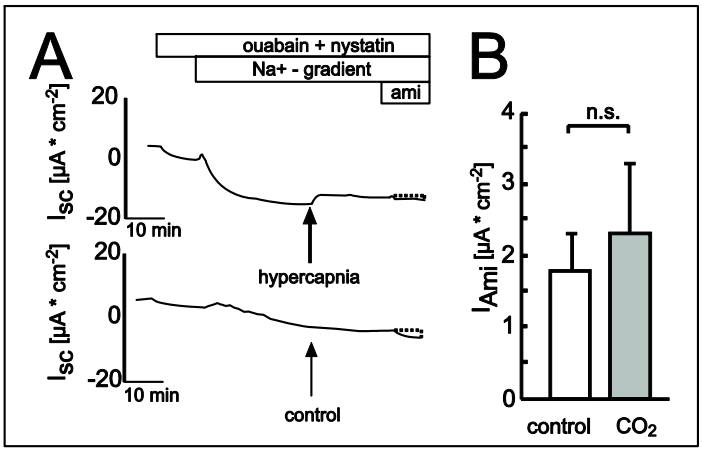

Figure 9 Amiloride-sensitive Na^+-transport during short-term hypercapnia

Ouabain-sensitive Na^+-transporter were inhibited with ouabain (1 mM) and the basolateral membrane permeabilized with nystatin (150 µM) and an artificial Na^+-gradient was generated. 20 min later, control or hypercapnic solution was also applied for 20 min and the amiloride-sensitive current measured (graphs show mean ± SEM; n = 4; *: $P < 0.05$).

3.1.4. Long-term hypercapnia affects the apical Na^+-conductance

To eliminate possible side-effects of the combination of additional Tris-base, artificial Na^+-gradient and Cl^--substitution and to elucidate the effect of chronic hypercapnia, H441 cells were incubated in Normocapnia- or Hypercapnia-medium for 24 h and the permeabilization was repeated with the buffers published previously (Ramminger et al., 2004; Woollhead et al., 2005) without any buffering and CO_2. Interestingly, the I_{Ami} of cells that were cultured in hypercapnic conditions was significantly reduced compared to control cells, even after approximately 30 min without CO_2 (**Figure 10**).

A reduction of the I_{Ami} can either be caused by a reduced open-probability (P_o) or a reduced number of channels in the membrane (N). Since the effect of 24 h hypercapnia was so stable, a change of P_o alone is most unlikely. Thus the endocytic pathway was targeted to investigate a contribution of the change of retrieval of channels from the membrane. Endocytosis of ENaC has been reported to be mediated by the 5' adenosine monophosphate-activated protein kinase (AMPK). Attempts to use the AMPK-inhibitor compound C or the proteasome-inhibitor MG-132, that is also commonly used to block endocytosis of transmembrane proteins (Gentzsch et al., 2010; Malik et al., 2006) prior to subjecting the cells to hypercapnia resulted in significant cell death, probably because of the long incubation times of more than 24 hours.

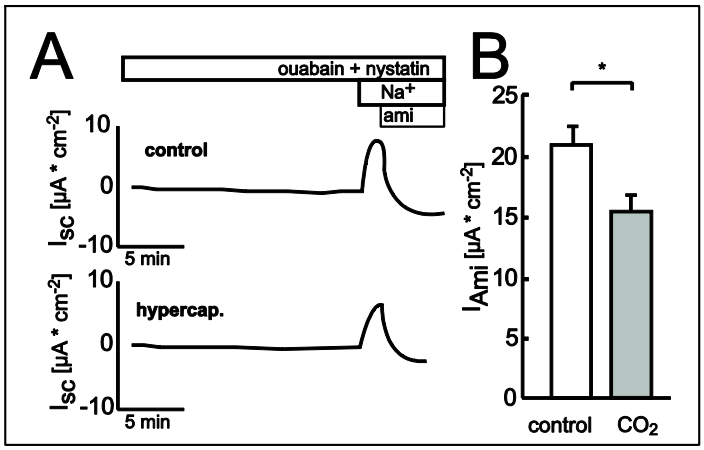

Figure 10 Effect of 24 h CO_2 on Na^+-conductance

H441 cells were incubated in normo- and hypercapnic conditions for 24 h. Apical permeabilization was performed immediately and the amiloride-sensitive current was determined (mean ± SEM; n = 3; *: P < 0.05).

3.2. rtPCR: Transcription levels of ENaC during hypercapnia

To rule out a regulation of ENaC-subunits on the transcriptional level H441 cells were exposed to normocapnia and hypercapnia and mRNA was isolated after 6 or 24 hours (**Figure 11**). Real-time rt-PCR revealed no change in transcription after 6 hours for all human ENaC subunits. After 24 hours only the expression of the ɔ-subunit was significantly decreased, although probably not to a biologically relevant extent (**Figure 12**).

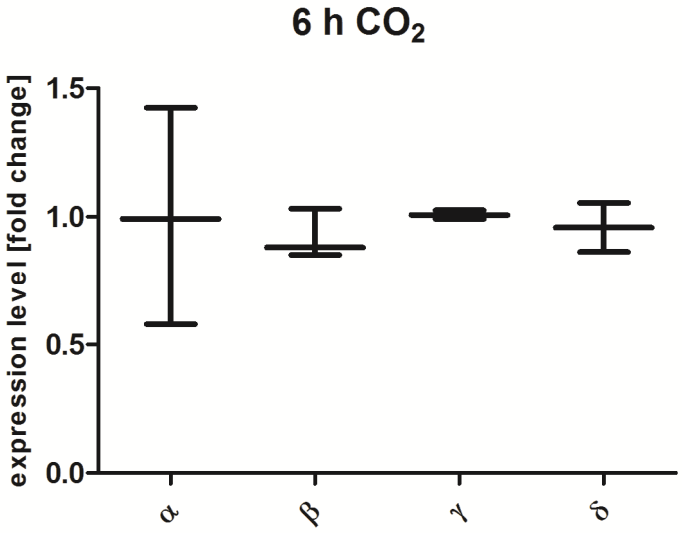

Figure 11 Transcription levels of ENaC subunits after 6 h CO_2

Native H441 cells were exposed to control conditions (40 mm CO_2) or hypercapnia (110 mm CO_2), pH 7.4 for 6 h prior to mRNA isolation and subsequent rtPCR (Graphs represent mean, whiskers mark the 5-95 percentile (n = 3) no significant differences were detected).

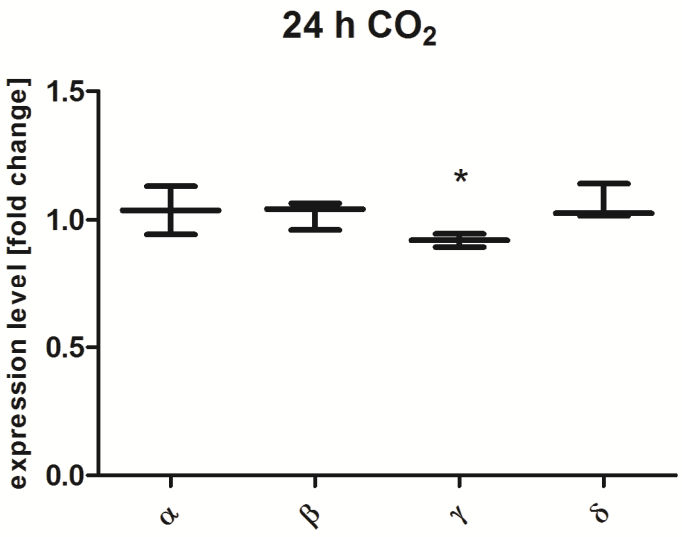

Figure 12 Transcription levels of ENaC subunits after 24 h CO_2

Native H441 cells were exposed to control-conditions (40 mm CO_2) or hypercapnia (110 mm CO_2), pH 7.4 for 24 h prior to mRNA isolation and subsequent rtPCR (Graphs represent mean, whiskers mark the 5-95 percentile; n = 3; unpaired Studentôs t-test compared to control; *: $P < 0.05$).

3.3. Expression cloning of modified human ENaC constructs

3.3.1. β-ENaC

Since a pharmacological manipulation of H441 cells during 24 hours hypercapnia was not feasible in the Ussing chamber setting, a different model had to be established. Mall et al. reported that overexpression of ϐ-ENaC is sufficient to increase the ENaC-complex membrane abundance and to cause a cystic-fibrosis-like phenotype in mice (Mall et al., 2004). Thus, a modified ϐ-ENaC was cloned and overexpressed in alveolar epithelial cells to enhance surface abundance of all ENaC-subunits. To improve the antibody recognition of the overexpressed ϐ-ENaC construct, the epitope-tag V5 was added to the C-terminus (**Figure 13**).

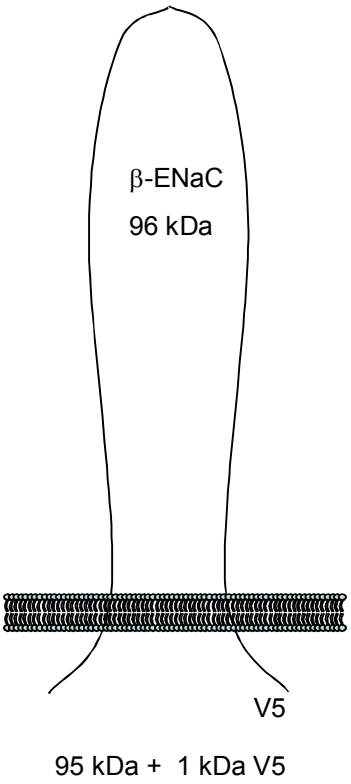

Figure 13 β-subunit of the human epithelial Na^+-channel was cloned from human lung tissue

The coding region corresponds to the NCBI Reference Sequence NM_000336.2. The epitope-tag V5 was added at the C-terminus, resulting in a predicted size of 96 kDa.

3.3.2. Cell surface abundance of β-ENaC-V5

To assess whether experimental difficulties using the buffered Ussing chamber solution rendered the effect of CO_2 on ENaC invisible, the newly generated ϐ-ENaC-V5 construct was transfected in A549 cells and the cell surface abundance and total cellular content was investigated by cell surface biotinylation. After one hour of hypercapnia no changes of the surface or total ENaC fraction were detected (**Figure 14**).

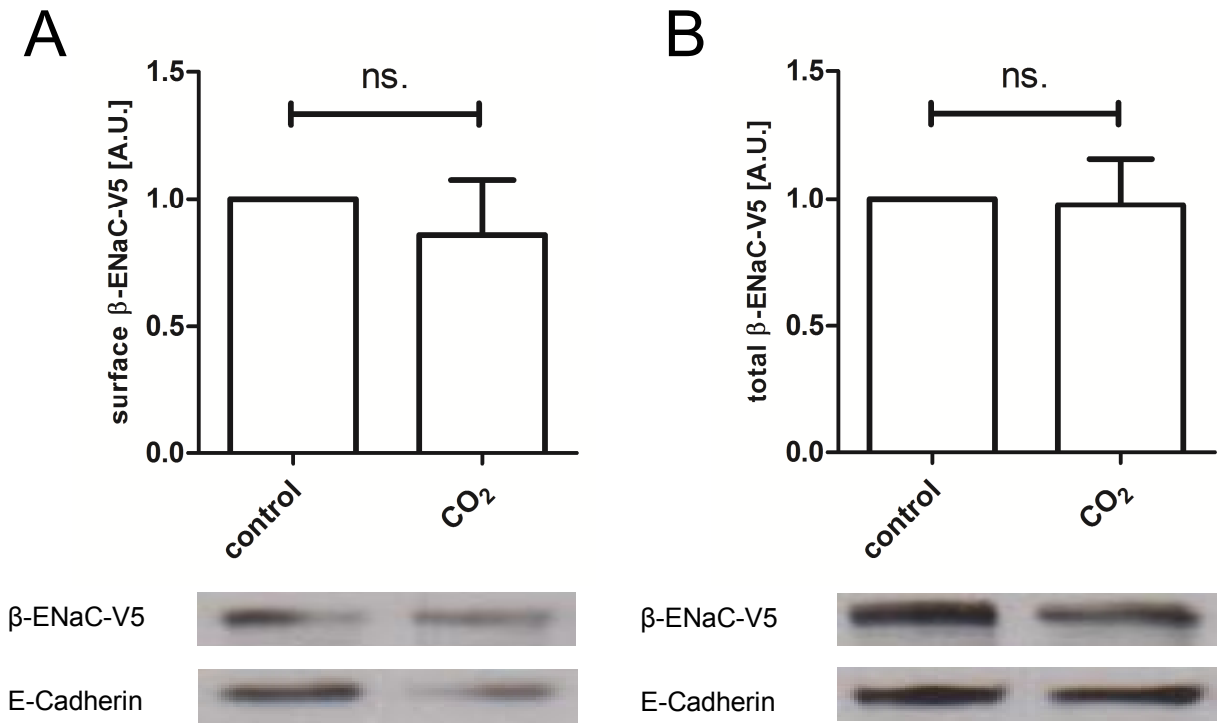

Figure 14 Short-term effect of CO_2 on β-ENaC-V5

A549 cells were transiently transfected with ϐ-ENaC-V5. 24 h later the cells were subjected to normocapnia or hypercapnia for 1 hour and the ϐ-ENaC-V5-levels were determined. (A) Biotin-streptavidin pulldown was performed to assess cell surface abundance of ϐ-ENaC-V5. (B) Whole cell lysate of the same samples was blotted to determine total ϐ-ENaC-V5 content (n = 4).

In the functional studies a significant decrease of the I_{Na} was detected (**Figure 10**). Consequently, cell surface expression of ɓ-ENaC-V5 was also investigated after 24 h hypercapnia. In line with the functional studies a marked decrease of the cell surface abundance could be observed that was not caused by generally lower total ENaC content (**Figure 15**). Pharmacological intervention using the endocytosis and proteasome inhibitor MG-132, the lysosome inhibitor chloroquine or the AMPK-inhibitor Compound C 2 hours before and during the 24 h hypercapnia incubation resulted again in significant cell death.

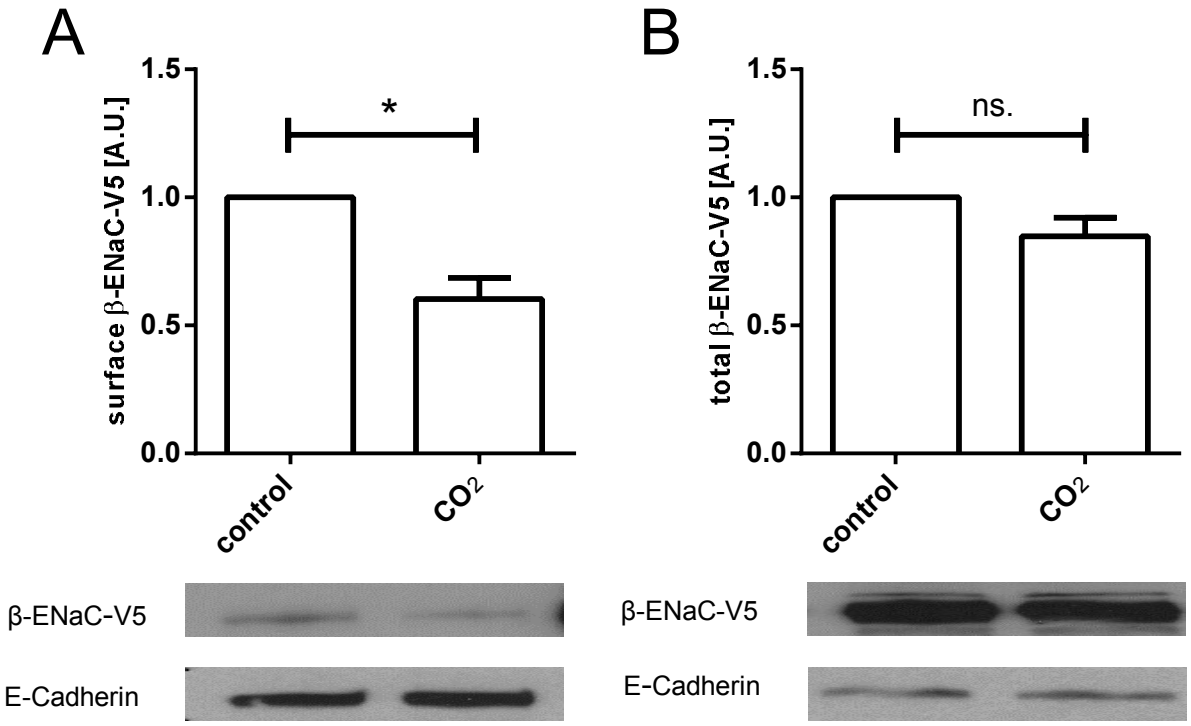

Figure 15 Long-term effect of CO_2 on β-ENaC-V5

A549 cells were transiently transfected with ɓ-ENaC-V5. Four hours later, cells were subjected to normocapnic (control) conditions or hypercapnic (CO_2) for 24 h. (A) Biotin-streptavidin pulldown was performed to assess cell surface abundance of ɓ-ENaC-V5. (B) Whole cell lysate of the same samples was blotted to determine total ɓ-ENaC-V5 content (n = 5; *: $P < 0.05$).

3.3.3. Expression cloning of human α- and γ-ENaC

Against the above mentioned evidence from the literature (chapter **1.3**) no acute regulation of ß-ENaC was observed. A possible explanation for that could be a different processing of individually expressed ENaC-subunits compared to a system in which all three subunits are expressed simultaneously, as reported for other cell types (Hughey et al., 2003). Thus, Ŭ- and ɔ-ENaC constructs were generated. Since both subunits undergo proteolytic processing during maturation, each subunit was tagged individually at the N-, as well as the C-terminus with different epitope tags (**Figure 16**) to provide a powerful tool for studying all aspects of post-translational ENaC-regulation, including but not limited to ubiquitination, phosphorylation and binding to the E3-ubiquitin ligase Nedd4-2.

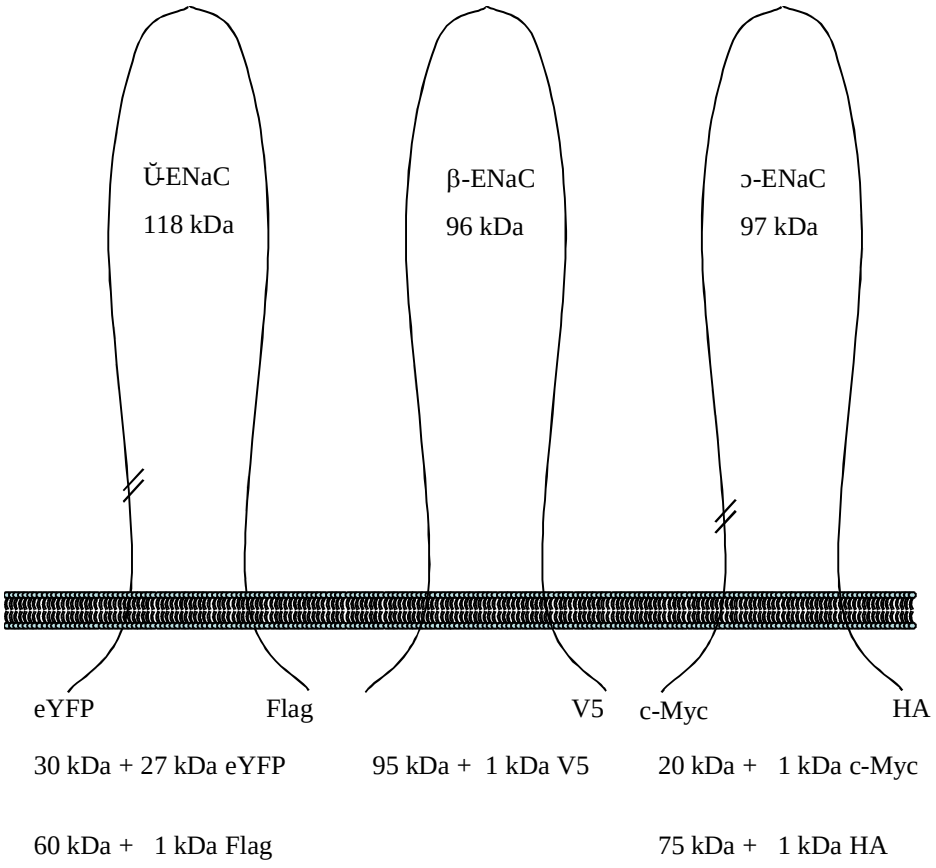

Figure 16 Overview about all ENaC-plasmids that were generated as part of this study

Expected sizes are given of the full length (top) as well as of the mature fragments (bottom) with the genetic modifications. Modified from R. Hughey (Hughey et al., 2003)

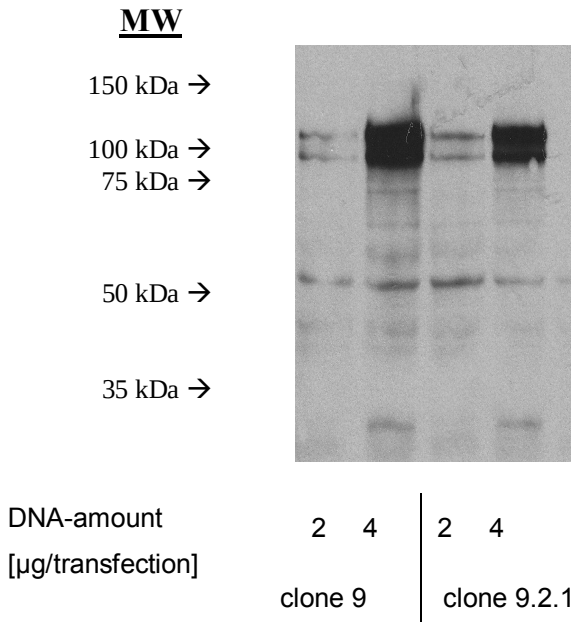

Figure 17 Expression pattern of α-ENaC before and after site-directed mutagenesis

The Ŭ-ENaC clone number 9 contained two single nucleotide polymorphisms (A334T, T663A), compared to the reference sequence NM_001038 (genebank, NIH), which were corrected using site-directed mutagenesis. The modified clone 9.2.1 contains a coding region identical to the reference sequence and does not exhibit alternative cleavage pattern when expressed individually in A549 cells (antibody used: anti-GFP, Roche).

Ŭ, ɓ and ɔ-ENaC could be expressed in A549 cells. The membrane abundance however was very variable and in many cases too low to be detected, even with the most sensitive, non-radioactive detection methods available for western-blotting. Further, cotransfection with plasmid amounts in the sublethal range resulted in only very low expression levels of Ŭand ɔ ENaC.

Trafficking of fully assembled ENaC-complexes to the cell membrane that are insoluble in the generally used non-ionic detergent-containing lysisbuffers were reported for different types of kidney cells (Prince and Welsh, 1998). Additionally a localization of ENaC in lipid rafts has been described in the mouse and frog kidney cells, also rendering it insoluble in the above mentioned buffers (Hill et al., 2007). An experiment was designed to evaluate, whether this was also the case for A549 cells, which exhibit formation of lipid rafts (Song et al., 2007). Ŭ-ENaC alone and Ŭ, ɓ and ɔ-ENaC together were transfected in A549 cells and the abundance of Ŭ-ENaC in the soluble fraction was compared to the insoluble fraction.

As can be seen in **Figure 18** Ŭ-ENaC was expressed when transfected alone and together with ɓ and ɔ (A: lanes 2a, 3a; whole cell lysate, Triton X-100 soluble). An immunoprecipitation was performed to compare the abundance of Ŭ-ENaC in the Triton X-100 soluble (b) and insoluble fraction (c) of the same cell lysate. Only faint bands were detected in the insoluble fraction (lane 2c), suggesting ENaC not to be present in lipid rafts in A549 cells. As a positive control for succesful immunoprecipitation also the soluble fractions were subjected to immunoprecipitation (b), which led to a distinct pull down (A and B; lanes 2b, 3b) that was detectable even after a brief exposure.

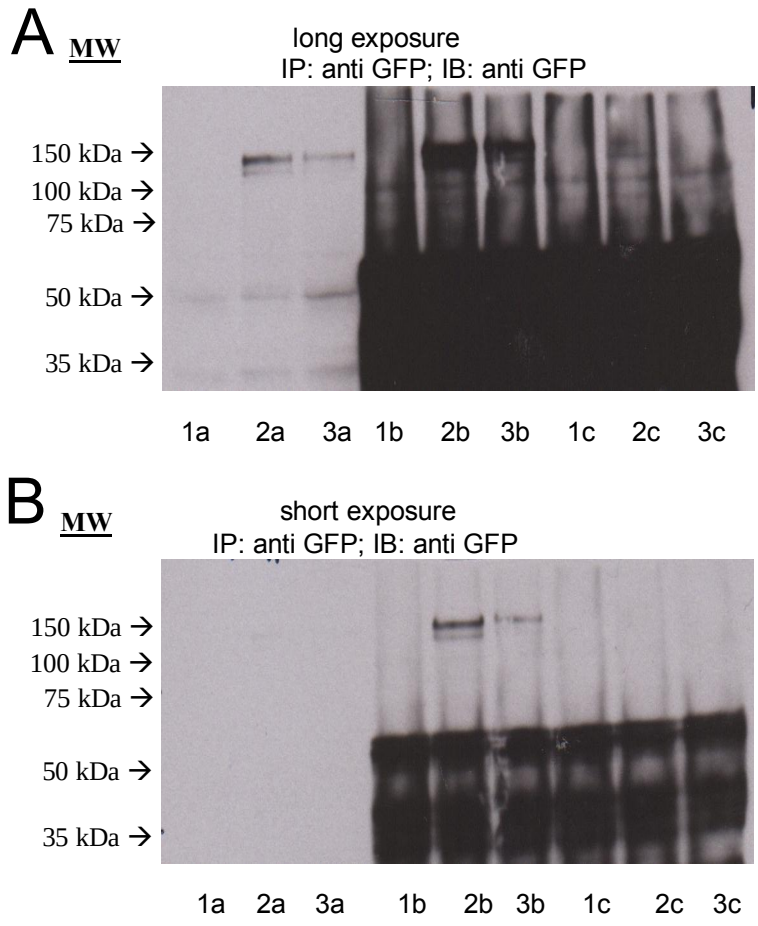

Figure 18 ENaC localisation in soluble fraction and in lipid rafts in A549 cells.

Cells were transfected without plasmid (1), Ŭ-ENaC-YFP alone (2) or Ŭ-ENaC-YFP, ɓ-ENaC-V5, ɔ-ENaC-HA combined (3) and lysed in TBS containing 1% Triton X-100. The insoluble pellet was boiled in solubilization buffer containing SDS and ɓ-mercaptoethanol and diluted in TBS containing 1% Triton X-100. Total cell lysate is presented in the first three lanes (a, 50 µg protein). Immunopreciptation was performed either from the Triton X-100- (b, ~ 600 µg protein), or the SDS-soluble fraction of the same amount of cells (c). Two different exposure times are shown to focus either on the total cell lysate (A) or the immunoprecipitated fraction (B). Depicted is a representative of three independent experiments.

Protein-turnover especially of ENaC is significantly influenced by the system used and the culture conditions. Before using the system to study the effect of CO_2, the baseline stability of cell surface Ŭ-ENaC was determined by pulse-chase experiments. For that, all membrane proteins are labeled with the membrane impermeable EZ-linked-sulpho-NHS-LC-biotin and the cells incubated again in preequilibrated medium for the duration indicated. After that the cells were lysed and remaining Ŭ-ENaC precipitated with streptavidin-agarose beads. A half-life of Ŭ-ENaC, inserted in the plasma-membrane of about 2 h was measured.

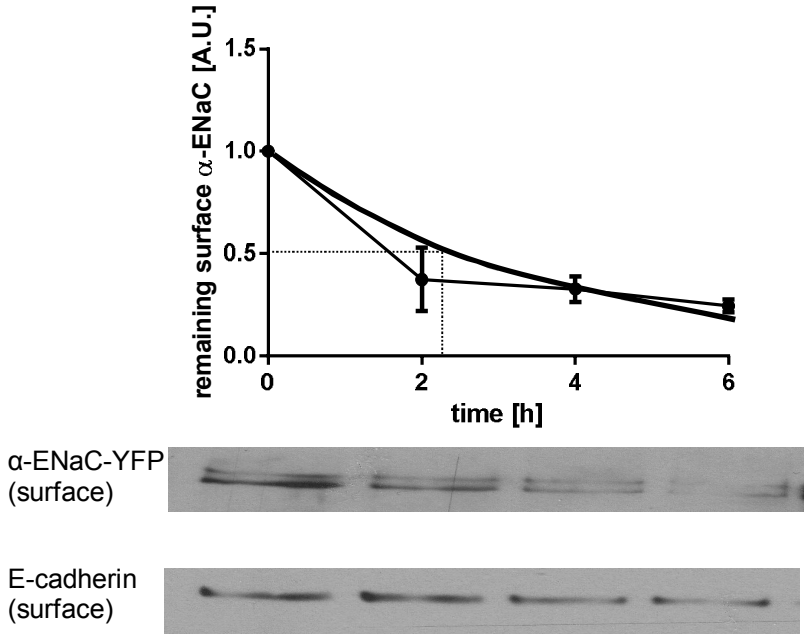

Figure 19 Stability of cell surface α-ENaC-YFP transfected in A549 cells

All proteins located in the plasma-membrane were labeled with biotin. The cells were then covered with preequilibrated medium and returned to the cell culture incubator. After the indicated time-points, cells were harvested, subjected to biotin-streptavidin pulldown and the remaining fraction of labeled Ŭ-ENaC-YFP was determined by western-blotting (means ± SEM, n = 3).

If CO_2 was a stimulus for ENaC to be retrieved from the plasma-membrane, decreased stability of the membrane fraction was to be expected. To adress this, membrane-proteins were biotinylated as described above, but the cells incubated in normocapnia or hypercapnia medium for 2 and 4 hours (**Figure 20**).

Observed was a slightly but not significantly decreased stability of Ŭ-ENaC during hypercapnia (**Figure 20**).

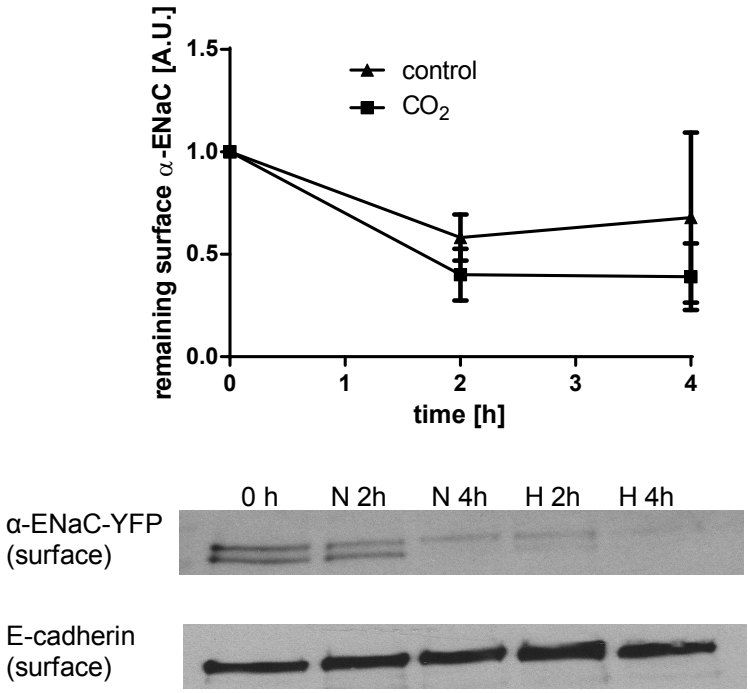

Figure 20 Stability of surface α-ENaC during normocapnia and hypercapnia

All membrane proteins were labeled with biotin. The cells were then covered with preequilibrated normocapnia (N) or hypercapnia (H) medium and returned to the cell culture incubator. After the indicated time-points, cells were harvested, subjected to biotin-streptavidin pulldown and the remaining fraction of labeled Ŭ-ENaC-YFP was determined by western-blotting (mean ± SEM, n = 3).

Degradation of ENaC is catalyzed by the E3-ubiquitin ligase Nedd4-2 (Itani et al., 2009; Kabra et al., 2008; Malik et al., 2005), and therefore it is anticipated, that its genetic inhibition should increase the total levels of ENaC and prevent the accelerated degradation during hypercapnia.

As depicted in **Figure 21**, the genetic inactivation of NEDD4-2 was highly effective.

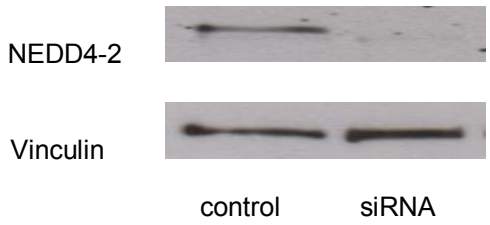

Figure 21 Nedd4-2 dependent cell surface expression of α-ENaC-YFP

(A) Nedd4-2 was efficiently downregulated by siRNA transfection (representative blot of 5 experiments).

The faster degradation of Ŭ-ENaC-YFP during hypercapnia was completely abolished when Nedd4-2 was silenced. Still, degradation of ENaC located in the plasma membrane was observed and the rate of degradation did not differ from cells that were expressing Nedd4-2 (**Figure 22**) . This finding did not correspond to the efficiency of the knockdown, which was reproducibly highly efficient.

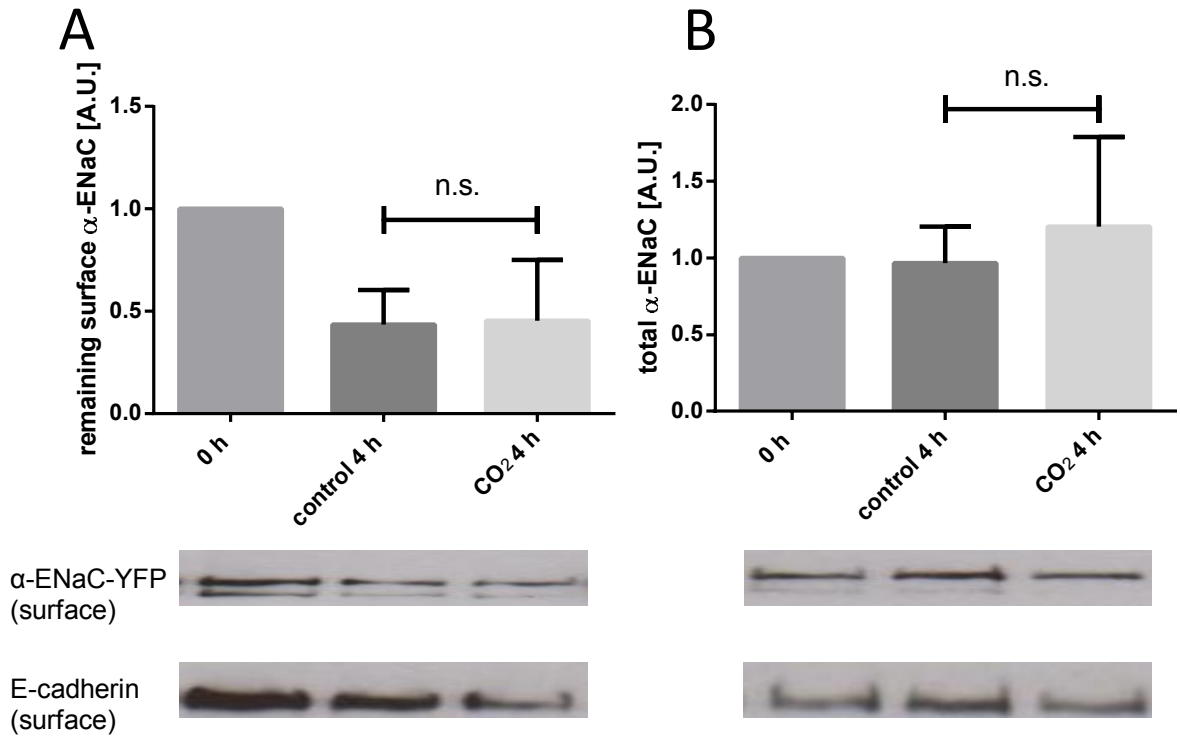

Figure 22 CO_2 dependent stability of α-ENaC-YFP during silencing of Nedd4-2.

The E3-ligase Nedd4-2 was silenced by siRNA transfection. The stability of Ŭ-ENaC-YFP was then compared after 4 hours of normocapnia or hypercapnia in the cell surface (A) and in the whole cell lysate (B) (mean ± SEM, n = 3).

3.3.1. Transfection of H441 cells

Compared to A549 cells, H441 cells are more widely used for studying Na^+-transport (Albert et al., 2008; Ramminger et al., 2004). Transfection of H441 cells with a new high-end 4D-Nucleofector-system was established to circumvent the poor antibodies raised against the endogenous ENaC subunits. The process called Nucleofection is based on electroporation and provides an elegant and fast technique for delivering nucleic acids directly into the nucleus.

After optimization of the Nucleofection H441 cells could efficiently be transfected (

Figure 23**)**. A mean transfection efficiency with the GFP control-plasmid pMaxGFP of ~ 60 % was achieved (**Figure 24**).

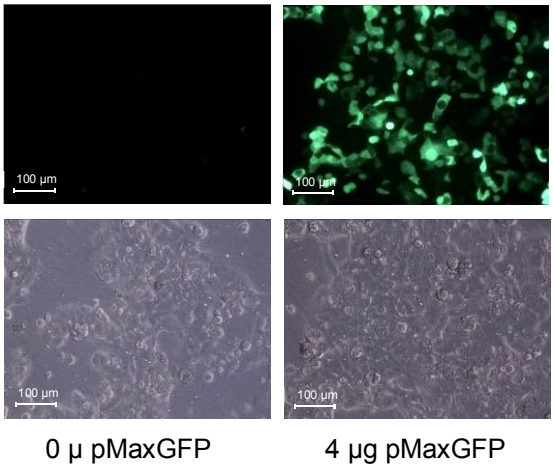

Figure 23 GFP expression of transfected H441 cells

H441 cells (1 x 10^6 cells/reaction) were nucleofected with and without 4 µg pMaxGFP. Depicted is a typical of seven independent experiments.

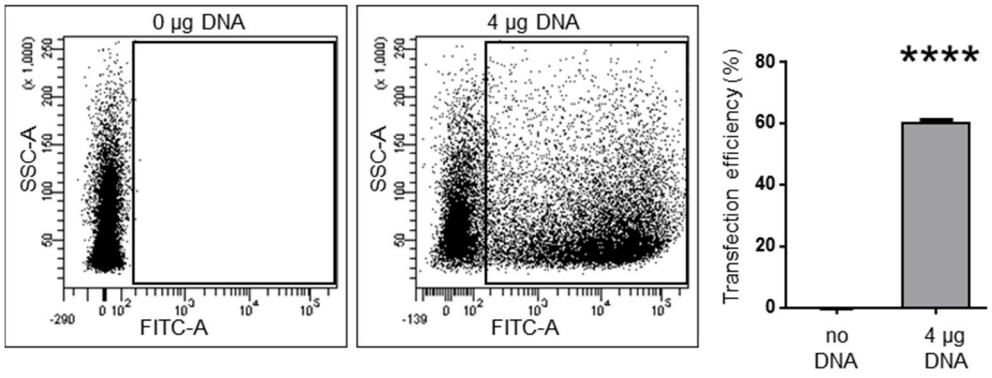

Figure 24 Transfection efficiency of H441 cells achieved by nucleofection

H441 cells (1 x 10^6 cells/reaction) were nucleofected with 4 µg pMaxGFP plasmid and the efficiency was determined by flow cytometry gating for GFP-positive cells (mean ± SEM; n = 3; ****: $P < 0.0001$).

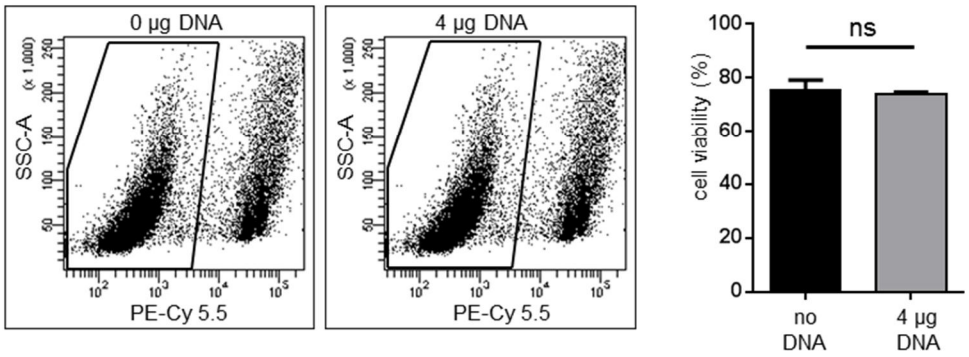

Figure 25 Viability of H441 cells after Nucleofection

H441 cells (1 x 10^6 cells/reaction) were nucleofected with 4 µg pMaxGFP plasmid, stained with the dye 7-AAD and the viability was determined by flow cytometry (mean ± SEM, n = 3).

Cotransfection of Ŭ, ɓ and ɔ-ENaC was also succesful, as shown in **Figure 26**. Every subunit was detected in the same cell lysate using the subunit specific antibodies (Ŭ: GPF, ɓ: V5, ɔ: HA). The transfection was transient, with fusion proteins being detectable after 24 hours but with a marked decrease in whole cell protein levels already after 48 hours.

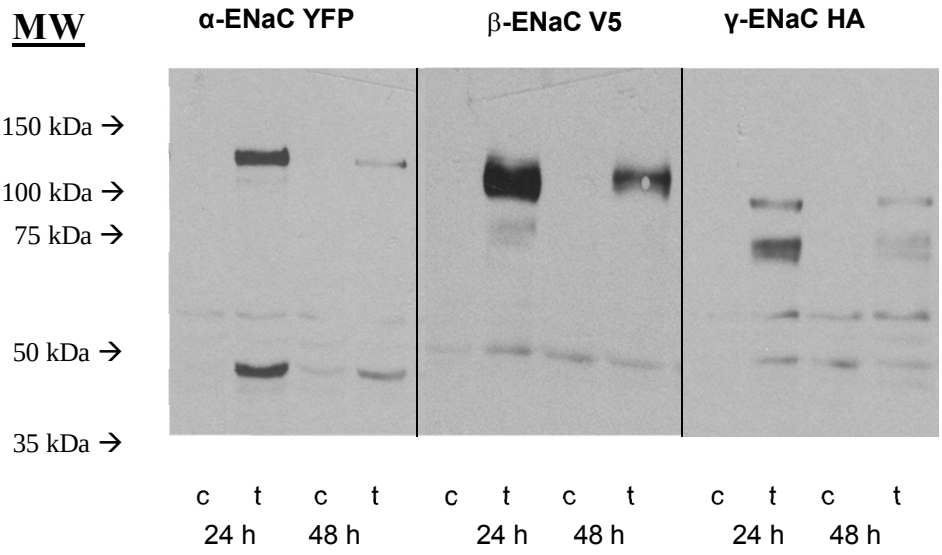

Figure 26 Cotransfection of α β and γ-ENaC in H441 cells

H441 cells were cotransfected without DNA (c) and with Ŭ-ENaC-YFP, ɓ-ENaC-V5, ɔ-ENaC-HA (t) and lysed 24 h respectively 48 h later and analysed by western immunoblotting using antibodies against the respective epitope tags.

However, detection of Ŭ and ɔ-ENaC in the cell membrane remained suboptimal. To optimize the cell surface expression of this two subunits, Ŭ and ɔ-ENaC constructs, both eGFP-tagged for recognition with the same antibody (**Figure 27**), were transfected in H441 cells and analyzed (**Figure 28**). Surface expression of Ŭ and ɔ-ENaC was evanescent, considering that the pulldown was performed from 1.8 mg total protein (surface) and the amount of total cell lysate that was loaded (50 µg / lane; (total)). The chemiluminescent signal was developed with the Supersignal West Femto substrate for maximal sensitivity. Treatment of the cells 5 days prior transfection and after transfection with dexamethasone, as well as aspiration of the apical liquid to expose the cells to air, did not increase the expression levels within the time-course of plasmid-expression (24 hours, data not shown).

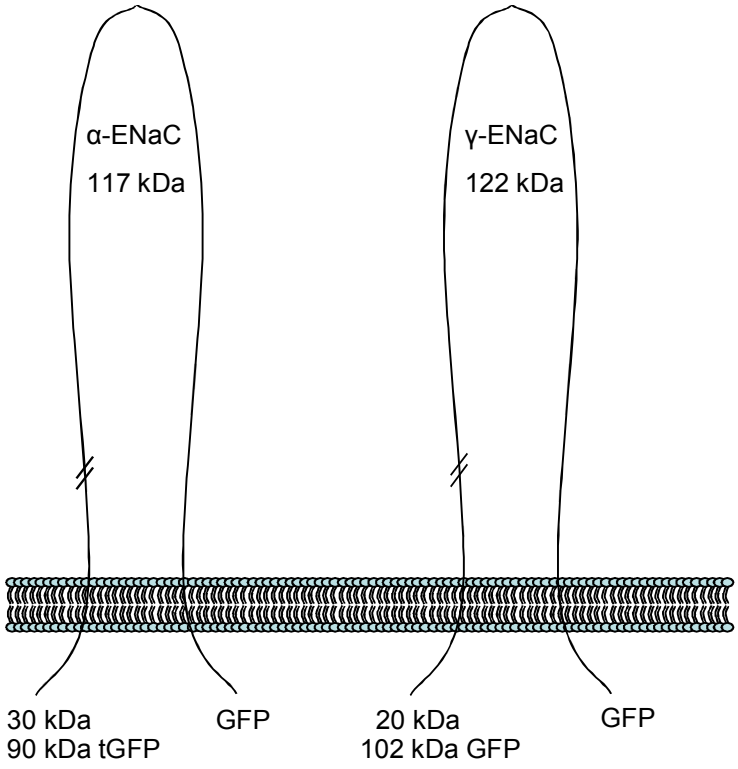

Figure 27 Scheme of the commercially available tGFP-tagged α- and γ-ENaC constructs (Origene) used in this study

Predicted sizes are given of full length forms (top) and after proteolytical processing (bottom).

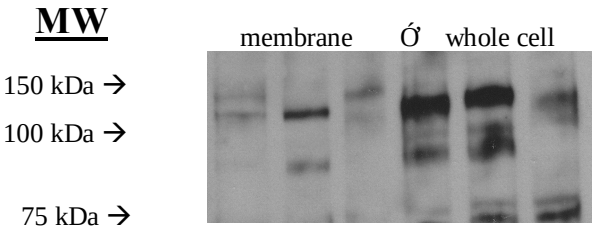

α-tGFP	+	+		+	+	
α-eYFP/Flag			+			+
β-V5	+	+	+	+	+	+
γ-tGFP	+		+	+		+
γ-HA		+			+	

Figure 28 Expression pattern of α and γ-ENaC in the cell-surface of H441 cells

Combinations of different ENaC-subunits were cotransfected in H441 cells and the cell membrane abundance compared to the whole cell content of Ŭand ɔ-ENaC (anti-tGFP). Shown is a biotin-streptavidin-pulldown of 1800 µg total protein (membrane) and 50 µg whole cell lysate.

3.3.2. Transfection of primary rat alveolar epithelial cells

Primary cells are in many ways superior to immortilized or tumor cell lines and represent a more physiologic system to study Na^+-transport. However, immunological detection of ENaC has always been difficult in primary cells. Another caveat is that genetic manipulation of primary cells by gene silencing and overexpression was usually associated with virus-mediated gene transfer, resulting in non-conventional experimental procedures that were limited by safety-regulations and complex and labour-intensive virus-production. As a proof of principle, ATII cells were transfected with Lipofectamine 2000 basically as described before (**2.1.2**). The amount of DNA per transfection was increased to achieve the same ratio of DNA to cells, as with Nucleofection. Subsequently, the amount of Lipofectamine 2000 was adjusted. The transfection resulted in only a few transfected cells, as depicted in **Figure 29,** confirming the dogma, that ATII cells can not efficiently be transfected by non-viral techniques.

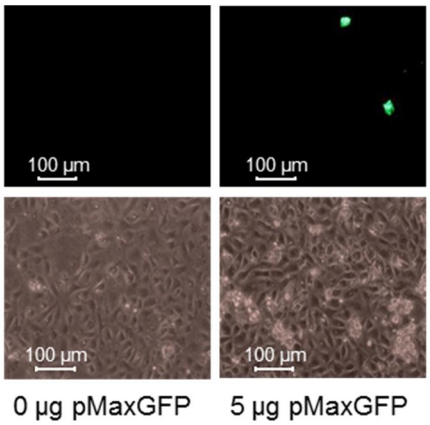

Figure 29 Lipofection of ATII cells

ATII cells were plated on 60 mm cell culture plates and allowed to recover for one day. They were then transfected with 15 µl Lipofectamine 2000 without or with 5 µg of the vector pMaxGFP. GFP expression was assessed 2 days later by fluorescence microscopy (n = 3).

Nucleofection is a transfection method, specifically designed for primary cells and other cells that are hard to transfect. This also applies to ATII cells, therefore a protocol was created to transfect them. For the first time a safe, reliable and efficient transfection procedure based on electroporation was established as part of this thesis to genetically manipulate primary ATII cells. Nucleofection proved to be dose-dependent, as depicted in

Figure 30 and **Figure 31**. The transfection efficiencies for 3, 5 and 8 µg pMaxGFP were 32.4 ± 0.5, 39.6 ± 1.2 and 48 ± 0.7 % respectively (**Figure 31**).

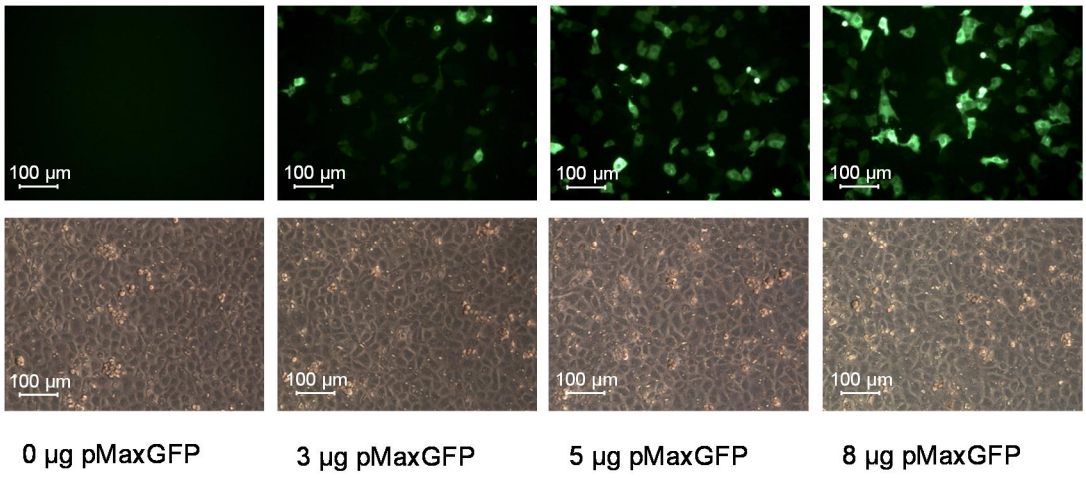

Figure 30 Nucleofection of primary rat alveolar epithelial type II cells.

Freshly isolated ATII cells were allowed to recover over night on a cell culture dish. The next day 3.5 x 10^6 cells were transfected with up to 8 µg pMaxGFP plasmid. The negative control was pulsed as all other cells, but without plasmid DNA and results were visualized 48 hours after transfection.

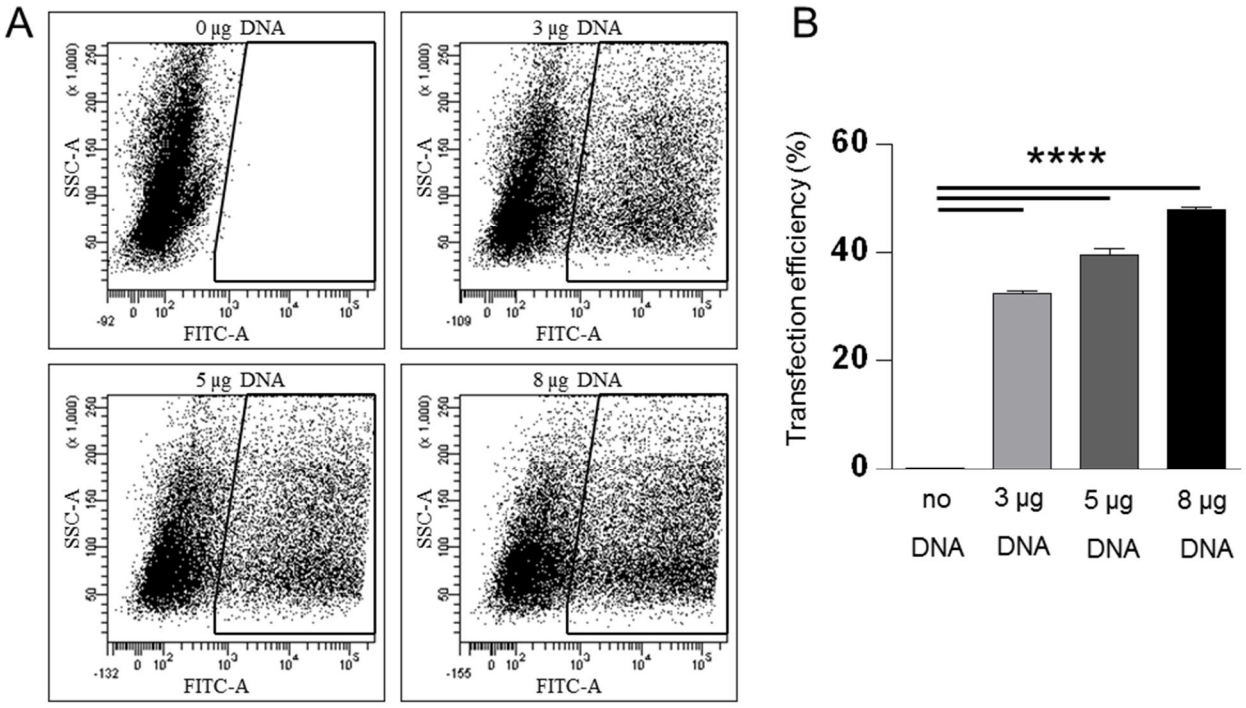

Figure 31 Transfection efficiency of ATII cells

Freshly isolated rat alveolar epithelial type II cells were allowed to recover on culture dishes over night, transfected with pMaxGFP (3-8 µg/reaction) and plated onto permeable supports at a density of 3.5 x 10^6 per

filter. Efficiency was assessed two days after transfection. (A) Scatter plot of GFP expression measured by FACS analysis. (B) Transfection efficiency of AT II cells transfected with the indicated DNA-amounts (bars indicate mean ± SEM; n = 2-3; ****: P < 0.0001).

Cells transfected with 8 µg DNA took longer to attach to the transwell-membrane after 24 h. To rule out early cell death due to the transfection procedure lactate-dehydrogenase (LDH) release was measured 4 and 24 h after transfection. After 4 h a strong release of LDH was detected only in cells that received the electrical pulse, which returned to baseline 20 h later. This LDH release is the result of the formation of pores in the cell membrane, which are the reason for delivery of nucleic acids by Nucleofection. At the later timepoint no significant LDH was measured (**Figure 32**). Counting the number of cells that remained on the permeable support 48 h after Nucleofection showed no significant differences (**Figure 33**).

However, viability was not significantly decreased 48 h after transfection compared to control cells as assessed by flow cytometry (**Figure 34**) and the cells formed electrically tight monolayers with a resistance of about 1200 q * cm^2, that did not differ from each other (**Figure 35**).

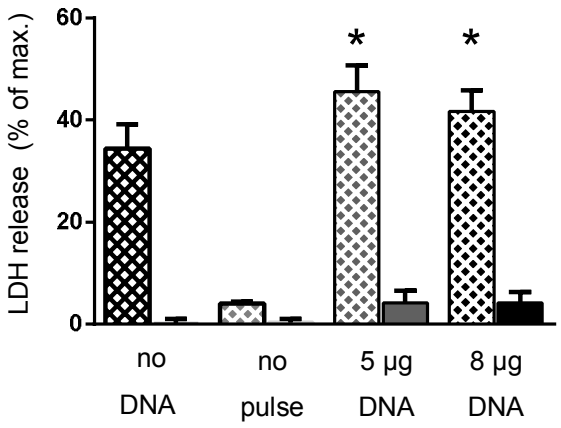

Figure 32 Evaluation of early cytotoxicity in transfected ATII cells

ATII cells were transfected as indicated and plated onto permeable supports. Four (patterned bars) and 24 h (full bars) after transfection medium was removed, cleared from cells and subjected to a lactate-dehydrogenase assay to screen for cell damage (mean ± SEM; n = 3; *: P < 0.05).

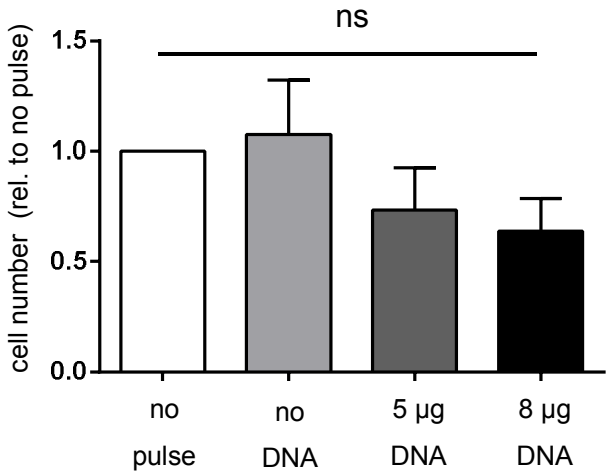

Figure 33 Cell number 48 h after Nucleofection

ATII cells were transfected as indicated, maintained for 48 h, trypsinized and the number of attached cells counted for each experimental condition (mean ± SEM; n = 3).

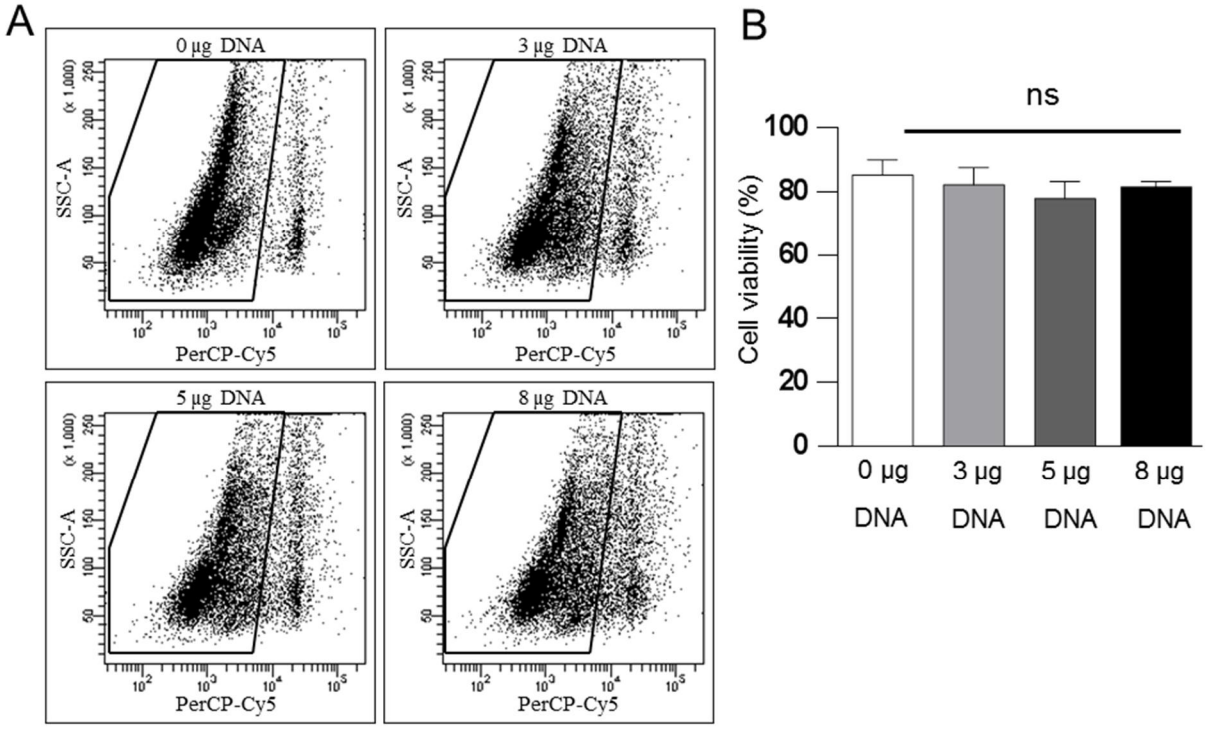

Figure 34 Viability of transfected ATII cells.

Rat alveolar epithelial type II cells were transfected with pMaxGFP, plated onto permeable supports at a density of 3.5 x 10^6 per filter. Control cells were sham transfected without the vector pMaxGFP but otherwise received the same treatment as cells receiving the GFP vector pMaxGFP (3-8 µg / reaction). Two days after transfection cells were trypsinized, stained with 7-AAD and subjected to flow cytometry. (A) Scatter plot of flow cytometry showing live cell population (inside the box). (B) Viability of transfected cells (bars indicate mean ± SEM; n = 3-4).

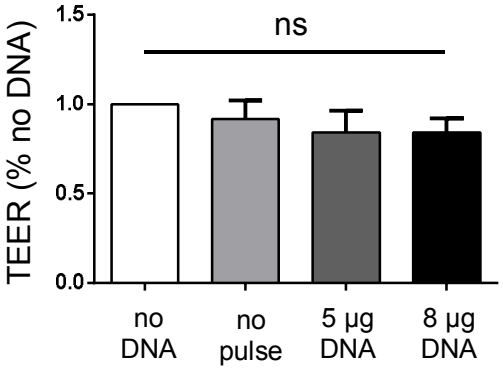

Figure 35 Electrical resistance 48 h after Nucleofection

Two days after Nucleofection the electrical resistance of the ATII cell monolayer was measured with an volt ohm meter (bars indicate mean ± SEM; n = 3).

3.3.3. ENaC transfection in ATII cells

To translate the newly established system to the initial project of studying ENaC and its regulation during hypercapnia Ŭ- and ɓ-ENaC individually and Ŭɓɔ-ENaC together were transfected into ATII cells. In the first experiments expression was evaluated two days after Nucleofection, but no signals were detected (not shown). When the analysis was carried out already after one day, relatively strong expression of individually transfected Ŭ- and ɓ-ENaC was detected and faint bands in the cotransfected sample. The low amount of protein that was available might explain the absence of ɔ-ENaC (**Figure 36**). Of note: Due to the low yield of protein the biotin-streptavidin pulldown was performed from only up to 200 µg protein and only 10-16 µg protein of whole cell lysate was blotted, as opposed to 1.8 mg that were used for the pulldown in H441 cells (chapter **3.3.1**).

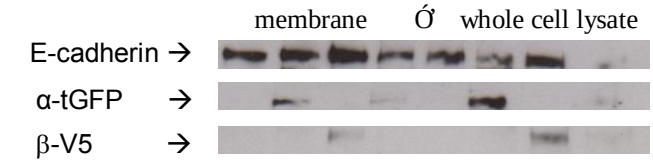

pMaxGFP	+				+			
α-tGFP		+		+		+		+
β-V5			+	+			+	+
γ-tGFP				+				+

Figure 36 Pilot experiment for transfection of ENaC subunits in ATII cells

Freshly isolated ATII cells were allowed to recover from isolation for 1 day. They were then transfected as indicated (equal ratios of subunits, total amount of DNA always 8 µg) and expression of recombinant ENaC subunits was monitored 24 h after transfection. Pulldown was performed from up to 200 µg protein and whole cell lysate shows 10 ï 16 µg protein.

4. Discussion

4.1. Hypercapnia modulated regulation of alveolar Na^+- transport

The alveolar fluid transport is tightly regulated in the intact lung due to secondary active Na^+-reabsorption creating an osmotic gradient for water to follow passively. The two key molecules involved in Na^+-transport are the Na^+,K^+-ATPase that actively exchanges Na^+ for K^+, thus lowering the intracellular Na^+-concentration. This drives Na^+ from the alveolar space to passively enter the cells through ENaCs (Matthay et al., 2002).

During different respiratory diseases ventilation is impaired leading to a reduced elimination of CO_2 in the body, a condition called hypercapnia. Hypercapnia can also be a consequence of lung protective ventilation during ARDS (Hickling et al., 1994).

Despite its immunoregulatory function hypercapnia has been reported to negatively affect alveolar fluid transport independent of pH. This finding has been reported from rats *in vivo*, isolated rat lungs as well as from isolated epithelial cells (Briva et al., 2007). The underlying mechanism is a CO_2 - triggered rapid increase in cytosolic Ca^{2+}. This leads to a *Ca^{2+}-calmodulin dependent kinase kinase ß*- (CaMKK-ß) mediated phosphorylation of the Ŭ-subunit of AMPK. One of the distal elements of this signaling cascade is *protein kinase-C-ζ* (PKC-ζ) which directly phosphorylates the Ŭ-subunit of the Na^+,K^+-ATPase at serine-18, leading to its endocytosis (Briva et al., 2007; Vadász et al., 2008). Phosphorylation of serine-18 has been shown to induce ubiquitination of the Ŭ-subunit of the Na^+,K^+-ATPase during hypoxia, so this is likely also the case in hypercapnia (Dada et al., 2007). Activation of AMPK was also shown to be dependent on e*xtracellular-signal regulated kinase* (ERK) activation.

In the present study, the effect of hypercapnia on Na^+-transport in H441 cells has been tested in Ussing chamber experiments. To rule out any contribution of pH changes, an initial experiment was performed, showing that variations of pH in the range of 7.2 ï 7.6 did not influence the I_{sc}. All other experiments were performed at a pH of 7.4. In line with the investigations mentioned above, hypercapnia resulted in a pronounced decrease in the total Na^+-transport which was caused by a strong inhibition of the Na^+,K^+-ATPase activity, as assessed by membrane permeabilization, supporting the established role of the Na^+,K^+-ATPase in hypercapnia. Interestingly this decrease was only present when hypercapnic solution was perfused in the apical compartment.

An explanation could be a distinguished difference in the CO_2 permeability of the apical and basolateral membrane caused for example by different subsets of transmembrane proteins, in especially gas permeating channels. Aquaporin 1 (AQP1) was demonstrated to be a physiologically relevant candidate to conduct CO_2 (Boron, 2010; Musa-Aziz et al., 2009; Wang et al., 2007) but its significance as a gas channel is highly controversial. A study using AQP1 deficient mice did not yield any differences in the CO_2 transport rate of the alveolo-capillary barrier (Fang et al., 2002). Additionally, AQP1 in the lung is predominantly expressed in endothelial cells (Jiao et al., 2002; King and Agre, 2001; King et al., 2002), so a potential differential expression pattern of AQP1 in the apical and basolateral membrane of H441 cells cannot be the reason for the absence of basolateral CO_2 mediated modulation of I_{Na}. Other channels that conduct CO_2 are AQP4 and AQP5 and AQP 5 is indeed expressed in ATI cells (Verkman et al., 2000). Another possibility could be an interference of the permeable support with the exposition of the cells to CO_2. These possibilities are currently under investigation in our laboratory.

Interestingly, many elements of the signaling cascade that induces downregulation of the Na^+,K^+-ATPase are also known direct or indirect regulators of ENaC function.

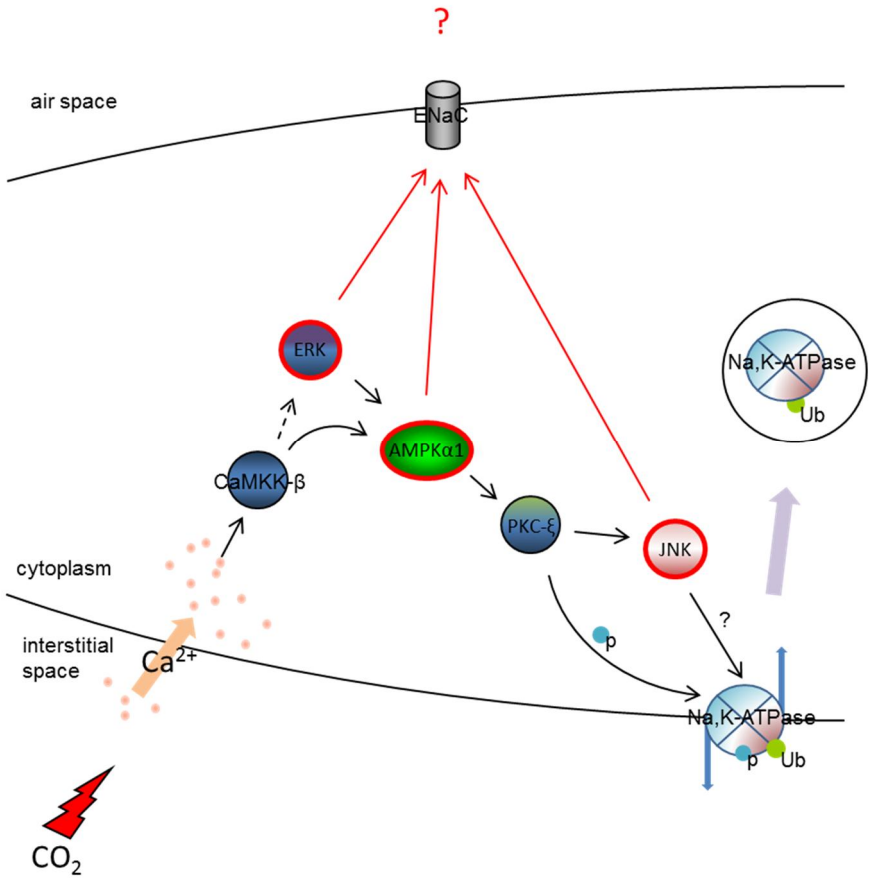

Figure 37 CO_2 induced signaling cascade leading to endocytosis of the Na^+,K^+-ATPase

Elements proven to regulate ENaC are highlighted in red.

ERK has been shown to phosphorylate ß- and ?-ENaC thereby mediating interaction with Nedd4-2 ultimately resulting in endocytosis and reduction of P_0 (Shi et al., 2002). Also ?-ENaC expression and additionally alveolar Na^+-transport have been shown to be regulated in an ERK dependent manner (Frank et al., 2003).

PKC mediates liquid regulation in the rat lung (Soukup et al., 2012). Also other groups report PKC-dependent ENaC regulation (Awayda et al., 1996; Shimkets et al., 1998; Stockand et al., 2000), but the CO_2-activated ?-isoform has never been directly linked to ENaC.

JNK on the other hand has been shown to phosphorylate the E-3 ligase Nedd4-2, which is known to ubiquitinate ENaC, causing its inhibition (Hallows et al., 2010).

AMPK dependent ENaC regulation has been extensively investigated. Activation of AMPK leads to decreased ENaC function and thus alveolar fluid clearance (Albert et al., 2008; Carattino et al., 2005; Myerburg et al., 2010; Woollhead et al., 2007). Two mechanisms seem likely to happen upon activation of AMPK: The classical way of interaction involves AMPK-dependent association of Nedd4-2 with ENaC subunits that induces retrieval of the channel from the membrane and thereby limiting Na^+-transport (Bhalla et al., 2006; Carattino et al., 2005). Another way of AMPK-dependent ENaC regulation is a reduction of single-channel P_0 rather than an effect on N as shown in H441 cells (Albert et al., 2008).

Since all these elements are activated during hypercapnia and are associated with ENaC regulation, the effect of CO_2 on ENaC function was investigated as part of the present study. As mentioned above, total Na^+-transport and activity of the Na^+,K^+-ATPase was reduced by CO_2. Elucidating the effect on the apical Na^+-permeability alone revealed no significant differences in normocapnia- versus hypercapnia-treated cells during up to 20 min.

However, when cells where incubated in normocapnic versus hypercapnic conditions for 24 hours, a marked decrease of the apical Na^+-permeability was detected, suggesting an immediate effect of CO_2 on the Na^+,K^+-ATPase and a delayed effect on ENaC in this system as postulated previously (Woollhead et al., 2007). Further experiments revealed that no change of mRNA-levels of all ENaC subunits occurred after 6 and 24 hour, pointing to a post-translational regulation as opposed to a change in gene-regulation. Unfortunately a pharmacological intervention with the AMPK-inhibitor Compound C even in a four fold lower concentration as published by others (Albert et al., 2008) and the proteasome-inhibitor MG-132 was not successful due to the much longer incubation times,

so there were no tools left to continue with functional experiments. Efficient transfection of H441 cells was not yet established so another system had to be used to study the effects of CO_2 on ENaC.

4.2. Molecular mechanism of CO_2-regulated ENaC function

The molecular basis of CO_2-mediated ENaC regulation was characterized in A549 cells. These cells are derived from a human alveolar cell carcinoma and contain multilamellar cytoplasmic inclusion bodies and secrete surfactant similar to primary ATII cells (Lieber et al., 1976). A549 cells are not ideal for functional alveolar epithelial barrier studies, for example Ussing chamber experiments, since they exhibit low transepithelial electrical resistance due to a reduced synthesis of tight-junction proteins such as *zona-occludens protein-1* (ZO-1) (Lehmann et al., 2011). But an extended range of mechanistic experiments is possible with this system, since genetic manipulation can be done easily.

In the present study A549 cells were used as recipients for epitope-tagged ENaC plasmids, since endogenous ENaC-proteins are difficult to detect using standard western blot techniques. In initial suudies, only the human ß-ENaC was cloned and modified with a small epitope V5-tag of the paramyxovirus *of simian virus 5* (SV5) for better antibody recognition. Some evidence from the literature suggests, that regulation of only ß-ENaC might be sufficient for a modulation of ENaC-function: In the human embryonic kidney cell line (HEK-293) activation of AMPK increased only the interaction of ß-ENaC with Nedd4-2, leading to reduced Na^+-transport (Bhalla et al., 2006). Further, overexpression of ß-ENaC alone, but not Ǔor ɔ in the mouse led to increased fluid reabsorption (Mall et al., 2004). Thus the rationale of the experiments described now was to produce an ENaC subunit that could be detected easily and to generally increase the protein levels of all ENaC subunits in the plasma membrane.

To investigate effects of hypercapnia, transfected cells were exposed to normocapnia and hypercapnia for 1 and 24 hours and the membrane as well as the whole cell abundance of ß-ENaC was determined. In line with the Ussing chamber experiments no change of ß-ENaC was detected after short term exposure to CO_2. After 24 hours of CO_2 a marked decrease of ß-ENaC in the cell membrane was observed that was not paralleled by a decrease of total ß-ENaC levels.

Also in line with the Ussing chamber experiments interference with the CO_2 induced signaling cascade using different drugs in ß-ENaC expressing A549 cells was not successful. Overexpression of single ENaC subunits compared to overexpression of the full

ŭɓɔ-ENaC might interfere with posttranscriptional modification and trafficking as reported by Hughey et al. for *Chinese hamster ovary* (CHO) and *Madin-Darby canine kidney type 1* (MDCK) cells (Hughey et al., 2003). To rule out effects of hypercapnia on the pore-forming ŭ- and the regulatory ɔ-subunit and effects that were limited to the fully functional ENaC complex, plasmids encoding these proteins modified with individual tags for the N- as well as the C-terminus were generated.

The coding sequence for ŭ-ENaC contained the two single-nucleotide polymorphisms A334T and T663A that were corrected before starting the actual experiments. Both polymorphisms are known, but especially T663A was important to correct, since degradation and activity of both polymorphisms seem to be different. A334T does not appear to change the physiologic properties of the channel (Tong et al., 2006; Yan et al., 2006). As demonstrated in the present study both polymorphisms have no effect on the size and posttranscriptional processing of ŭ-ENaC.

Next, all three ENaC subunits were cotransfected in A549 cells. ɓ-ENaC could be detected best, but the ŭ- and the ɔ-subunit were hardly detectable, especially in the membrane. Now, the ENaC subunits could be recognized by antibodies, but the expression level was extremely low and in most cases below the detection limit. In the kidney cell lines COS-7 and HEK-293 it has been demonstrated, that ENaC subunits form a complex that is largely insoluble in conventional detergent-based cell lysis buffers and that ENaC detection was largely improved, when the detergent-insoluble fraction was denatured in SDS and ɓ-mercaptoethanol containing buffer at 90 °C (Prince and Welsh, 1998). Also a trafficking of ENaC into lipid rafts in kidney cells of the mouse was reported, although the ratio of insoluble ENaC was smaller in that study compared to detergent-insoluble proteins (Hill et al., 2007).

In this study, the detergent insoluble fraction of the cell lysate of A549 cells was denatured as published previously (Prince and Welsh, 1998), but an insoluble complex composed of ŭɓɔ-ENaC could not be detected. Also an incorporation of ŭ-ENaC alone into lipid rafts that are solubilized by the protocol used could not be shown, indicating that differential solubility might be a feature of ENaC that is limited to renal cell lines.

Coexpression of all three ENaC-subunits in A549 cells was not succesful. To test whether ŭ-ENaC alone would be regulated during hypercapnia the half-life of ŭ-ENaC located in the plasma membrane was determined by pulse chase experiments which revealed a half-life of about two hours. Next, the stability of ŭ-ENaC located in the membrane was compared during normocapnia and hypercapnia in which a clear trend to reduction in

hypercapnia, compared to normocapnia, was evident, although no statistical significance was apparent.

Since the stability of ENaC is described to be markedly affected by its ubiquitin ligase Nedd4-2 (Kabra et al., 2008; Rotin and Staub, 2012; Staub et al., 2000) a genetic approach was chosen in which Nedd4-2 was downregulated by siRNA in A549 cells. Ŭ-ENaC was transfected two days later, to match its maximal expression with the time of best knockdown of Nedd4-2. Baseline degradation seems not to be critically dependent on Nedd4-2, since about 60 % of Ŭ-ENaC located in the membrane was degraded within four hours independently of the presence of Nedd4-2.

To sum up all experiments involving hypercapnia and A549 cells: ɓ-ENaC is down regulated after sustained hypercapnia by an unknown posttranslational mechanism, whereas Ŭ-ENaC might already be affected earlier, but definitive evidence is missing. Nedd4-2 does not seem to play an important role in ENaC degradation in A549 cells, neither under normal conditions nor during hypercapnia, at least not in the conditions that were used in this study.

4.3. Transfection of H441 cells – Seeking the right system

After the addition of the 27 kDa eYFP tag, the full size Ŭ-ENaC has a predicted size of about 120 kDa and two fragments of approximately 60 kDa when cleaved. Interestingly, only the bigger of the two detected bands (~ 100 and 120 kDa) for Ŭ-ENaC matched the predicted size. To complement the experiments that were performed in A549 cells, another cell line was used for further studies.

An alternative for A549 cells as recipients for genetically modified ENaC constructs are H441 cells. As mentioned above these cells were used for functional studies of ENaC activity, but transfection has been difficult and its efficiency in H441 cells has rarely been published. Low efficiencies of 5 ï 10 % were achieved by Polyfect transfection agent (Lazrak et al., 2009). Virus-mediated gene transfer has been reported to work very well, since lentiviral transduction reached an efficiency of up to 100 % (Aarbiou et al., 2012). But virus mediated gene transfer is associated with strict safety regulations and it is very time and labour intensive.

In the present study, a non-viral protocol was established to transfect H441 cells by Nucleofection. As shown by fluorescence microscopy and flow cytometry about 60 % of H441 cells expressed the eGFP encoded in the transfected control plasmid.

Using the generated ENaC plasmids encoding ŭɓɔ-subunits it was possible to transiently coexpress all three subunits in the same cells. Surprisingly the cleavage pattern of the ŭ-subunit (~ 45 and 130 kDa) was different from the one seen in A549 cells (~ 100 and 120 kDa), although the exact same plasmid was used for transfection. The predicted sizes for the eYFP-tag containing cleaved and full length forms are ~ 60 and 120 kDa based on the observations from Hughey and Carattino (Carattino et al., 2006; Hughey et al., 2004), so the pattern found in H441 cells hints more to a proteolytically activated form of ŭ-ENaC. Also the cleavage pattern of the ɔ-subunit was close to the predicted sizes of 76 and 97 kDa, indicating that the posttranslational processing of ENaC in H441 cells was more likely to function properly compared to A549 cells. However, membrane expression in H441 cells especially of the ŭ- and ɔ-subunit was extremely low, close to the detection limit, although large amounts of proteins were used for the pulldown. Despite extensive effort on optimization the system could not be fully applied to mechanistic experiments.

Identification of ENaC on the protein level and its interpretation is generally difficult. Results vary widely dependent on the type of cells that is used and the culture conditions. And even in the same cell type the sizes for ENaC subunits can be different. Possible explanations are different states of glycosylation and proteolysis. A brief overview about endogenous ENaC sizes that have been published is provided in **Table 24**.

Many investigators use overexpression of hetero- or homologous ENaC subunits, thus complicating the comparison of different studies. Westernblot results vary from many nonspecific bands and smears (Bhalla et al., 2006) to a single band for all forms of cotransfected ŭɓɔ-ENaC modified with the same epitope tag (Lee et al., 2009).

Table 24 Reported sizes [kDa] of endogenous ENaC in different cell types (n.d.: not detected)

Cell type	Species	α	β	γ	Publication
ATI/II	Rat	180-200			(Johnson et al., 2002)
H441	Human	65 / 67; 90-100	88		(Albert et al., 2008)
ATII	Rat	60; 90			(Frank et al., 2003)
ATII	Rat	65; 70-75; 97; 150	n.d.	150	(Lazrak et al., 2012)
A6	Xenopus	< 90	90	95	(Eaton et al., 2010)
A6	Xenopus	75; 150; 180	97	95	(Weisz et al., 2000)
A549 cells	Human	100; 120	100		present work
H441	Human	45; 130	100	76; 100	present work
ATII	Rat	120	100	n.d.	present work

4.4. Novel technique for transfection of primary alveolar epithelial cells

A549 and H441 cells are both immortalized cell lines that resemble alveolar epithelial cells, but show clear differences to freshly isolated primary cells (Lieber et al., 1976; Ramminger et al., 2004). So the most physiologic attempt to study the function of alveolar epithelia would be to use primary cells.

To combine the generated ENaC constructs with the advantage of primary cells, a novel technique was established to genetically manipulate primary rat alveolar epithelial type II (ATII) cells.

ATII cells are hard to transfect. This is basically due to two reasons: Primary alveolar cells do not proliferate, at least not to a significant extent and contain large amount of multilamellar bodies.

Only a very small fraction (0.5-1 %) of freshly isolated ATII cells has been reported to be proliferative (Kalina et al., 1993). Many transfection methods are based on the exposure of the nuclear machinery to the cytosol during mitosis (Kirton et al., 2013). One example that was also used in this thesis for A549 cells is lipofection, a lipid based transfection procedure that works well in rapidly dividing cell lines. This technique incorporates nucleic acids into liposomes that fuse with the cell membrane, thereby releasing the nucleic acids into the cytosol (Felgner et al., 1987). As shown in the present thesis the transfection rate by Lipofection is minimal.

Further, ATII cells contain a large amount of lamellar bodies. Even if siRNA or cDNA can be delivered to ATII cells, it is trapped and unable to translocate into the nucleus (Friend et al., 1996).

Two publications suggest that freshly isolated ATII cells take up ñnakedò siRNA without any additional treatment (Jain 1999, Jain 2001), but this technique has not been applied and published any further.

Adenovirus mediated gene transfer, the only efficient way to deliver nucleic acids to ATII cells, has been reported by several investigators (Berger et al., 2011; Factor et al., 1998; Roux et al., 2005; Vadász et al., 2012). The transfection efficiency ranges somewhere around 50 ï 60 %. But virus infection is associated with increased safety regulations and the preparation of the reagents is expensive and time consuming.

During the present study, an innovative transfection method has been established for ATII cells. The process called Nucleofection is based on electroporation and combines special nucleofection solutions with distinct electrical pulses to drive nucleic acids directly into the

nucleus of hard-to-transfect cell lines (Gresch et al., 2004). The best combination is specific for each cell type and has to be determined empirically.

For optimization purposes an GFP expressing vector was used, so that the successfully transfected cells could be identified by flow cytometry and fluorescence microscopy. After optimization the transfection efficiency was approximately 50 %. The determination of the transepithelial electrical resistance showed no significant reduction of monolayer integrity of transfected compared to untransfected cells. Immediately after Nucleofection a transient release of lactate-dehydrogenase was observed in cells that received the electrical pulse. This LDH release was limited to the transfection procedure and can be explained by the formation of pores in the cell membrane that enable entry of nucleic acids (Gresch et al., 2004). LDH release one day after Nucleofection showed no increased cell damage and also determination of viability two days after Nucleofection was not different from control cells as assessed by flow cytometry, indicating that the described procedure does not interfere with cell viability.

Nucleofection of rat ATII cells has already been published before, but the transfection efficiency for cells harvested from adult animals, as in the present study, was only ~ 13 %. The authors were using an earlier device and different solutions and electrical pulses (McCoy et al., 2006). The present study, which has been recently published in part (Grzesik et al., 2013), demonstrates for the first time highly efficient transfection of primary rat alveolar epithelial type II cells and thus represents an important advance in studying physiology of primary alveolar epithelial cells. The non-viral procedure is highly efficient, non-cytotoxic, fast and since the electrical properties of the plated cells were not impaired, which indicates that nucleofected ATII cells can be used in a variety of experimental settings, including electrophysiology.

The newly established Nucleofection protocol was finally used to transfect ATII cells with ENaC subunits. For convenience, the already described commercially available Ŭ- and ɔ-ENaC constructs (Origene) were used. Preliminary results show that the cell surface abundance of at least Ŭ- and ɓ-ENaC are drastically increased in ATII cells, compared to H441 cells. Thus, Nucleofection of epitope tagged ENaC-subunits into ATII cells could be the solution to overcome the poor detectability and low expression levels of ENaC in other systems.

5. Summary

Acute respiratory distress syndrome is a life threatening condition triggered by a variety of pulmonary and extrapulmonary causes, that is characterized by pulmonary edema and subsequently impaired gas exchange. Due to lung protective ventilation strategies, its treatment is often associated with systemic accumulation of CO_2, a condition termed permissive hypercapnia. Recent studies report a negative effect of CO_2 on alveolar fluid clearance, a process mediated by its two key elements the Na^+,K^+-ATPase and epithelial Na^+-channels (ENaCs). A reduced activity of the Na^+,K^+-ATPase during hypercapnia has already been demonstrated, but regulation of ENaC has never been directly linked to CO_2. Many molecular signaling events that are activated during hypercapnia are known to regulate ENaC function, so the present study aimed to generate and subsequently apply techniques to investigate a possible contribution of ENaC to the reduction of alveolar epithelial fluid transport upon hypercapnia.

ENaC function was studied in H441 cells by Ussing chamber experiments which revealed no significant regulation during short term hypercapnia, but a clear reduction of ENaC function during sustained hypercapnia.

To identify the signaling mechanism on the molecular level, epitope-tagged human ENaC constructs for the Ŭ-, ɓ- and ɔ-subunit were cloned and initially expressed in A549 cells. Exposition to hypercapnia up to 4 hours did not significantly reduce cell surface expression of the ENaC-subunits, but after 24 hours, a significant decrease of ɓ-ENaC was observed. Since the molecular sizes of Ŭ- and ɔ-ENaC expressed in A549 cells were differing from previously published studies, transfection of ENaC was continued in other cells. H441 cells are commonly used for ENaC studies, so their transfection was established, yielding an efficiency of about 60 %. The molecular sizes of transfected ENaC subunits matched the pattern that was expected, but expression levels were evanescent and too low for further experiments. Since ENaC detection in these two cell lines remained problematic, a novel methodology was applied. Since the primary site of ENaC expression in the lung are epithelial cells, rat primary alveolar epithelial cells type II were used as recipients for ENaC plasmids. Non-viral transfection of ATII cells has been inefficient in the past, but during the present study a protocol was generated to efficiently deliver nucleic acids to exactly this cell type. ENaC expression was largely increased in ATII cells, compared to the cell lines used, indicating that established system might be extremely useful for further studies involving ENaC turnover.

Thus, a new and highly relevant, non-viral transfection technique for primary alveolar epithelial type II cells was established, providing ground-breaking opportunities for future pulmonary research.

6. Zusammenfassung

Das Atemnotsyndrom des Erwachsenen ist eine lebensbedrohliche Erkrankung, ausgelöst durch eine Reihe von Faktoren, die direkt oder indirekt auf die Lunge einwirken . Charakteristisch für dieses Syndrom sind pulmonare Ödeme und daraus resultierend ein eingeschränkter Gasaustausch. Die daher benötigte künstliche Beatmung führt im Zuge von protektiven Beatmungsstrategien oft zu einer systemischen Anreicherung von CO_2 (Hyperkapnie). Einige Studien zeigen, dass erhöhte CO_2-Level den Flüssigkeitstransport der Lunge einschränken. Dieser aktive Prozess wird maßgeblich durch zwei Komponenten, die Na^+,K^+-ATPase und epitheliale Na^+-Kanäle (ENaCs), kontrolliert. Eine Beeinträchtigung der Na^+,K^+-ATPase durch CO_2 gezeigt, für ENaCs ist dies bislang nicht bekannt. Einige bekannte Regulatoren von ENaCs werden jedoch während Hyperkapnie aktiviert. Das Ziel der vorliegenden Arbeit war, Methoden zu etablieren und anzuwenden, die einen möglichen Einfluss von CO_2 auf ENaC zeigen.

Funktionelle Versuche wurden an H441-Zellen mit Ussing-Kammer-Messungen durchgeführt. Während akuter Hyperkapnie konnte keine signifikante Regulation von ENaC nachgewiesen werden, jedoch war die ENaC-Funktion bei anhaltender Hyperkapnie deutlich verringert.

Um die Signalwege auf molekularer Ebene zu untersuchen, wurde die Ŭ-, ɓ- und ɔ-Untereinheit des humanen ENaC kloniert, genetisch modifiziert und in A549 Zellen überexprimiert. Nach bis zu vierstündiger Hyperkapnie erfolgte keine Regulation von ENaC, jedoch wurde nach 24 Stunden eine deutlich verminderte Menge ɓ-ENaC in der Zellmembran nachgewiesen. Da die Größen von Ŭ- und ɔ-ENaC von den bisher publizierten abwichen, wurden weitere Versuche in H441 Zellen durchgeführt. Die Transfektion dieser Zelllinie wurde etabliert und erreichte eine Effizienz von ungefähr 60 %. Die posttranslationale Regulation der Ŭ- und ɔ-Untereinheiten, insbesondere die proteolytische Aktivierung funktionierten wie in der Literatur beschrieben, jedoch waren die Expressionslevel zu gering für weitere Versuche. In der Lunge werden ENaCs überwiegend in epithelialen Zellen exprimiert. Diese Zellen konnten bisher jedoch nicht effizient transfiziert werden, ohne Viren einzusetzen. In der vorliegenden Arbeit wurde jedoch eine effiziente Methode zur Transfektion von primären epithelialen Zellen der Ratte erarbeitet. Die Expression von transfizierten ENaC-Untereinheiten war in diesen Zellen deutlich erhöht, weswegen die Etablierung dieses Systems ausschlaggebend für weitere Versuche ist.

Die vorliegende Arbeit beschreibt daher zum ersten Mal die nicht-virale, effiziente Transfektion von primären alveolaren Zellen und liefert damit ein bedeutendes neues Werkzeug für die Lungenforschung.

7. Literature

Aarbiou, J., Copreni, E., Buijs-Offerman, R.M., van der Wegen, P., Castellani, S., Carbone, A., Tilesi, F., Fradiani, P., Hiemstra, P.S., Yueksekdag, G., et al. (2012). Lentiviral small hairpin RNA delivery reduces apical sodium channel activity in differentiated human airway epithelial cells. The Journal of Gene Medicine *14*, 733ï 745.

Adamson, I.Y., and Bowden, D.H. (1974). The type 2 cell as progenitor of alveolar epithelial regeneration. A cytodynamic study in mice after exposure to oxygen. Laboratory Investigation; a Journal of Technical Methods and Pathology *30*, 35ï 42.

Albert, A.P., Woollhead, a M., Mace, O.J., and Baines, D.L. (2008). AICAR decreases the activity of two distinct amiloride-sensitive Na^+-permeable channels in H441 human lung epithelial cell monolayers. American Journal of Physiology. Lung Cellular and Molecular Physiology *295*, L837ï 48.

Almaça, J., Kongsuphol, P., Hieke, B., Ousingsawat, J., Viollet, B., Schreiber, R., Amaral, M.D., and Kunzelmann, K. (2009). AMPK controls epithelial Na^+ channels through Nedd4-2 and causes an epithelial phenotype when mutated. Pflügers Archiv ز European Journal of Physiology *458*, 713ï 721.

Ashbaugh, D.G., Bigelow, D.B., Petty, T.L., and Levine, B.E. (1967). Acute respiratory distress in adults. Lancet *2*, 319ï 323.

Awayda, M.S., Ismailov, I.I., Berdiev, B.K., Fuller, C.M., and Benos, D.J. (1996). Protein kinase regulation of a cloned epithelial Na^+ channel. The Journal of General Physiology *108*, 49ï 65.

Awayda, M.S., Boudreaux, M.J., Reger, R.L., and Hamm, L.L. (2000). Regulation of the epithelial Na^+ channel by extracellular acidification. American Journal of Physiology. Cell Physiology.

Babini, E., Geisler, H.-S., Siba, M., and Gründer, S. (2003). A new subunit of the epithelial Na^+ channel identifies regions involved in Na^+ self-inhibition. The Journal of Biological Chemistry *278*, 28418ï 28426.

Bachofen, M., and Weibel, E.R. (1977). Alterations of the gas exchange apparatus in adult respiratory insufficiency associated with septicemia. The American Review of Respiratory Disease *116*, 589ï 615.

Bentley, P.J. (1968). Amiloride: a potent inhibitor of sodium transport across the toad bladder. The Journal of Physiology *195*, 317ï 330.

Berger, G., Guetta, J., Klorin, G., Badarneh, R., Braun, E., Brod, V., Saleh, N.A., Katz, A., Bitterman, H., and Azzam, Z.S. (2011). Sepsis impairs alveolar epithelial function by downregulating Na-K-ATPase pump. American Journal of Physiology. Lung Cellular and Molecular Physiology *301*, L23ï 30.

Bernard, G.R., Artigas, A., Brigham, K.L., Carlet, J., Falke, K., Hudson, L., Lamy, M., Legall, J.R., Morris, A., and Spragg, R. (1994). The American-European Consensus Conference on ARDS. Definitions, mechanisms, relevant outcomes, and clinical trial coordination. American Journal of Respiratory and Critical Care Medicine *149*, 818ï 824.

Bhalla, V., Oyster, N.M., Fitch, A.C., Wijngaarden, M. a, Neumann, D., Schlattner, U., Pearce, D., and Hallows, K.R. (2006). AMP-activated kinase inhibits the epithelial Na^+ channel through functional regulation of the ubiquitin ligase Nedd4-2. The Journal of Biological Chemistry *281*, 26159ï 26169.

Biehl, M., Kashiouris, M.G., and Gajic, O. (2013). Ventilator-Induced Lung Injury: Minimizing Its Impact in Patients With or at Risk for ARDS. Respiratory Care *58*, 927ï 937.

Blazer-Yost, B.L., Esterman, M. a, and Vlahos, C.J. (2003). Insulin-stimulated trafficking of ENaC in renal cells requires PI 3-kinase activity. American Journal of Physiology. Cell Physiology *284*, C1645ï 53.

Boncoeur, É., Tardif, V., Tessier, M., and Morneau, F. (2009). Modulation of epithelial sodium channel activity by lipopolysaccharide in alveolar type II cells ز Involvement of purinergic signaling. American Journal Of Physiology *8000*.

Boron, W.F. (2010). The Sharpey-Schafer Lecture: Gas Channels. Experimental Physiology.

Briel, M., Meade, M., Mercat, A., Brower, R.G., Talmor, D., Walter, S.D., Slutsky, A.S., Pullenayegum, E., Zhou, Q., Cook, D., et al. (2010). Higher vs lower positive end-expiratory pressure in patients with acute lung injury and acute respiratory distress syndrome: systematic review and meta-analysis. JAMAز the Journal of the American Medical Association *303*, 865ï 873.

Briva, A., Vadász, I., Lecuona, E., Welch, L.C., Chen, J., Dada, L.A., Trejo, H.E., Dumasius, V., Azzam, Z.S., Myrianthefs, P.M., et al. (2007). High CO_2 levels impair alveolar epithelial function independently of pH. PloS One *2*, e1238.

Brown, S.G., Gallacher, M., Olver, R.E., and Wilson, S.M. (2008). The regulation of selective and nonselective Na^+ conductances in H441 human airway epithelial cells. American Journal of Physiology. Lung Cellular and Molecular Physiology *294*, L942ï 54.

Buchäckert, Y., Rummel, S., Vohwinkel, C.U., Gabrielli, N.M., Grzesik, B.A., Mayer, K., Herold, S., Morty, R.E., Seeger, W., and Vadász, I. (2012). Megalin mediates transepithelial albumin clearance from the alveolar space of intact rabbit lungs. The Journal of Physiology *590*, 5167ï 5181.

Butterworth, M.B. (2010). Regulation of the epithelial sodium channel (ENaC) by membrane trafficking. Biochimica et Biophysica Acta *1802*, 1166ï 1177.

Canessa, C.M., Horisberger, J.D., and Rossier, B.C. (1993). Epithelial sodium channel related to proteins involved in neurodegeneration. Nature *361*, 467ï 470.

Canessa, C.M., Schild, L., Buell, G., Thorens, B., Gautschi, I., Horisberger, J.D., and Rossier, B.C. (1994). Amiloride-sensitive epithelial Na^+ channel is made of three homologous subunits. Nature *367*, 463ï 467.

Carattino, M.D., Edinger, R.S., Grieser, H.J., Wise, R., Neumann, D., Schlattner, U., Johnson, J.P., Kleyman, T.R., and Hallows, K.R. (2005). Epithelial sodium channel inhibition by AMP-activated protein kinase in oocytes and polarized renal epithelial cells. The Journal of Biological Chemistry *280*, 17608ï 17616.

Carattino, M.D., Sheng, S., Bruns, J.B., Pilewski, J.M., Hughey, R.P., and Kleyman, T.R. (2006). The epithelial Na^+ channel is inhibited by a peptide derived from proteolytic processing of its alpha subunit. The Journal of Biological Chemistry *281*, 18901ï 18907.

Carattino, M.D., Hughey, R.P., and Kleyman, T.R. (2008). Proteolytic processing of the epithelial sodium channel gamma subunit has a dominant role in channel activation. The Journal of Biological Chemistry *283*, 25290ï 25295.

Carlton, D.P., Cummings, J.J., Poulain, F.R., and Bland, R.D. (1992a). Increased pulmonary vascular filtration pressure does not alter lung liquid secretion in fetal sheep. Journal of Applied Physiology (Bethesda, Md.ز 1985) *72*, 650ï 655.

Carlton, D.P., Cummings, J.J., Chapman, D.L., Poulain, F.R., and Bland, R.D. (1992b). Ion transport regulation of lung liquid secretion in foetal lambs. Journal of Developmental Physiology *17*, 99ï 107.

Cassin, S., Gause, G., and Perks, A.M. (1986). The effects of bumetanide and furosemide on lung liquid secretion in fetal sheep. Proceedings of the Society for Experimental Biology and Medicine. Society for Experimental Biology and Medicine (New York, N.Y.) *181*, 427ï 431.

Caudrillier, A., Kessenbrock, K., Gilliss, B.M., Nguyen, J.X., Marques, M.B., Monestier, M., Toy, P., Werb, Z., and Looney, M.R. (2012). Platelets induce neutrophil extracellular traps in transfusion-related acute lung injury. The Journal of Clinical Investigation *122*, 2661ï 2671.

Chalfie, M., and Wolinsky, E. (1990). The identification and suppression of inherited neurodegeneration in Caenorhabditis elegans. Nature *345*, 410ï 416.

Chapman, H.A., Li, X., Alexander, J.P., Brumwell, A., Lorizio, W., Tan, K., Sonnenberg, A., Wei, Y., and Vu, T.H. (2011). Integrin Ŭб4 identifies an adult distal lung epithelial population with regenerative potential in mice. The Journal of Clinical Investigation *121*, 2855ï 2862.

Chen, England, S., Akopian, A.N., and Wood, J.N. (1998). A sensory neuron-specific, proton-gated ion channel. Proceedings of the National Academy of Sciences of the United States of America *95*, 10240ï 10245.

Chen, J., Lecuona, E., Briva, A., Welch, L.C., and Sznajder, J.I. (2008). Carbonic anhydrase II and alveolar fluid reabsorption during hypercapnia. American Journal of Respiratory Cell and Molecular Biology *38*, 32ï 37.

Chen, X.L., Nam, J.-O., Jean, C., Lawson, C., Walsh, C.T., Goka, E., Lim, S.-T., Tomar, A., Tancioni, I., Uryu, S., et al. (2012). VEGF-induced vascular permeability is mediated by FAK. Developmental Cell *22*, 146ï 157.

Cheng, I.W., Eisner, M.D., Thompson, B.T., Ware, L.B., and Matthay, M.A. (2005). Acute effects of tidal volume strategy on hemodynamics, fluid balance, and sedation in acute lung injury. Critical Care Medicine *33*, 63ï 70; discussion 239ï 40.

Clegg, G.R., Tyrrell, C., McKechnie, S.R., Beers, M.F., Harrison, D., and McElroy, M.C. (2005). Coexpression of RTI40 with alveolar epithelial type II cell proteins in lungs following injury: Identification of alveolar intermediate cell types. American Journal of Physiology. Lung Cellular and Molecular Physiology *289*, L382ï 90.

Collier, D.M., and Snyder, P.M. (2009). Extracellular protons regulate human ENaC by modulating Na^+ self-inhibition. The Journal of Biological Chemistry *284*, 792ï 798.

Connors, A.F., Dawson, N. V, Thomas, C., Harrell, F.E., Desbiens, N., Fulkerson, W.J., Kussin, P., Bellamy, P., Goldman, L., and Knaus, W.A. (1996). Outcomes following acute exacerbation of severe chronic obstructive lung disease. The SUPPORT investigators (Study to Understand Prognoses and Preferences for Outcomes and Risks of Treatments). American Journal of Respiratory and Critical Care Medicine *154*, 959ï 967.

Crapo, J.D., Barry, B.E., Gehr, P., Bachofen, M., and Weibel, E.R. (1982). Cell number and cell characteristics of the normal human lung. The American Review of Respiratory Disease *126*, 332ï 337.

Curley, G., Hayes, M., and Laffey, J.G. (2011). Can ñpermissiveò hypercapnia modulate the severity of sepsis-induced ALI/ARDS? Critical Care (London, England) *15*, 212.

Dada, L.A., Welch, L.C., Zhou, G., Ben-Saadon, R., Ciechanover, A., and Sznajder, J.I. (2007). Phosphorylation and ubiquitination are necessary for Na,K-ATPase endocytosis during hypoxia. Cellular Signalling *19*, 1893ï 1898.

Dagenais, A., Denis, C., Vives, M., Girouard, S., Nguyen, T., Yamagata, T., Grygorczyk, C., Berthiaume, Y., and Masse, C. (2008). Modulation of alpha-ENaC and alpha1-Na-K-ATPase by cAMP and dexamethasone in alveolar epithelial cells. Am J Physiol Lung Cell Mol Physiol 217ï 230.

Debonneville, C., Flores, S.Y., Kamynina, E., Plant, P.J., Tauxe, C., Thomas, M.A., Mu, C., Chraõ, A., Pearce, D., Lof, J., et al. (2001). Phosphorylation of Nedd4-2 by Sgk1 regulates epithelial Na^+ channel cell surface expression. EMBO Journal *20*, 7052ï 7059.

Deng, W., Li, C.-Y., Tong, J., Zhang, W., and Wang, D.-X. (2012). Regulation of ENaC-mediated alveolar fluid clearance by insulin via PI3K/Akt pathway in LPS-induced acute lung injury. Respiratory Research *13*, 29.

Dobbs, L.G. (1990). Isolation and culture of alveolar type II cells. Am J Physiol Lung Cell Mol Physiol *258*, L134ï L147.

Downs, C. a, Kumar, A., Kreiner, L.H., Johnson, N.M., and Helms, M.N. (2013). H_2O_2 regulates lung ENaC via ubiquitin-like protein Nedd8. The Journal of Biological Chemistry.

Eaton, D.C., Malik, B., Bao, H.-F., Yu, L., and Jain, L. (2010). Regulation of epithelial sodium channel trafficking by ubiquitination. Proceedings of the American Thoracic Society *7*, 54ï 64.

Edinger, R.S., Lebowitz, J., Li, H., Alzamora, R., Wang, H., Johnson, J.P., and Hallows, K.R. (2009). Functional regulation of the epithelial Na^+ channel by IkappaB kinase-beta occurs via phosphorylation of the ubiquitin ligase Nedd4-2. The Journal of Biological Chemistry *284*, 150ï 157.

Evans, M.J., Cabral, L.J., Stephens, R.J., and Freeman, G. (1973). Renewal of alveolar epithelium in the rat following exposure to NO_2. The American Journal of Pathology *70*, 175ï 198.

Factor, P., Saldias, F., Ridge, K., Dumasius, V., Zabner, J., Jaffe, H.A., Blanco, G., Barnard, M., Mercer, R., Perrin, R., et al. (1998). Augmentation of lung liquid clearance via adenovirus-mediated transfer of a Na,K-ATPase beta1 subunit gene. The Journal of Clinical Investigation *102*, 1421ï 1430.

Fang, X., Yang, B., Matthay, M. a, and Verkman, a S. (2002). Evidence against aquaporin-1-dependent CO_2 permeability in lung and kidney. The Journal of Physiology *542*, 63ï 69.

Farman, N., Talbot, C.R., Boucher, R., Fay, M., Canessa, C., Rossier, B., and Bonvalet, J.P. (1997). Noncoordinated expression of alpha-, beta-, and gamma-subunit mRNAs of epithelial Na^+ channel along rat respiratory tract. American Journal of Physiology - Cell Physiology *272* , C131ï C141.

Feihl, F., and Perret, C. (1994). Permissive hypercapnia. How permissive should we be? American Journal of Respiratory and Critical Care Medicine *150*, 1722ï 1737.

Felgner, P.L., Gadek, T.R., Holm, M., Roman, R., Chan, H.W., Wenz, M., Northrop, J.P., Ringold, G.M., and Danielsen, M. (1987). Lipofection: a highly efficient, lipid-mediated DNA-transfection procedure. Proceedings of the National Academy of Sciences of the United States of America *84*, 7413ï 7417.

Firsov, D., Gautschi, I., Merillat, a M., Rossier, B.C., and Schild, L. (1998). The heterotetrameric architecture of the epithelial sodium channel (ENaC). The EMBO Journal *17*, 344ï 352.

Frank, J., Roux, J., Kawakatsu, H., Su, G., Dagenais, A., Berthiaume, Y., Howard, M., Canessa, C.M., Fang, X., Sheppard, D., et al. (2003). Transforming growth factor-beta1 decreases expression of the epithelial sodium channel alphaENaC and alveolar epithelial vectorial sodium and fluid transport via an ERK1/2-dependent mechanism. The Journal of Biological Chemistry *278*, 43939ï 43950.

Friend, D.S., Papahadjopoulos, D., and Debs, R.J. (1996). Endocytosis and intracellular processing accompanying transfection mediated by cationic liposomes. Biochimica et Biophysica Acta *1278*, 41ï 50.

Fronius, M., Bogdan, R., Althaus, M., Morty, R.E., and Clauss, W.G. (2010). Epithelial Na^+ channels derived from human lung are activated by shear force. Respiratory Physiology & Neurobiology *170*, 113ï 119.

Fuchs, W., Larsen, E.H., and Lindemann, B. (1977). Current-voltage curve of sodium channels and concentration dependence of sodium permeability in frog skin. The Journal of Physiology *267*, 137ï 166.

Fujino, N., Kubo, H., Suzuki, T., Ota, C., Hegab, A.E., He, M., Suzuki, S., Suzuki, T., Yamada, M., Kondo, T., et al. (2011). Isolation of alveolar epithelial type II progenitor cells from adult human lungs. Laboratory Investigation; a Journal of Technical Methods and Pathology *91*, 363ï 378.

Fuller, C.M., Awayda, M.S., Arrate, M.P., Bradford, A.L., Morris, R.G., Canessa, C.M., Rossier, B.C., and Benos, D.J. (1995). Cloning of a bovine renal epithelial Na^+ channel subunit. The American Journal of Physiology *269*, C641ï 54.

Gambling, L., Dunford, S., Wilson, C. a, McArdle, H.J., and Baines, D.L. (2004). Estrogen and progesterone regulate alpha, beta, and gammaENaC subunit mRNA levels in female rat kidney. Kidney International *65*, 1774ï 1781.

Gates, K.L., Wang, N., Nair, A., Sznajder, J.I., and Sporn, P.H.S. (2011). Hypercapnia Inhibits Bacterial Phagocytosis And Reactive Oxygen Species Generation In Neutrophils. American Journal of Respiratory and Critical Care Medicine *183*, A1793 [abstract].

Gentzsch, M., Dang, H., Dang, Y., Garcia-Caballero, A., Suchindran, H., Boucher, R.C., and Stutts, M.J. (2010). The cystic fibrosis transmembrane conductance regulator impedes proteolytic stimulation of the epithelial Na^+ channel. The Journal of Biological Chemistry *285*, 32227ï 32232.

Goldstein, O., Asher, C., and Garty, H. (1997). Cloning and induction by low NaCl intake of avian intestine Na^+ channel subunits. Am J Physiol Cell Physiol *272*, C270ï 277.

Gottardi, C.J., Dunbar, L.A., and J, C. (1995). Biotinylation and essessment of membrane polarity: caveats and methodological concerns. American Journal of Physiology. Renal Physiology *262*, F285ï 95.

Gresch, O., Engel, F.B., Nesic, D., Tran, T.T., England, H.M., Hickman, E.S., Körner, I., Gan, L., Chen, S., Castro-Obregon, S., et al. (2004). New non-viral method for gene transfer into primary cells. Methods (San Diego, Calif.) *33*, 151ï 163.

Grzesik, B.A., Vohwinkel, C.U., Morty, R.E., Mayer, K., Herold, S., Seeger, W., and Vadász, I. (2013). Efficient gene delivery to primary alveolar epithelial cells by nucleofection. American Journal of Physiology. Lung Cellular and Molecular Physiology.

Guérin, C., Reignier, J., Richard, J.-C., Beuret, P., Gacouin, A., Boulain, T., Mercier, E., Badet, M., Mercat, A., Baudin, O., et al. (2013). Prone positioning in severe acute respiratory distress syndrome. The New England Journal of Medicine *368*, 2159ï 2168.

Günther, A., Ruppert, C., Schmidt, R., Markart, P., Grimminger, F., Walmrath, D., and Seeger, W. (2001). Surfactant alteration and replacement in acute respiratory distress syndrome. Respiratory Research *2*, 353ï 364.

Hallows, K.R., Bhalla, V., Oyster, N.M., Wijngaarden, M.A., Lee, J.K., Li, H., Chandran, S., Xia, X., Huang, Z., Chalkley, R.J., et al. (2010). Phosphopeptide screen uncovers novel phosphorylation sites of Nedd4-2 that potentiate its inhibition of the epithelial Na^+ channel. The Journal of Biological Chemistry *285*, 21671ï 21678.

Hanwell, D., Ishikawa, T., Saleki, R., and Rotin, D. (2002). Trafficking and cell surface stability of the epithelial Na^+ channel expressed in epithelial Madin-Darby canine kidney cells. The Journal of Biological Chemistry *277*, 9772ï 9779.

Helenius, I.T., Krupinski, T., Turnbull, D.W., Gruenbaum, Y., Silverman, N., Johnson, E.A., Sporn, P.H.S., Sznajder, J.I., and Beitel, G.J. (2009). Elevated CO_2 suppresses specific Drosophila innate immune responses and resistance to bacterial infection. Proceedings of the National Academy of Sciences of the United States of America *106*, 18710ï 18715.

Helms, M.N., Jain, L., Self, J.L., and Eaton, D.C. (2008). Redox regulation of epithelial sodium channels examined in alveolar type 1 and 2 cells patch-clamped in lung slice tissue. The Journal of Biological Chemistry *283*, 22875ï 22883.

Herwig, M.C., Tsokos, M., Hermanns, M.I., Kirkpatrick, C.J., and Müller, A.M. (2013). Vascular endothelial cadherin expression in lung specimens of patients with sepsis-induced acute respiratory distress syndrome and endothelial cell cultures. Pathobiology ز Journal of Immunopathology, Molecular and Cellular Biology *80*, 245ï 251.

Hickling, K.G., Walsh, J., Henderson, S., and Jackson, R. (1994). Low mortality rate in adult respiratory distress syndrome using low-volume, pressure-limited ventilation with permissive hypercapnia: a prospective study. Critical Care Medicine *22*, 1568ï 1578.

Higgins, B.D., Ph, D., Costello, J., and Contreras, M. (2009). Differential Effects of Buffered Hypercapnia versus Hypercapnic Acidosis on Shock and Lung Injury Induced by Systemic Sepsis. Anesthesiology *111*, 1317ï 1326.

Hill, W.G., Butterworth, M.B., Wang, H., Edinger, R.S., Lebowitz, J., Peters, K.W., Frizzell, R. a, and Johnson, J.P. (2007). The epithelial sodium channel (ENaC) traffics to apical membrane in lipid rafts in mouse cortical collecting duct cells. The Journal of Biological Chemistry *282*, 37402ï 37411.

Hong, K., and Driscoll, M. (1994). A transmembrane domain of the putative channel subunit MEC-4 influences mechanotransduction and neurodegeneration in C. elegans. Nature *367*, 470ï 473.

Huang, M., and Chalfie, M. (1994). Gene interactions affecting mechanosensory transduction in Caenorhabditis elegans. Nature *367*, 467ï 470.

Hughey, R.P., Mueller, G.M., Bruns, J.B., Kinlough, C.L., Poland, P. a, Harkleroad, K.L., Carattino, M.D., and Kleyman, T.R. (2003). Maturation of the epithelial Na+ channel involves proteolytic processing of the alpha- and gamma-subunits. The Journal of Biological Chemistry *278*, 37073ï 37082.

Hughey, R.P., Bruns, J.B., Kinlough, C.L., Harkleroad, K.L., Tong, Q., Carattino, M.D., Johnson, J.P., Stockand, J.D., and Kleyman, T.R. (2004). Epithelial sodium channels are activated by furin-dependent proteolysis. The Journal of Biological Chemistry *279*, 18111ï 18114.

Itani, O. a, Stokes, J.B., and Thomas, C.P. (2009). Nedd4ï 2 isoforms differentially associate with ENaC and regulate its activity. Renal Physiology *289*, 334ï 346.

Jain, L., Chen, X.J., Malik, B., Al-Khalili, O., and Eaton, D.C. (1999). Antisense oligonucleotides against the alpha-subunit of ENaC decrease lung epithelial cation-channel activity. The American Journal of Physiology *276*, L1046ï 51.

Jain, L., Chen, X., Ramosevac, S., Brown, L.A., and C, D. (2008). Expression of highly selective sodium channels in alveolar type II cells is determined by culture conditions. Society 646ï 658.

Ji, H.-L., Zhao, R.-Z., Chen, Z.-X., Shetty, S., Idell, S., and Matalon, S. (2012). ŭ ENaC: A Novel Divergent Amiloride-Inhibitable Sodium Channel. American Journal of Physiology. Lung Cellular and Molecular Physiology.

Jiao, G., Li, E., and Yu, R. (2002). Decreased expression of AQP1 and AQP5 in acute injured lungs in rats. Chinese Medical Journal *115*, 963ï 967.

Johnson, M.D., Widdicombe, J.H., Allen, L., Barbry, P., and Dobbs, L.G. (2002). Alveolar epithelial type I cells contain transport proteins and transport sodium, supporting an active role for type I cells in regulation of lung liquid homeostasis. Proceedings of the National Academy of Sciences of the United States of America *99*, 1966ï 1971.

Kabra, R., Knight, K.K., Zhou, R., and Snyder, P.M. (2008). Nedd4-2 induces endocytosis and degradation of proteolytically cleaved epithelial Na^+ channels. The Journal of Biological Chemistry *283*, 6033ï 6039.

Kalina, M., Riklis, S., and Blau, H. (1993). Pulmonary epithelial cell proliferation in primary culture of alveolar type II cells. Experimental Lung Research *19*, 153ï 175.

Kawada, H., Shannon, J.M., and Mason, R.J. (1990). Improved maintenance of adult rat alveolar type II cell differentiation in vitro: effect of serum-free, hormonally defined medium and a reconstituted basement membrane. American Journal of Respiratory Cell and Molecular Biology *3*, 33ï 43.

King, L.S., and Agre, P. (2001). Man Is not a rodent: aquaporins in the airways. American Journal of Respiratory Cell and Molecular Biology *24*, 221ï 223.

King, L.S., Nielsen, S., Agre, P., and Brown, R.H. (2002). Decreased pulmonary vascular permeability in aquaporin-1-null humans. Proceedings of the National Academy of Sciences of the United States of America *99*, 1059ï 1063.

Kirton, H.M., Pettinger, L., and Gamper, N. (2013). Transient overexpression of genes in neurons using nucleofection. Methods in Molecular Biology (Clifton, N.J.) *998*, 55ï 64.

Knight, K.K., Wentzlaff, D.M., and Snyder, P.M. (2008). Intracellular sodium regulates proteolytic activation of the epithelial sodium channel. The Journal of Biological Chemistry *283*, 27477ï 27482.

Komwatana, P., Dinudom, A., Young, J.A., and Cook, D.I. (1996). Cytosolic Na^+ controls and epithelial Na^+ channel via the Go guanine nucleotide-binding regulatory protein. Proceedings of the National Academy of Sciences of the United States of America *93*, 8107ï 8111.

Kosari, F., Sheng, S., Li, J., Mak, D.O., Foskett, J.K., and Kleyman, T.R. (1998). Subunit stoichiometry of the epithelial sodium channel. The Journal of Biological Chemistry *273*, 13469ï 13474.

Lai, C.C., Hong, K., Kinnell, M., Chalfie, M., and Driscoll, M. (1996). Sequence and transmembrane topology of MEC-4, an ion channel subunit required for mechanotransduction in Caenorhabditis elegans. The Journal of Cell Biology *133*, 1071ï 1081.

Lazrak, A., Iles, K.E., Liu, G., Noah, D.L., Noah, J.W., Matalon, S., and Communication, R. (2009). Influenza virus M2 protein inhibits epithelial sodium channels by increasing reactive oxygen species. The FASEB Journalز Official Publication of the Federation of American Societies for Experimental Biology *23*, 3829ï 3842.

Lazrak, A., Chen, L., Jurkuvenaite, A., Doran, S.F., Liu, G., Li, Q., Lancaster, J.R., and Matalon, S. (2012). Regulation of alveolar epithelial Na^+ channels by ERK1/2 in chlorine-breathing mice. American Journal of Respiratory Cell and Molecular Biology *46*, 342ï 354.

Lee, I.-H., Campbell, C.R., Cook, D.I., and Dinudom, A. (2008). Regulation of epithelial Na^+ channels by aldosterone: role of Sgk1. Clinical and Experimental Pharmacology & Physiology *35*, 235ï 241.

Lee, I.-H., Campbell, C.R., Song, S.-H., Day, M.L., Kumar, S., Cook, D.I., and Dinudom, A. (2009). The activity of the epithelial sodium channels is regulated by caveolin-1 via a Nedd4-2-dependent mechanism. The Journal of Biological Chemistry *284*, 12663ï 12669.

Lehmann, A.D., Daum, N., Bur, M., Lehr, C.-M., Gehr, P., and Rothen-Rutishauser, B.M. (2011). An in vitro triple cell co-culture model with primary cells mimicking the human alveolar epithelial barrier. European Journal of Pharmaceutics and Biopharmaceuticsز Official Journal of Arbeitsgemeinschaft Für Pharmazeutische Verfahrenstechnik e.V *77*, 398ï 406.

Letz, B., Ackermann, A., Canessa, C.M., Rossier, B.C., and Korbmacher, C. (1995). Amiloride-sensitive sodium channels in confluent M-1 mouse cortical collecting duct cells. The Journal of Membrane Biology *148*, 127ï 141.

Lewis, S.A., Eaton, D.C., Clausen, C., and Diamond, J.M. (1977). Nystatin as a probe for investigating the electrical properties of a tight epithelium. The Journal of General Physiology *70*, 427ï 440.

Li, X.J., Xu, R.H., Guggino, W.B., and Snyder, S.H. (1995). Alternatively spliced forms of the alpha subunit of the epithelial sodium channel: distinct sites for amiloride binding and channel pore. Molecular Pharmacology *47*, 1133ï 1140.

Lieber, M., Smith, B., Szakal, A., Nelson-rees, W., and Todaro, G. (1976). A continuous tumor-cell line from a human lung carcinoma with properties of type II alveolar epithelial cells. Leukemia and Lymphoma *70*, 62ï 70.

Lingueglia, E., de Weille, J.R., Bassilana, F., Heurteaux, C., Sakai, H., Waldmann, R., and Lazdunski, M. (1997). A modulatory subunit of acid sensing ion channels in brain and dorsal root ganglion cells. The Journal of Biological Chemistry *272*, 29778ï 29783.

Looney, M.R., Nguyen, J.X., Hu, Y., Ziffle, J.A. Van, Lowell, C.A., Matthay, M.A., and Van Ziffle, J.A. (2009). Platelet depletion and aspirin treatment protect mice in a two-event model of transfusion-related acute lung injury. The Journal of Clinical Investigation *119*, 3450ï 3461.

Malik, B., Yue, Q., Yue, G., Chen, X.J., Price, S.R., Mitch, W.E., and Eaton, D.C. (2005). Role of Nedd4-2 and polyubiquitination in epithelial sodium channel degradation in untransfected renal A6 cells expressing endogenous ENaC subunits. American Journal of Physiology. Renal Physiology *289*, F107ï 16.

Malik, B., Price, S.R., Mitch, W.E., Yue, Q., and Eaton, D.C. (2006). Regulation of epithelial sodium channels by the ubiquitin-proteasome proteolytic pathway. American Journal of Physiology. Renal Physiology *290*, F1285ï 94.

Mall, M., Grubb, B.R., Harkema, J.R., OôNeal, W.K., and Boucher, R.C. (2004). Increased airway epithelial Na^+ absorption produces cystic fibrosis-like lung disease in mice. Nature Medicine *10*, 487ï 493.

Mano, I., and Driscoll, M. (1999). DEG/ENaC channels: a touchy superfamily that watches its salt. Bioessays *21*, 568ï 578.

Masilamani, S., Kim, G., Mitchell, C., Wade, J.B., and Knepper, M.A. (1999). Aldosterone-mediated regulation of ENaC. Journal of Clinical Investigation *104*, 19ï 23.

Matthay, M. a, Folkesson, H.G., and Clerici, C. (2002). Lung epithelial fluid transport and the resolution of pulmonary edema. Physiological Reviews *82*, 569ï 600.

Matthay, M.A., Ware, L.B., and Zimmerman, G.A. (2012). The acute respiratory distress syndrome. The Journal of Clinical Investigation *122*, 2731ï 2740.

McCoy, D.M., Fisher, K., Robichaud, J., Ryan, A.J., and Mallampalli, R.K. (2006). Transcriptional regulation of lung cytidylyltransferase in developing transgenic mice. American Journal of Respiratory Cell and Molecular Biology *35*, 394ï 402.

Musa-Aziz, R., Chen, L.-M., Pelletier, M.F., and Boron, W.F. (2009). Relative CO2/NH3 selectivities of AQP1, AQP4, AQP5, AmtB, and RhAG. Proceedings of the National Academy of Sciences of the United States of America *106*, 5406ï 5411.

Mutlu, G.M., Factor, P., Schwartz, D.E., and Sznajder, J.I. (2002). Severe status asthmaticus: management with permissive hypercapnia and inhalation anesthesia. Critical Care Medicine *30*, 477ï 480.

Myerburg, M.M., King, J.D., Oyster, N.M., Fitch, A.C., Magill, A., Baty, C.J., Watkins, S.C., Kolls, J.K., Pilewski, J.M., and Hallows, K.R. (2010). AMPK Agonists Ameliorate Sodium and Fluid Transport and Inflammation in Cystic Fibrosis Airway Epithelial Cells. American Journal of Respiratory Cell and Molecular Biology *42*, 676ï 684.

Natalini, G., Minelli, C., Rosano, A., Ferretti, P., Militano, C.R., De Feo, C., and Bernardini, A. (2013). Cardiac index and oxygen delivery during low and high tidal volume ventilation strategies in patients with acute respiratory distress syndrome: a crossover randomized clinical trial. Critical Care (London, England) *17*, R146.

Nuckton, T.J., Alonso, J.A., Kallet, R.H., Daniel, B.M., Pittet, J.-F., Eisner, M.D., and Matthay, M.A. (2002). Pulmonary dead-space fraction as a risk factor for death in the acute respiratory distress syndrome. The New England Journal of Medicine *346*, 1281ï 1286.

OôCroinin, D.F., Nichol, A.D., Hopkins, N., Boylan, J., OôBrien, S., OôConnor, C., Laffey, J.G., and McLoughlin, P. (2008). Sustained hypercapnic acidosis during pulmonary infection increases bacterial load and worsens lung injury. Critical Care Medicine *36*, 2128ï 2135.

OôToole, D., Hassett, P., Contreras, M., Higgins, B.D., McKeown, S.T.W., McAuley, D.F., OôBrien, T., and Laffey, J.G. (2009). Hypercapnic acidosis attenuates pulmonary epithelial wound repair by an NF-kappaB dependent mechanism. Thorax *64*, 976ï 982.

Olver, R.E., and Strang, L.B. (1974). Ion fluxes across the pulmonary epithelium and the secretion of lung liquid in the foetal lamb. The Journal of Physiology *241*, 327ï 357.

Opitz, B., Laak, V. Van, Eitel, J., and Suttorp, N. (2010). State of the Art Innate Immune Recognition in Infectious and Noninfectious Diseases of the Lung. *181*, 1294ï 1309.

Palmer, L.G. (1992). Epithelial Na channels: Function and diversity. Annual Review of Physiology *54*, 51ï 66.

Parsons, P.E., Eisner, M.D., Thompson, B.T., Matthay, M.A., Ancukiewicz, M., Bernard, G.R., and Wheeler, A.P. (2005). Lower tidal volume ventilation and plasma cytokine markers of inflammation in patients with acute lung injury. Critical Care Medicine *33*, 1ï 6; discussion 230ï 2.

Press, E.B., Dobbs, L.G., Mason, R.J., Williams, M.C., Benson, B.J., and Sueishi, K. (1982). Secretion of surfactant by primary cultures of alveolar type II cells isolated from rats. Culture *13*, 118ï 127.

Prince, L.S., and Welsh, M.J. (1998). Cell surface expression and biosynthesis of epithelial Na^+ channels. The Biochemical Journal *336 (Pt 3*, 705ï 710.

Ramminger, S.J., Richard, K., Inglis, S.K., Land, S.C., Olver, R.E., and Wilson, S.M. (2004). A regulated apical Na^+ conductance in dexamethasone-treated H441 airway epithelial cells. American Journal of Physiology. Lung Cellular and Molecular Physiology *287*, L411ï L419.

Randrianarison, N., Clerici, C., Ferreira, C., Pradervand, S., Fowler-jaeger, N., Hummler, E., Bernard, C., Planès, C., Fontayne, A., Rossier, B.C., et al. (2008). Low expression of the beta-ENaC subunit impairs lung fluid clearance in the mouse. 409ï 416.

Ranieri, V.M. (1999). Effect of Mechanical Ventilation on Inflammatory Mediators in Patients With Acute Respiratory Distress Syndrome: A Randomized Controlled Trial. JAMA: The Journal of the American Medical Association *282*, 54ï 61.

Ranieri, V.M., Giunta, F., Suter, P.M., and Slutsky, A.S. (2000). Mechanical ventilation as a mediator of multisystem organ failure in acute respiratory distress syndrome. JAMAز the Journal of the American Medical Association *284*, 43ï 44.

Ranieri, V.M., Rubenfeld, G.D., Thompson, B.T., Ferguson, N.D., Caldwell, E., Fan, E., Camporota, L., and Slutsky, A.S. (2012). Acute respiratory distress syndrome: the Berlin Definition. JAMAز the Journal of the American Medical Association *307*, 2526ï 2533.

Renard, S., Lingueglia, E., Voilley, N., Lazdunski, M., and Barbry, P. (1994). Biochemical analysis of the membrane topology of the amiloride-sensitive Na^+ channel. The Journal of Biological Chemistry *269*, 12981ï 12986.

Rotin, D., and Staub, O. (2012). Nedd4-2 and the regulation of epithelial sodium transport. Frontiers in Physiology *3*, 212.

Roux, J., Kawakatsu, H., Gartland, B., Pespeni, M., Sheppard, D., Matthay, M. a, Canessa, C.M., and Pittet, J.-F. (2005). Interleukin-1beta decreases expression of the epithelial sodium channel alpha-subunit in alveolar epithelial cells via a p38 MAPK-dependent signaling pathway. The Journal of Biological Chemistry *280*, 18579ï 18589.

Rubenfeld, G.D., and Herridge, M.S. (2007). Epidemiology and outcomes of acute lung injury. Chest *131*, 554ï 562.

Ruffieux-Daidie, D., and Staub, O. (2010). Intracellular ubiquitylation of the epithelial Na^+ channel controls extracellular proteolytic channel activation via conformational change. The Journal of Biological Chemistry *2*.

Ryu, J., Haddad, G., and Carlo, W.A. (2012). Clinical effectiveness and safety of permissive hypercapnia. Clinics in Perinatology *39*, 603ï 612.

Santa Cruz, R., Rojas, J.I., Nervi, R., Heredia, R., and Ciapponi, A. (2013). High versus low positive end-expiratory pressure (PEEP) levels for mechanically ventilated adult patients with acute lung injury and acute respiratory distress syndrome. Cochrane Database of Systematic Reviews (Online) *6*, CD009098.

Sheikh, H.S., Tiangco, N.D., Harrell, C., and Vender, R.L. (2011). Severe hypercapnia in critically ill adult cystic fibrosis patients. Journal of Clinical Medicine Research *3*, 209ï 212.

Sheng, S., Carattino, M.D., Bruns, J.B., Hughey, R.P., and Kleyman, T.R. (2006). Furin cleavage activates the epithelial Na+ channel by relieving Na^+ self-inhibition. American Journal of Physiology. Renal Physiology *290*, F1488ï 96.

Shi, H., Asher, C., Chigaev, A., Yung, Y., Reuveny, E., Seger, R., and Garty, H. (2002). Interactions of beta and gamma ENaC with Nedd4 can be facilitated by an ERK-mediated phosphorylation. The Journal of Biological Chemistry *277*, 13539ï 13547.

Shimkets, R. a, Lifton, R., and Canessa, C.M. (1998). In vivo phosphorylation of the epithelial sodium channel. Proceedings of the National Academy of Sciences of the United States of America *95*, 3301ï 3305.

Snyder, P.M., Cheng, C., Prince, L.S., Rogers, J.C., and Welsh, M.J. (1998). Electrophysiological and biochemical evidence that DEG/ENaC cation channels are composed of nine subunits. The Journal of Biological Chemistry *273*, 681ï 684.

Song, J.H., Tse, M.C.L., Bellail, A., Phuphanich, S., Khuri, F., Kneteman, N.M., and Hao, C. (2007). Lipid rafts and nonrafts mediate tumor necrosis factor related apoptosis-inducing ligand induced apoptotic and nonapoptotic signals in non small cell lung carcinoma cells. Cancer Research *67*, 6946ï 6955.

Soukup, B., Benjamin, A., Orogo-Wenn, M., and Walters, D. (2012). Physiological effect of protein kinase C on ENaC-mediated lung liquid regulation in the adult rat lung. American Journal of Physiology. Lung Cellular and Molecular Physiology *302*, L133ï 9.

Sporn, P.H.S., Nair, A., Gates, K.L., Andreeva, A. V, and Wang, N. (2011). Hypercapnia Selectively Modulates Gene Expression In Lipopolysaccharide-Stimulated Macrophages. American Journal of Respiratory and Critical Care Medicine *183*, A2907 [abstract].

Staub, O., Gautschi, I., Ishikawa, T., Breitschopf, K., Ciechanover, A., Schild, L., and Rotin, D. (1997). Regulation of stability and function of the epithelial Na^+ channel (ENaC) by ubiquitination. EMBO J *16*, 6325±6336.

Staub, O., Abriel, H., Plant, P., Ishikawa, T., Kanelis, V., Saleki, R., Horisberger, J.D., Schild, L., and Rotin, D. (2000). Regulation of the epithelial Na^+ channel by Nedd4 and ubiquitination. Kidney International *57*, 809ï 815.

Stewart, A.P., Haerteis, S., Diakov, A., Korbmacher, C., and Edwardson, J.M. (2011). Atomic force microscopy reveals the architecture of the epithelial sodium channel (ENaC). The Journal of Biological Chemistry *286*, 31944ï 31952.

Stockand, J.D., Bao, H.F., Schenck, J., Malik, B., Middleton, P., Schlanger, L.E., and Eaton, D.C. (2000). Differential effects of protein kinase C on the levels of epithelial Na^+ channel subunit proteins. The Journal of Biological Chemistry *275*, 25760ï 25765.

Su, A.I., Wiltshire, T., Batalov, S., Lapp, H., Ching, K.A., Block, D., Zhang, J., Soden, R., Hayakawa, M., Kreiman, G., et al. (2004). A gene atlas of the mouse and human protein-encoding transcriptomes. Proceedings of the National Academy of Sciences of the United States of America *101*, 6062ï 6067.

Talbot, C.L., Bosworth, D.G., Briley, E.L., Fenstermacher, D.A., Boucher, R.C., Gabriel, S.E., and Barker, P.M. (1999). Quantitation and localization of ENaC subunit expression in fetal, newborn, and adult mouse lung. American Journal of Respiratory Cell and Molecular Biology *20*, 398ï 406.

Tamarapu Parthasarathy, P., Galam, L., Huynh, B., Yunus, A., Abuelenen, T., Castillo, A., Kollongod Ramanathan, G., Cox, R., and Kolliputi, N. (2012). MicroRNA 16 modulates epithelial sodium channel in human alveolar epithelial cells. Biochemical and Biophysical Research Communications *426*, 203ï 208.

Tavernarakis, N., Shreffler, W., Wang, S., and Driscoll, M. (1997). unc-8, a DEG/ENaC family member, encodes a subunit of a candidate mechanically gated channel that modulates C. elegans locomotion. Neuron *18*, 107ï 119.

Taylor, A.E., and Gaar, K.A. (1970). Estimation of equivalent pore radii of pulmonary capillary and alveolar membranes. The American Journal of Physiology *218*, 1133ï 1140.

The Acute Respiratory Distress Syndrome Network (2000). Ventilation with lower tidal volumes as compared with traditional tidal volumes for acute lung injury and the acute respiratory distress syndrome. The New England Journal of Medicine *342*, 1301ï 1308.

The National Heart, Lung, and B.I.A.R.D.S. (ARDS) C.T.N. (2006). Comparison of Two Fluid-Management Strategies in Acute Lung Injury. The New England Journal of Medicine *354*, 2564ï 2575.

Tong, Q., Menon, A.G., and Stockand, J.D. (2006). Functional polymorphisms in the alpha-subunit of the human epithelial Na^+ channel increase activity. American Journal of Physiology. Renal Physiology *290*, F821ï 7.

Uchida, T., and Clerici, C. (2002). Hypoxia and beta2 -Agonists Regulate Cell Surface Expression of the Epithelial Sodium Channel in Native Alveolar Epithelial Cells*. Biochemistry *277*, 47318 ï 47324.

Uchiyama, T., Fujita, T., Gukasyan, H.J., Kim, K.-J., Borok, Z., Crandall, E.D., and Lee, V.H.L. (2008). Functional characterization and cloning of amino acid transporter B(0,+) (ATB(0,+)) in primary cultured rat pneumocytes. Journal of Cellular Physiology *214*, 645ï 654.

Vadász, I., Dada, L.A., Briva, A., Trejo, H.E., Welch, L.C., Chen, J., Tóth, P.T., Lecuona, E., Witters, L.A., Schumacker, P.T., et al. (2008). AMP-activated protein kinase regulates CO_2 -induced alveolar epithelial dysfunction in rats and human cells by promoting Na,K-ATPase endocytosis. Online *118*.

Vadász, I., Dada, L.A., Briva, A., Helenius, I.T., Sharabi, K., Welch, L.C., Kelly, A.M., Grzesik, B.A., Budinger, G.R.S., Liu, J., et al. (2012). Evolutionary conserved role of c-Jun-N-terminal kinase in CO_2-induced epithelial dysfunction. PloS One *7*, e46696.

Verkman, A.S., Matthay, M.A., and Song, Y. (2000). Aquaporin water channels and lung physiology. American Journal of Physiology. Lung Cellular and Molecular Physiology *278*, L867ï 79.

Waldmann, R., Champigny, G., Bassilana, F., Voilley, N., and Lazdunski, M. (1995). Molecular cloning and functional expression of a novel amiloride-sensitive Na^+ channel. The Journal of Biological Chemistry *270*, 27411ï 27414.

Waldmann, R., Champigny, G., Bassilana, F., Heurteaux, C., and Lazdunski, M. (1997). A proton-gated cation channel involved in acid-sensing. Nature *386*, 173ï 177.

Wang, S., and Hubmayr, R.D. (2011). Type I alveolar epithelial phenotype in primary culture. American Journal of Respiratory Cell and Molecular Biology *44*, 692ï 699.

Wang, N., Gates, K.L., Trejo, H., Favoreto, S., Schleimer, R.P., Sznajder, J.I., Beitel, G.J., and Sporn, P.H.S. (2010). Elevated CO_2 selectively inhibits interleukin-6 and tumor necrosis factor expression and decreases phagocytosis in the macrophage. FASEB Journalز Official Publication of the Federation of American Societies for Experimental Biology *24*, 2178ï 2190.

Wang, Y., Cohen, J., Boron, W.F., Schulten, K., and Tajkhorshid, E. (2007). Exploring gas permeability of cellular membranes and membrane channels with molecular dynamics. Journal of Structural Biology *157*, 534ï 544.

Ware, L.B., and Matthay, M.A. (2001). Alveolar fluid clearance is impaired in the majority of patients with acute lung injury and the acute respiratory distress syndrome. American Journal of Respiratory and Critical Care Medicine *163*, 1376ï 1383.

Weisz, O.A., Wang, J., Edinger, R.S., and Johnson, J.P. (2000). Non-coordinate Regulation of Endogenous Epithelial Sodium Channel (ENaC) Subunit Expression at the Apical Membrane of A6 Cells in Response to Various Transporting Conditions*. Biochemistry *275*, 39886 ï 39893.

Welch, L.C., Lecuona, E., Briva, A., Trejo, H.E., Dada, L.A., and Sznajder, J.I. (2010). Extracellular signal-regulated kinase (ERK) participates in the hypercapnia-induced Na,K-ATPase downregulation. FEBS Letters *584*, 3985ï 3989.

Wiedemann, H.P., Wheeler, A.P., Bernard, G.R., Thompson, B.T., Hayden, D., deBoisblanc, B., Connors, A.F., Hite, R.D., and Harabin, A.L. (2006). Comparison of two fluid-management strategies in acute lung injury. The New England Journal of Medicine *354*, 2564ï 2575.

Wiener-Kronish, J.P., Albertine, K.H., and Matthay, M.A. (1991). Differential responses of the endothelial and epithelial barriers of the lung in sheep to Escherichia coli endotoxin. The Journal of Clinical Investigation *88*, 864ï 875.

Woollhead, A., Sivagnanasundaram, J., Kalsi, K.K., Pucovsky, V., Pellatt, L.J., Scott, J.W., Mustard, K.J., Hardie, D.G., and Baines, D.L. (2007). Pharmacological activators of AMP-activated protein kinase have different effects on Na^+ transport processes across human lung epithelial cells. British Journal of Pharmacology *151*, 1204ï 1215.

Woollhead, A.M., Scott, J.W., Hardie, D.G., and Baines, D.L. (2005). Phenformin and 5-aminoimidazole-4-carboxamide-1-beta-D-ribofuranoside (AICAR) activation of AMP-activated protein kinase inhibits transepithelial Na^+ transport across H441 lung cells. The Journal of Physiology *566*, 781ï 792.

Yan, W., Suaud, L., Kleyman, T.R., and Rubenstein, R.C. (2006). Differential modulation of a polymorphism in the COOH terminus of the alpha-subunit of the human epithelial sodium channel by protein kinase Cdelta. American Journal of Physiology. Renal Physiology *290*, F279ï 88.

Yang, L., Rinke, R., and Korbmacher, C. (2006). Stimulation of the Epithelial Sodium Channel (ENaC) by cAMP Involves Putative ERK Phosphorylation Sites in the C Termini of the Channelôs beta - and gamma -Subunit *. Journal of Biological Chemistry *281*, 9859 ï 9868.

Young, D., Lamb, S.E., Shah, S., MacKenzie, I., Tunnicliffe, W., Lall, R., Rowan, K., and Cuthbertson, B.H. (2013). High-frequency oscillation for acute respiratory distress syndrome. The New England Journal of Medicine *368*, 806ï 813.

Yue, G., Russell, W.J., Benos, D.J., Jackson, R.M., Olman, M.A., and Matalon, S. (1995). Increased expression and activity of sodium channels in alveolar type II cells of hyperoxic rats. Proceedings of the National Academy of Sciences of the United States of America *92*, 8418ï 8422.

Figure Index

Tables

8. Eidesstattliche Versicherung

ÄIch erkläre: Ich habe die vorgelegte Dissertation selbständig und ohne unerlaubte fremde Hilfe und nur mit den Hilfen angefertigt, die ich in der Dissertation angegeben habe. Alle Textstellen, die wörtlich oder sinngemäß aus veröffentlichten Schriften entnommen sind, und alle Angaben, die auf mündlichen Auskünften beruhen, sind als solche kenntlich gemacht.
Bei den von mir durchgeführten und in der Dissertation erwähnten Untersuchungen habe ich die Grundsätze guter wissenschaftlicher Praxis, wie sie in der ÄSatzung der Justus-Liebig-Universität Gießen zur Sicherung guter wissenschaftlicher Praxisñ niedergelegt sind, eingehalten.ñ

Benno Buchbinder

9. Danksagung

Während der Durchführung dieser Arbeit haben mich viele Menschen begleitet, unterstützt und gefördert und bei diesen möchte ich mich an dieser Stelle herzlich bedanken:

Meinem Betreuer Dr. István Vadász möchte ich danken für die Bereitstellung des Themas, für die Freiheiten während der Planung und Durchführung der Experimente, sowie für die Unterstützung und Kameradschaft, die ich in dieser Zeit bekommen habe.

Ich danke Prof. Werner Seeger für die Aufnahme ins Graduiertenkolleg ÄMBMLñ, die mir nicht nur die Durchführung dieser Arbeit, sondern auch umfassendes wissenschaftliches Training und die rege Teilnahme an internationalen Kongressen ermöglichte. Des Weiteren danke ich ihm für die Betreuung dieser Arbeit, die ich dadurch extern am Fachbereich Medizin durchführen durfte.

Prof. Wolfgang Clauss begleitete mich bereits während meiner Diplomarbeit. Ihm danke ich für die Betreuung im Fachbereich Biologie.

Ein besonderer Dank geht an Ingrid Breitenborn-Müller und Andrea Mohr für ihre bedingungslose Unterstützung im Laboralltag. Ohne sie wäre diese Arbeit nicht möglich gewesen.

Bei meinen Kollegen möchte ich mich ebenfalls bedanken, insbesondere Miriam Wessendorf, Yasmin Buchäckert und Nieves Gabrielli, die mich über weite Strecken in den letzten Jahren begleitet haben.

Ganz besonders möchte ich meiner Frau Anja danken, die unendlich viel Geduld bewiesen hat und mich trotz der Entbehrungen oder gerade wegen ihnen bestärkt hat diese Arbeit abzuschließen.

Zuletzt möchte ich mich für die fortwährende Unterstützung meiner Familie bedanken, die mir ein finanziell absolut sorgenfreies Studium ermöglichte. Vielen Dank auch für eure Anteilnahme am Gelingen dieser Arbeit.

Der Lebenslauf wurde aus der elektronischen Version der Arbeit entfernt.

The curriculum vitae was removed from the electronic version of the paper.

Orginale Publikationen

BA Grzesik, CU Vohwinkel, RE Morty, K Mayer, S Herold, W Seeger, I Vadász **„*Efficient gene delivery to primary alveolar epithelial cells by nucleofection*"** Am J Physiol Lung Cell Mol Physiol. [in press]

K Richter, KP Kiefer, **BA Grzesik**, WG Clauss, M Fronius **„*Hydrostatic pressure activates ATP-sensitive K^+ channels in lung epithelium by ATP-release through pannexin/connexin hemichannels*** FASEB Journal [in press]

I Vadász, LA Dada, A Briva, IT Helenius, K Sharabi, LC Welch, AM Kelly, **BA Grzesik**, GR Budinger, J Liu, W Seeger, GJ Beitel, Y Gruenbaum, JI Sznajder. **„*Evolutionary conserved role of c-Jun-N-terminal kinase in CO_2-induced epithelial dysfunction.ò*** PLoS One. 2012;7(10):e46696

Y Buchaeckert, S Rummel, CU Vohwinkel, NM Gabrielli, **BA Grzesik**, K Mayer, S Herold, RE Morty, W Seeger, I Vadász. **„*Megalin mediates transepithelial albumin clearance from the alveolar space of intact rabbit lungs.ò*** J Physiol. 2012 Oct 15;590(Pt 20):5167-81

Vorträge und Poster

BA Grzesik, R Ruhl, N Gabrielli, W Seeger, W Kummer, U Pfeil, I Vadasz. ***ĂIntermedinEnhances Alveolar Edema Clearance By Promoting Na,K-ATPase Exocytosis In A Protein Kinase A-Dependent But cAMP-Independent Mannerñ*** Am J Respir Crit Care Med 185; 2012: A3521

BA Grzesik, NM Gabrielli, M Fronius, RE Morty, W Seeger, JI Sznajder, I Vadasz. **"*Long-Term Hypercapnia Impairs ENaC Function In Alveolar Epithelial Monolayers: A Role For Ubiquitination?*"** Am J Respir Crit Care Med 183; 2011: A4228

NM Gabrielli, **BA Grzesik**, LA Dada, W Seeger, JI Sznajder, I Vadasz. ***ĂEffects Of Hypercapnia On Na,K-ATPase Stability And Epithelial Cell Adhesion In Human Alveolar Epithelial Cellsò*** Am J Respir Crit Care Med 183; 2011: A4232

BA Grzesik, M Fronius, W Seeger, RE Morty, JI Sznajder, I Vadasz. **„*Short-term Hypercapnia Differentially Regulates Na,K-ATPase And ENaC Function In Polarized H441 Cell Monolayers*"** Am. J. Respir. Crit. Care Med. 2010; 181: A6462.

K Richter, **BA Grzesik**, R Bogdan, W Clauss, M Fronius. ***„ATP-sensitive K^+-channels In Pulmonary Epithelium (Xenopus laevis) Are Activated By Mechanical Stress.ñ*** Acta Physiologica 2010; Volume 198, Supplement 677:P-TUE-42

I Vadasz, LA Dada, A Briva, HE Trejo, LC Welch, AM Kelly, K Sharabi, **BA Grzesik**, J Liu, Y Gruenbaum, W Seeger, JI Sznajder. ***„Central Role Of C-Jun N-terminal Kinase In Hypercapnia-induced Alveolar Epithelial Dysfunctionò*** Am J Respir Crit Care Med 181;2010:A6459

C Veith, **BA Grzesik**, R Bogdan, WG Clauss, M Fronius. **"*Mechanical Stress Stimulates ATP Release And Activates K_{ATP}-channels In Xenopus Lung Epithelium*"** Acta Physiologica 2008; Volume 192, P140